

UCLA

UCLA Electronic Theses and Dissertations

Title

Quantum oscillations in cuprates and Cooper pairing in half filled Landau level

Permalink

<https://escholarship.org/uc/item/4r29w8q5>

Author

Wang, Zhiqiang

Publication Date

2016

Peer reviewed|Thesis/dissertation

UNIVERSITY OF CALIFORNIA

Los Angeles

**Quantum oscillations in cuprates and Cooper pairing
in half filled Landau level**

A dissertation submitted in partial satisfaction
of the requirements for the degree
Doctor of Philosophy in Physics

by

Zhiqiang Wang

2016

© Copyright by
Zhiqiang Wang
2016

ABSTRACT OF THE DISSERTATION

**Quantum oscillations in cuprates and Cooper pairing
in half filled Landau level**

by

Zhiqiang Wang

Doctor of Philosophy in Physics

University of California, Los Angeles, 2016

Professor Sudip Chakravarty, Chair

The observation of quantum oscillations in hole under-doped cuprate is a big breakthrough to reveal its normal state nature. To understand the observed oscillation frequencies, in chapter 2, we consider the normal state to be a Fermi liquid and in a symmetry broken phase, whose order parameter is a novel period-8 d -density wave. This order gives rise to a complex Fermi surface consisting of not only an electron pocket, which can explain the major observed oscillation frequency $F \sim 530$ T, but also a small hole pocket, which corresponds to a newly predicted slower oscillation. This slower oscillation has received some experimental supports recently.

In chapter 3, we study how superconductivity fluctuations, which exist in the form of random vortices, could affect the normal state quasiparticle quantum oscillation. We find that the Onsager rule, which connects extremal normal state Fermi surface areas to quantum oscillation frequencies, remains intact to an excellent approximation in the mixed-vortex state. We also show that the oscillations of the magnetic field B dependent density of states, $\rho(B)$, ride on top of a field independent background in the high field quantum oscillation regime. This feature appears to agree with the most recent specific heat measurement on $\text{YBa}_2\text{Cu}_3\text{O}_{6+\delta}$. At lower fields the superconductivity fluctuations are quenched and form an ordered vortex lattice. We show that the density of states follows $\rho(B) \propto \sqrt{B}$ as $B \rightarrow 0$, in agreement with the semiclassical results by Volovik.

In chapter 4, we turn to the Cooper pairing problem of composite fermions in the half-filled Landau level. We apply a new pairing mechanism from repulsive forces to the

Halperin-Lee-Read composite fermion liquid. This mechanism takes advantage of the dynamical screening at finite frequency from the finite density composite fermions and makes a net attraction possible. We show that the transition from the composite fermion liquid state to a chiral Cooper pairing state, with odd angular momentum channels, is continuous, in disagreement with the previous conclusion that the transition is discontinuous if the bare interaction is short-ranged. We also construct the phase diagrams for different angular momentum channels ℓ and show that the $\ell = 1$ channel is quite different from higher channels $\ell \geq 3$. Similar analysis has been carried out for the bilayer Hall system with a total filling fraction $\nu = \frac{1}{2} + \frac{1}{2}$ and it is found that the previously established results remain qualitatively unaltered.

Finally, in chapter 5 we apply the above pairing mechanism to the recently proposed particle-hole symmetric Dirac composite fermion liquid theory for the half-filled Landau level. We find that a continuous transition to different chiral pairing states, with angular momentum channels $|\ell| \geq 1$, is possible. These include the Moore-Read Pfaffian and the anti-Pfaffian state. However, the $\ell = 0$ channel particle-hole symmetric pairing state, turns out to be energetically impossible although it is symmetry allowed.

The dissertation of Zhiqiang Wang is approved.

Marek Biskup

Ni Ni

Rahul Roy

Sudip Chakravarty, Committee Chair

University of California, Los Angeles

2016

To my parents ...

TABLE OF CONTENTS

1	Introduction	1
1.1	Quantum oscillations in underdoped Cuprates	2
1.1.1	High temperature superconductor: a short introduction	2
1.1.2	Quantum oscillations	3
1.1.3	d -density wave orders	10
1.1.4	Superconductivity fluctuations in the mixed vortex state	14
1.2	Pairing in half filled Landau level	16
1.2.1	Half filled Landau level problem: a brief overview	18
1.2.2	New pairing mechanism from repulsive forces	27
1.2.3	Particle-hole symmetric composite fermion theory of the half filled Landau level	28
1.3	Outline of this thesis	33
2	Quantum oscillations in $\text{YBa}_2\text{Cu}_3\text{O}_{6+\delta}$ from period-8 d-density wave or- der	36
2.1	Introduction	36
2.2	The Model	38
2.2.1	Band structure	38
2.2.2	Incommensurate DDW without disorder	39
2.2.3	The real space Hamiltonian including disorder	41
2.3	The transfer matrix method	42
2.4	Results	43
2.4.1	Specific heat without disorder	43
2.4.2	Charge modulation without disorder	43
2.4.3	Oscillation spectra in the presence of correlated disorder	45

2.5	Discussion	47
3	Onsager rule, quantum oscillation frequencies, and the density of states in the mixed-vortex state of cuprates	52
3.1	Introduction	52
3.2	The Model Hamiltonians	54
3.2.1	The diagonal component H	54
3.2.2	The off-diagonal component Δ_{ij}	56
3.3	The recursive Green function	58
3.4	Results	59
3.4.1	The Onsager rule for quantum oscillation frequencies	59
3.4.2	The Density of states at high fields	62
3.4.3	Vortex solid at low fields	66
3.5	Conclusion	70
4	Pairing in half-filled Landau level within the HLR picture	71
4.1	Introduction	71
4.2	The Effective action and the BCS gap equation for a single layer system .	73
4.3	Numerical results for single layer system	79
4.4	BCS gap equation for the double layer system	82
4.5	Conclusion	86
5	Pairing of particle-hole symmetric composite fermions in half-filled Lan- dau level	89
5.1	Introduction	89
5.2	Model	90
5.3	Results	95
5.3.1	The effective interaction $\tilde{V}_\ell(\tilde{\Omega})$	95
5.3.2	Solution to the pairing gap equation	96

5.4	Discussion	98
5.5	Conclusion	100
A	Appendices for Chapter 3	102
A.1	Recursive Green's function method	102
A.1.1	Surface Green's function G_s^L, G_s^R of the leads	105
A.2	Bond phase field θ_{ij} of Δ_{ij}	107
A.3	The ansatz $(\frac{\xi}{r_{\text{eff}}})^q = \sum_n (\frac{\xi}{r_n})^q$	109
A.4	Check of the results in Ref.[1]	111
B	Appendices for Chapter 5	116
B.1	The transverse current-current response function $\mathcal{R}_T(\Omega, \mathbf{q})$	116
B.1.1	The RPA equation	116
B.1.2	The computation of $\mathcal{R}_T(\Omega, \mathbf{q})$	117
B.2	Particle-hole symmetry transformation of the order parameter $\hat{\Delta}$	119
B.3	Pairing channels ℓ of particle hole symmetric CFs for the Moore-Read Pfaffian and anti-Pfaffian wavefunctions	120
B.3.1	The shift \mathcal{S} of the Moore-Read Pfaffian and anti-Pfaffian wavefunctions	122
B.3.2	The relativistic shift κ of the Dirac fermions in the 0th Landau level	125
B.3.3	The shift κ of chiral Dirac CF pairing condensates	126
	References	128

LIST OF FIGURES

1.1	Schematic temperature-hole doping phase diagram of cuprates	4
1.2	Current pattern of a two-fold d -density wave order	12
1.3	Current pattern of a period-8 d -density wave order	14
1.4	Mean field $H - T$ phase diagram of a type II superconductor	15
2.1	Reconstructed Fermi surface due to a period-8 d -density wave order . .	40
2.2	Total density of states of the period-8 d -density wave reconstructed band structure	44
2.3	Fourier transform of the oscillation spectra in the presence of a period-8 DDW (I).	47
2.4	Fourier transform of the oscillation spectra in the presence of a period-8 DDW (II).	48
2.5	Fourier transform of the oscillation spectra in the presence of a period-8 DDW (III)	48
2.6	Fourier transform of the oscillation spectra in the presence of a period-8 DDW (IV)	49
3.1	Illustrations of the vortices on the lattice	57
3.2	The Fermi surface and FFT spectrum for the two-fold DDW order case .	60
	(a) Fermi surface	60
	(b) FFT spectrum	60
3.3	The Fermi surface and FFT spectrum for the bi-directional CDW order .	61
	(a) Fermi surface	61
	(b) FFT spectrum	61
3.4	The Fermi surface and FFT spectrum for the period-8 DDW order . . .	63
	(a) Fermi surface	63
	(b) FFT spectrum	63

3.5	Field dependence of the density of states for the two-fold DDW order case	64
3.6	Field dependence of the density of states for the bi-directional CDW order	65
3.7	Field dependence of the density of states for the period-8 DDW order	65
3.8	Schematic diagram of a square vortex lattice	66
3.9	The density of states of a pure d-wave vortex lattice without any particle-hole density wave order at low fields	69
3.10	The density of states of a d -wave vortex lattice coexisting with a two fold DDW order at low fields	70
4.1	Diagrammatic representation of the Dyson equation for the off-diagonal anomalous self-energy $\Delta(i\omega_n, \mathbf{k})$	75
4.2	$\frac{\gamma_\ell(i\omega)}{\alpha_\ell}$ versus $2\pi\alpha_\ell\omega$ for the short-range interaction case	78
4.3	Zero frequency gap Δ_ℓ versus ξ_ℓ for the short-range interaction	79
4.4	Phase diagram for $\ell = 3$ in the ξ_ℓ - ζ_ℓ plane, for the case of short-range interaction.	80
4.5	Phase diagram for $\ell = 1$ in the ξ_ℓ - ζ_ℓ plane, for the case of short-range interaction	81
4.6	Pairing gap Δ for different values of β , in the s -wave channel.	84
4.7	The bilayer pairing gap Δ as a function of the parameter β	86
5.1	Loglinear plots of the effective interaction as a function of the coupling constant for different angular momentum channels	96
5.2	The plot of gap $\Delta_\ell(\omega)$ as a function of the frequency ω for angular momentum channel $\ell = 1$	97
5.3	Plot of gap $\Delta_\ell = \Delta_\ell(\omega = 0)$ as a function of the effective coupling constant α for angular momentum channel $\ell = 1$.	97
5.4	Plots of the gap $\Delta_\ell = \Delta_\ell(\omega = 0)$ as a function of the effective coupling constant α for angular momentum channel $\ell = 1, 2, 3$	99
A.1	Schematic diagram of the recursive Green's function calculation	103

A.2	Schematic diagram for the computation of the Green's function G_{i-1}^L . . .	104
A.3	Schematic diagram for definition of bond phases of the superconductivity order parameter	108
	(a) Bond \overline{ij} does not cross the branch cut: $ \phi_i - \phi_j < \pi$	108
	(b) Bond \overline{ij} crosses the branch cut: $ \phi_i - \phi_j > \pi$	108
A.4	Oscillation spectrum of the density of states for the two fold DDW order model with different q values but a fixed Δ	111
A.5	Numerical check of the density of states results in Fig.1 of Ref.[1]	112
A.6	Numerical check of the density of states results in Fig.3 of Ref.[1]	113
B.1	Schematic sketches of the three steps of constructing the Dirac CF theory in Ref. [2]	122

LIST OF TABLES

- B.1 Summary of the shift values and the corresponding pairing channels ℓ for the Moore-Read Pfaffian wavefunction and the anti-Pfaffian wavefunction 127

ACKNOWLEDGMENTS

There are many people who have helped me during my PhD journey. In this section I would like to express my sincere thanks to them. The completion of my dissertation would be probably impossible without their help.

First and foremost, I am fortunate to have Professor Sudip Chakravarty as my advisor and I am very grateful to him for his numerous support in many aspects. Ever since I joined our group he has kept suggesting to me many important and interesting research topics with his kin eyesight and has guided me towards the right direction in my research. I have benefited tremendously from him in discussing physics problems. I also thank him for his support of me to attend many conferences so that I have the opportunities to present my work and interact with other physicists.

There are also other colleagues in this department that I have learnt a lot from. Among them are especially Professor Yaroslav Tserkovnyak and Professor Rahul Roy who have taught some wonderful classes on special topics of condensed matter physics that have broadened my knowledge. Professor Elihu Abrahams has given many suggestions on my research in our group meeting, which I appreciate a lot.

I am also fortunate to have some wonderful members in our group: Jonghyoun Eun, Chen-Hsuan Hsu, Ipsita Mandal, Arash Bellafard, Antonio Russo and Jian Wang. Jonghyoun Eun has helped me initiate my first PhD project. Chen-Hsuan used to be my office neighbor who I have bothered a lot during the past. He has given me many advices and help on all kinds of things related to my PhD. I have also enjoyed many conversations on physics with our other group members.

In addition, I would also like to acknowledge Dr. Suk-Bum Chung, who used to be a postdoc here in Professor Rahul Roy's group, and Dr. Ipsita Mandal for collaborations and many enlightening discussions.

This dissertation is based on several of my research papers. Specifically, Chapter 2 is a modified version of the paper "Quantum oscillations in $\text{YBa}_2\text{Cu}_3\text{O}_{6+\delta}$ from period-8 d -density wave order", Jonghyoun Eun, Zhiqiang Wang, Sudip Chakravarty, Proc. Natl. Acad. Sci. USA, **109**,13198(2012); Chapter 3 is a modified version of the paper "Onsager rule, quantum oscillation frequencies, and the density of states in the

mixed-vortex state of cuprate”, Zhiqiang Wang, Sudip Chakravarty, Phys. Rev. B, **93**, 184505(2016); Chapter 4 is a modified version of the paper “Pairing in half-filled Landau level”, Zhiqiang Wang, Ipsita Mandal, Suk-Bum Chung, Sudip Chakravarty, Annals of Physics, **351**, 727(2014); Chapter 5 is based on an unpublished manuscript “Pairing of particle-hole symmetric composite fermions in half filled Landau level”, Zhiqiang Wang, Sudip Chakravarty, 2016, which has been submitted to Phys. Rev. B journal. I would like to thank the co-authors, Dr. Jonghyoun Eun, Dr. Ipsita Mandal, and Dr. Suk-Bum Chung for their permission to reuse the papers in my dissertation.

I am also lucky to have some great friends in UCLA who have enriched my graduate life a lot. Among them are especially Brian Xiaoyu Zhu, Phuc Hoang, Yunfeng Xi. They have given me numerous suggestions and advices on different aspects of life.

At last I owe most to my parents, who have always valued education above everything else since I was a kid. Without them I would not have gone this far in my academic journey. They and my other family members are always there as my final support in my whole life. This dissertation is dedicated to them.

Zhiqiang Wang

August 30, 2016

Los Angeles, California, USA

VITA

- 2009 B.S. (Applied Physics), University of Science and Technology of China, Hefei, Anhui, China.
- 2009–2010 Research Assistant, Hefei National Laboratory for Physical Sciences at Microscale, Hefei, Anhui, China
- 2010–present PhD Student (advanced to candidacy in 2013), Condensed Matter Theory, Department of Physics and Astronomy, University of California, Los Angeles, USA.
- 2011 M.S. (Physics), UCLA.
- 2010–2016 Teaching Assistant, Physics and Astronomy Department, University of California, Los Angeles, USA.

PUBLICATIONS AND PRESENTATIONS

- **Zhiqiang Wang**, and Sudip Chakravarty, “Pairing of particle-hole symmetric composite fermions in the half-filled Landau level”, arXiv preprint 2016, <http://arxiv.org/abs/1606.00899>.
- **Zhiqiang Wang**, and Sudip Chakravarty, “Onsager rule, quantum oscillation frequencies, and the density of states in the mixed-vortex state of cuprates”, Phys. Rev. B **93**, 184505(2016)
- **Zhiqiang Wang**, Ipsita Mandal, Suk-Bum Chung and Sudip Chakravarty, “Pairing in half-filled Landau level”, Annals of Physics, **351**, 727(2014)
- Jonghyoun Eun, **Zhiqiang Wang**, and Sudip Chakravarty, “Quantum oscillations in $\text{YBa}_2\text{Cu}_3\text{O}_{6+\delta}$ from period-8 d -density wave order”, Proc. Natl. Acad. Sci. USA, **109**, 13198 (2012)

- Chen-Hsuan Hsu, **Zhiqiang Wang**, and Sudip Chakravarty, “Spin dynamics of possible density wave states in the pseudogap phase of the high temperature superconductors”, Phys. Rev. B, **86**, 214510 (2012)

- *Onsager rule, quantum oscillation frequencies, and the density of states in the mixed-vortex state of cuprates* (Oral)
 APS March Meeting, Baltimore, Maryland, USA, 2016

- *Pairing in half-filled Landau level*(Oral)
 APS March Meeting, San Antonio, Texas, USA, 2015

- *Pairing in half-filled Landau level*(Poster)
 Gordon Research Conference Correlated Electron Systems, Mount Holyoke College, South Hadley, MA, USA, 2014

- *Quantum oscillations in $\text{YBa}_2\text{Cu}_3\text{O}_{6+\delta}$ from period-8 d-density wave order*(Oral)
 APS March Meeting, Baltimore, Maryland, USA, 2013

- *Quantum oscillations in $\text{YBa}_2\text{Cu}_3\text{O}_{6+\delta}$ from period-8 d-density wave order*(Poster)
 Gordon Research Conference Correlated Electron Systems, Mount Holyoke College, South Hadley, MA, USA, 2012

CHAPTER 1

Introduction

The subject of this thesis consists of two most fascinating research topics in strongly correlated electronic systems. One is the high temperature superconductor [3]; the other is the fractional quantum Hall effect(FQHE) [4].

Among many open questions of high temperature superconductors the nature of the normal state of hole underdoped cuprates(copper based high temperature superconductor) is especially puzzling [5]. Different experimental observations seem to point to conflicting physical pictures [6]. In this thesis we focus on a sub-set of these experiments, namely the quantum oscillation experiments [7], which indicate that the concept of Fermi liquid quasiparticles [8] is still valid in the normal state of hole underdoped cuprates despite of strong electron electron interactions. The first half of this thesis will be devoted to understanding these experiments. Specifically we address the following questions:

1. How to understand the quantum oscillation frequencies observed in hole underdoped cuprates from a d -density wave perspective [9, 10]?
2. What are the possible effects of superconductivity fluctuations on the normal state quasiparticle quantum oscillations?

In the FQHE field the odd denominator fractional quantum Hall plateaus have been already understood well by Laughlin's wavefunctions [11], Haldane's hierarchy construction [12], and Jain's composite fermion picture [13]. However our understanding of the even denominator filling fraction states are still far from being satisfactory, although numerous progress has been made in the past. These include both the compressible gapless state [14, 15] and the incompressible gapped states [16] in the half filled Landau level. The gapped states at $\nu = 1/2$ has been proposed to be a Pfaffian state [17, 18], whose quasiparticles posses exotic non-Abelian statistics and can be potentially useful for build-

ing fault-tolerant quantum computers [19]. This state can be interpreted as a Cooper pairing state of composite fermions developed from the compressible state [20, 21, 22]. The second half of this thesis will be devoted to understanding the pairing mechanism behind this transition. In particular we answer the following questions:

1. What is the pairing mechanism behind this transition if the gapless state is described by the Halperin-Lee-Read composite fermion liquid picture [23]? What's the nature of the transition?
2. What is the possible pairing mechanism for the transition if the gapless state is described by the recently proposed particle-hole symmetric Dirac composite fermions [2]? What are the possible pairing angular momentum channels?

1.1 Quantum oscillations in underdoped Cuprates

1.1.1 High temperature superconductor: a short introduction

The copper based high temperature superconductor(cuprates) was first discovered in 1986 by J. G. Bednorz and K. A. Müller [3]. Since 2008 a new generation of the iron-based high temperature superconductor [24, 25, 26] has been discovered. In this thesis we only discuss the cuprates and the term of high temperature superconductor will implicitly mean cuprates.

Although conventional superconductors have been satisfactorily explained by Bardeen, Cooper, and Schrieffer(BCS) [27], there is still no consensus [28] on the pairing mechanism for high temperature superconductivity. One reason is that the normal state, from which the superconductivity arises, is very complicated and difficult to understand. This can be seen from the schematic temperature-hole doping phase diagram of cuprates in Fig. 1.1. In this phase diagram the superconducting state itself is well understood as a Cooper paired state and its superconducting order parameter has a d -wave symmetry [29, 30]. However, the normal state phases at temperatures above the superconducting transition temperature T_c , including the pseudogap phase [31, 5] in the underdoped regime and the strange metal phase [32] at around the optimal doping level, are notoriously difficult to understand. Many anomalous features, such as Fermi arcs [33, 34, 35] in the pseudogap

regime, linear temperature dependent resistivity [36, 37] in the strange metal regime, and etc., have been observed experimentally. They defy satisfactory explanation within the conventional Fermi liquid framework and therefore point to a non-Fermi liquid picture [38, 39].

However, in 2007, to the surprise of the high- T_c community, quantum oscillations [7] have been successfully observed in the hole under doped cuprates. These experiments are performed at very low temperatures and high magnetic fields are applied to kill the superconductivity so that the normal state property could be revealed. Our conventional understanding of quantum oscillation is that it is a direct consequence of Landau level quantization of the cyclotron orbits of some conventional Fermi liquid quasiparticles. Therefore the successful observations of quantum oscillations in cuprates indicate that despite of enormously strong interactions, the physics of the normal state can still be well described by Fermi liquid quasiparticles picture [52, 53], although to today it is still unclear whether non-Fermi liquids can give rise to quantum oscillations or not [6]. In this thesis we take a view that the observed quantum oscillations have truly revealed some conventional Fermi liquid quasiparticles instead of originate from some non-Fermi liquid physics.

Some key issues [6] such as how to reconcile the anomalous non-Fermi liquid physics, observed in the high temperature normal state at zero magnetic field, with the conventional Fermi liquid picture of the low temperature but high magnetic field normal state, suggested by the quantum oscillation experiments, are still far from being well understood. These issues are interesting in their own. However, in this thesis we only focus on some particular issues pertinent to the understanding of the quantum oscillation experiments themselves. In the next section we give a short introduction to the quantum oscillation experiments.

1.1.2 Quantum oscillations

Quantum oscillations [54, 55] are periodic oscillations of physical quantities in the magnetic field inverse $\frac{1}{B}$ when a strong field B is applied to a material at very low temperature T . The measured physical quantities can be magnetization (de Haas-Van Alphen effect), heat capacity, resistivity (Shubnikov-de Haas effect), Hall coefficient, etc.

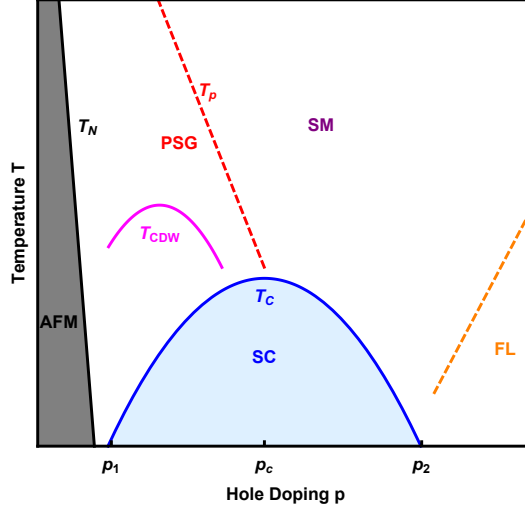


Figure 1.1: Schematic phase diagram of a hole doped cuprate. The vertical axis is temperature T . The horizontal axis is hole doping percentage p . In this phase diagram there are several lines dividing the diagram into different regimes. T_N , the black line, is the phase transition boundary for the anti-ferromagnetic (AFM) order [40, 41, 42]. T_c , the blue line, is the superconductivity transition temperature line bounding the superconducting (SC) dome [43, 44], shaded in light blue. p_1, p_2 are the two critical hole doping values at which the superconductivity order disappears. p_c is the optimal doping level at which T_c is maximum. In the regime $p < p_c$, the cuprate is underdoped; while in the regime $p > p_c$ it is overdoped. The solid pink line T_{CDW} is the transition temperature line for a charge density wave order [45, 46, 47, 48, 49], whose nature is still under hot debate. The red dashed line T_p stands for a temperature scale for the pseudogap (PSG) phase [31, 5]. Whether T_p should be understood as a genuine phase transition line or an energy crossover is still controversial. In this thesis we take the position that T_p represents a transition line below which a novel kind of density wave order, the d -density wave order [9, 10], is developed. The symbol “SM” stands for the strange metal phase [39], which exhibits many anomalous behaviors that deviate from the Fermi liquid picture. The orange dashed line is a crossover temperature scale below which the system behaves like a conventional Fermi liquid (FL) metal [50, 51].

1.1.2.1 Semi-classical picture

The quantum oscillation is a macroscopic manifestation of the Landau level quantization of the underlying quasiparticles near the Fermi surface. It could be viewed as a precursor of the quantum Hall effect (QHE), whose observation requires a much stronger magnetic field and purer sample. Although understanding of the QHE requires a full quantum theory, the quantum oscillation can be understood within a semi-classical quantization scheme.

Consider applying a perpendicular magnetic field $\mathbf{B} = B\hat{z}$ to a two dimensional non-interacting electron gas in a crystal. Then under the Lorentz force a quasiparticle, represented by a wavepacket with a crystal momentum \mathbf{k} , will execute cyclotron motion. This motion is described by the Newton equation [54]

$$\hbar\dot{\mathbf{k}} = -\frac{e}{c}\dot{\mathbf{r}} \times \mathbf{B}, \quad (1.1)$$

where e is the fundamental electric charge and c is the light velocity. The group velocity of the wavepacket is

$$\dot{\mathbf{r}} = \frac{1}{\hbar} \frac{\partial \epsilon(\mathbf{k})}{\partial \mathbf{k}}, \quad (1.2)$$

where $\epsilon(\mathbf{k})$ is the dispersion of the underlying quasiparticles. Integrating Equation (1.1) over time gives

$$\mathbf{k} - \mathbf{k}_0 = -\frac{e}{\hbar c} [\mathbf{r} - \mathbf{r}_0] \times \mathbf{B}, \quad (1.3)$$

where $\mathbf{k}_0, \mathbf{r}_0$ are the initial positions of the wavepacket's trajectories in the momentum and real space respectively. This equation shows that the trajectory in the momentum space can be obtained by a rotation of the real space trajectory along the magnetic field \mathbf{B} direction by a 90 degree angle. Therefore the wavepacket's motion in the momentum space is also cyclotron and it is along a constant energy $\epsilon(\mathbf{k})$ contour because the Lorentz force does not do any work. Furthermore the momentum space cyclotron orbit area $\mathcal{A}_{\mathbf{k}}$ is proportional to the real space orbit area $\mathcal{A}_{\mathbf{r}}$

$$\mathcal{A}_{\mathbf{k}} = \frac{e^2 B^2}{\hbar^2 c^2} \mathcal{A}_{\mathbf{r}}. \quad (1.4)$$

Therefore the quantization condition for $\mathcal{A}_{\mathbf{k}}$ can be obtained from that of $\mathcal{A}_{\mathbf{r}}$. Within the Bohr-Sommerfeld semi-classical quantization scheme, the real space motion satisfies

the following condition

$$\oint [\hbar\mathbf{k} - e\mathbf{A}/c] \cdot d\mathbf{r} = (n + \gamma)2\pi\hbar, \quad (1.5)$$

where n is a non-negative integer, γ is a constant, and \mathbf{A} is the vector potential that satisfies $\mathbf{B} = \nabla \times \mathbf{A} = B\hat{z}$. The integral contour in Equation (1.5) is along a closed cyclotron orbit in real space. In this equation the left hand side bracket has two terms. The first term can be rewritten as follows by using the Equation (1.3)

$$\oint \hbar\mathbf{k} \cdot d\mathbf{r} = \frac{eB}{c} 2 \frac{1}{2} \hat{z} \cdot \oint \mathbf{r} \times d\mathbf{r} = \frac{2e}{c} B\mathcal{A}_{\mathbf{r}}. \quad (1.6)$$

The second term gives nothing but the Aharonov-Bohm phase accumulated along the orbit and is equal to $-eB\mathcal{A}_{\mathbf{r}}/c$. Adding the two terms together gives a net result of $eB\mathcal{A}_{\mathbf{r}}/c$. Substituting this result back into Equation (1.5) leads to

$$B\mathcal{A}_{\mathbf{r}} = (n + \gamma) \frac{2\pi\hbar c}{e} = (n + \gamma)\Phi_0, \quad (1.7)$$

where $\Phi_0 \equiv 2\pi\hbar c/e$ is the magnetic flux quantum. This is the quantization condition for $\mathcal{A}_{\mathbf{r}}$. Then from Equation (1.4), the cyclotron orbit area $\mathcal{A}_{\mathbf{k}}$ in momentum space is also quantized as

$$\mathcal{A}_{\mathbf{k}} \ell_B^2 = (n + \gamma) 2\pi, \quad (1.8)$$

where

$$\ell_B \equiv \sqrt{\frac{\hbar c}{eB}} \quad (1.9)$$

is the magnetic length. Because of this orbit quantization, as the magnetic field is varied, the density of states at the Fermi energy level will have a peak whenever one of these orbit areas $\mathcal{A}_{\mathbf{k}}$ coincides with the extremal Fermi surface area, which in $2D$ is simply the Fermi surface area \mathcal{A}_F . In other words the density of states at the Fermi energy oscillates periodically and the period is determined by

$$\Delta(\mathcal{A}_F \ell_B^2) = 2\pi \quad \Rightarrow \quad \Delta\left(\frac{1}{B}\right) = \frac{2\pi e}{\hbar c} \frac{1}{\mathcal{A}_F}. \quad (1.10)$$

So the oscillation is periodic in the magnetic field inverse $\frac{1}{B}$ instead of the magnetic field B itself. The oscillation frequency F is then given by

$$F \equiv \frac{1}{\Delta(1/B)} = \frac{\hbar c}{2\pi e} \mathcal{A}_F. \quad (1.11)$$

This is the well-known Onsager relation [56] which relates the area \mathcal{A}_F of an extremal Fermi surface cross section perpendicular to the magnetic field to the quantum oscillation frequency F . This relation is remarkable because it directly relates a macroscopic measurable quantity F to a microscopic quantity \mathcal{A}_F with some universal proportionality constant. It makes the quantum oscillation experiment a powerful Fermiology analysis tool [55, 57].

The above analysis applies to a single piece of closed Fermi surface sheet case. If there are more than one piece, then each individual sheet contributes an oscillation with a frequency that is proportional to its own Fermi surface area, as long as different Fermi surface sheets are well separated in the momentum space so that tunneling effects such as magnetic breakdown [55] between different sheets are absent. However, if a Fermi surface sheet contains open orbits, the open orbits do not contribute to quantum oscillations. This is because their corresponding motion in real space is not closed and therefore not periodic. Hence the above semi-classical quantization scheme does not work.

1.1.2.2 Lifshitz-Kosevich formula

A more quantitative analysis of quantum oscillation experiments needs to go beyond the above discussions in order to extract more information. Experimentally this is typically done by fitting data to the Lifshitz-Kosevich(LK) formula [58].

The LK formula can be exactly derived for a free $2d$ electron gas with a dispersion $\epsilon(\mathbf{k}) = \hbar^2(k_x^2 + k_y^2)/2m$. In the presence of a perpendicular magnetic field $\mathbf{B} = B\hat{z}$, the energy levels are quantized into discrete Landau levels $E_n = (n + 1/2)\hbar\omega_c$, where $\omega_c = eB/mc$ is the cyclotron frequency. Then the thermodynamic free energy density Ω can be computed by summing up the contribution from each Landau level. This kind of derivation can be found in Shoenberg [55](also see the PhD thesis of Dr. Brad Ramshaw [59]). The final result of the oscillatory part of Ω , denoted as $\tilde{\Omega}$, is then given by the LK formula which takes the following form

$$\tilde{\Omega} = \frac{\hbar\omega_c}{2\pi\ell_B^2} \sum_{s=1}^{\infty} (-1)^s \frac{1}{\pi^2 s^2} \cos\left(2\pi s \frac{F}{B}\right) \quad (1.12)$$

at zero temperature and without disorder. F is identical to the frequency given in Equation (1.11). In the above summation the $s = 1$ term oscillates in $\frac{1}{B}$ with a frequency

F . Other $s \geq 2$ terms are higher order harmonics of the fundamental mode $s = 1$. The higher order terms are typically much less important, because their amplitudes are suppressed by the factor $1/s^2$ in the above summation and are further damped much more severely by the finite temperature and disorder effects compared with the $s = 1$ term.

When applied to particles with an arbitrary band dispersion $\epsilon(\mathbf{k})$ in a crystal, the LK formula can not be derived exactly in general. However, with the help of the above semi-classical quantization scheme, the LK formula can still be obtained approximately. The major modification is that the bare electron mass m in ω_c should be replaced by an effective cyclotron mass m^* , which depends on the band dispersion $\epsilon(\mathbf{k})$ and is given by [55]

$$m^* = \frac{\hbar^2}{2\pi} \left. \frac{\partial \mathcal{A}_{\mathbf{k}}}{\partial \epsilon} \right|_{\epsilon=\epsilon_F}, \quad (1.13)$$

where ϵ is a short hand notation of $\epsilon(\mathbf{k})$ and ϵ_F is the Fermi energy. $\mathcal{A}_{\mathbf{k}}$ is the \mathbf{k} space area bounded by the energy contour $\epsilon(\mathbf{k}) = \epsilon$, as defined previously.

1.1.2.3 Disorder effects

If disorders are taken into account, then due to random incoherent scattering the Landau levels are broadened and the quasiparticles will have a finite lifetime τ . The effects on the quantum oscillations are two fold. First, the oscillation amplitude will get damped. This can be accounted for by multiplying an additional Dingle damping factor R_D :

$$R_D = e^{-s\pi/\omega_c\tau} \quad (1.14)$$

to each term of the LK formula in Equation (1.12). Again s is the harmonic order index. Because of the exponential dependence of R_D on s , the disorder has a much more severe effect in suppressing the higher order ($s \geq 2$) harmonics oscillations than in suppressing the fundamental mode ($s = 1$) oscillation.

The disorder could also affect the quantum oscillation frequency F in principle. However, as is shown in Ref. [60], the correction is of order $(\hbar/\epsilon_F\tau)^2$. This is typically very small and can be ignored.

1.1.2.4 Finite temperature effects

Similar to the disorder effects, at finite temperature T , the random thermal fluctuations can also broaden the Landau levels. They induce another damping factor

$$R_T = \frac{X}{\sinh(X)} \quad \text{with } X \equiv s \frac{2\pi^2 k_B T}{\hbar\omega_c}, \quad (1.15)$$

that should be multiplied to each term of the LK formula. At high temperature $X \gg 1$, $R_T \approx X e^{-X}$. We see clearly that this factor damps the oscillation amplitude in a way similar to the disorder effects.

1.1.2.5 Electron-electron interactions

So far all the analysis is based on a single particle picture and nothing has been said about the electron-electron interaction effects. However, investigating the effects of electron-electron interactions on quantum oscillations can be very important to fully understand the quantum oscillations in cuprates as it is well known that the electron-electron interaction in cuprates is very strong. However, despite its great interest the current understanding of electron-electron interactions on quantum oscillations is very primitive. In the case that the interaction can be treated as a weak perturbation without completely destroying the underlying Landau levels it can be shown that the quantum oscillation survives with a new frequency which is determined by the interaction renormalized single particle energy dispersion (see Luttinger [61]). However, if the interaction is so strong that the Landau quasi-particle concept breaks down, then whether the quantum oscillations can still survive or not is not clear at all [6].

As emphasized previously, in this thesis we take the view that quantum oscillations observed in underdoped cuprates truly reveal some well-defined Landau quasi-particles despite of strong interactions.

1.1.2.6 Quantum oscillations in the hole doped cuprates

Back to the quantum oscillation problem in the hole doped cuprates, experimentally the major frequency observed is $F \sim 530\text{T}$ [7]. From the Onsager relation this corresponds to a closed Fermi surface pocket occupying only $\mathcal{A}_F/(2\pi/a)^2 \sim 2\%$ of the Brillouin

zone if the lattice spacing constant is chosen to be $a \sim 3.8\text{\AA}$ for a hole doped cuprate. This small 2% does not agree with a single large hole like Fermi surface as we would naively expect. This is because if we assume that the oscillations result from a single large hole pocket that can be produced by bare band hoppings, then according to the Luttinger volume counting [62] rule this hole pocket should occupy $(1 + p)/2 \sim 56\%$ of the first Brillouin zone, in contrast to the observed 2%. Notice that the nominal hole doping percentage range within which quantum oscillations have been established in underdoped cuprates is $p \sim 11 - 14\%$ [6]. The apparent contraction suggests that the bare band structure must have been reconstructed by some mean field order. Since the first observation of quantum oscillations in hole underdoped cuprates, many different types of orders have been proposed to explain the experiments, such as the d -density wave order [63, 6], bi-directional charge density wave order [52, 64], charge/spin stripe order [65, 66], etc. Among these orders the d -density wave order is a natural choice given that it not only can explain the observed oscillation in Hall coefficient well [63] but also can be naturally connected to the high temperature pseudogap phase at zero magnetic field [10]. In Chapter 2 we employ a particular type of the d -density wave order: the period-8 stripe d -density wave order [67], to understand the quantum oscillation frequencies observed in hole underdoped cuprates.

1.1.3 d -density wave orders

As its name suggests, the d -density wave (DDW) [9] is a generalization of the concept of the charge density wave (CDW) and spin density wave (SDW). It is a condensate in the particle-hole channel, in contrast to the superconductivity order parameter which is a particle-particle channel condensate. The major difference of the DDW order from the CDW and SDW order is that its orbital angular momentum channel is $\ell = 2$ instead of $\ell = 1$ as for the CDW and SDW case. The DDW order parameter can also have different structures in the electron spin space. It can be transformed as either a singlet or a triplet under the spin rotation. Among the different types of DDW order parameters, we shall discuss singlet DDW orders only and consider two different kinds that are relevant to the Chapter 2 and Chapter 3.

1.1.3.1 The two-fold DDW order

The simplest DDW order order parameter is the two-fold DDW order. Defined on a square lattice this order parameter can be written as follows(the spin indices are suppressed)

$$\langle c_{\mathbf{r}}^{\dagger} c_{\mathbf{r}'} \rangle = i(-1)^{x+y} \Phi \{ \delta_{\mathbf{r}, \mathbf{r}'+a\hat{x}} + \delta_{\mathbf{r}, \mathbf{r}'-a\hat{x}} - \delta_{\mathbf{r}, \mathbf{r}'+a\hat{y}} - \delta_{\mathbf{r}, \mathbf{r}'-a\hat{y}} \}, \quad (1.16)$$

where $\mathbf{r} = (x a, y a)$ is a site on the square lattice. Because of the pure imaginary i factor on the right hand side this order parameter is a current and breaks the time reversal symmetry locally. The factor $(-1)^{x+y}$ indicates that the ordering wavevector is $\mathbf{Q} = (\pi/a, \pi/a)$. Therefore the order parameter has a period of $2a$ in each direction. This explains its name ‘‘two-fold’’. Φ is a spatial independent real constant that characterizes the order parameter magnitude. The last factor $\{\dots\}$ explicitly shows that the order parameter is defined on a bond and has a local d -wave symmetry at each site. A schematic diagram of the current pattern of this order parameter is given in Fig. 1.2. The current plotted in this diagram is defined as

$$J_{\mathbf{r}, \mathbf{r}'} = \frac{1}{2i} \left[\langle c_{\mathbf{r}}^{\dagger} c_{\mathbf{r}'} \rangle - \langle c_{\mathbf{r}'}^{\dagger} c_{\mathbf{r}} \rangle \right]. \quad (1.17)$$

Notice that the circulating current pattern in Fig. 1.2 is staggered from one square plaquette to its neighboring ones so that globally the time reversal symmetry is still preserved. In the momentum space the two-fold DDW order parameter can be obtained from Equation (1.2) by a Fourier transform and is given by

$$\langle c_{\mathbf{k}'}^{\dagger} c_{\mathbf{k}} \rangle = i \Phi 2 (\cos k_x a - \cos k_y a) \{ \delta_{\mathbf{k}', \mathbf{k}+\mathbf{Q}} + \delta_{\mathbf{k}', \mathbf{k}-\mathbf{Q}} \}. \quad (1.18)$$

Again the factor $(\cos k_x a - \cos k_y a)$ explicitly shows that the two-fold DDW order parameter has a $d_{x^2-y^2}$ symmetry.

1.1.3.2 Relevance of the DDW order to cuprates

The possible relevance of the DDW order to the high temperature superconductor was first emphasized in Ref. [10]. In that paper the authors proposed the idea that the pseudogap phase in the schematic phase diagram of Fig. 1.1 is a genuine symmetry broken phase with the DDW order its order parameter. Under this picture many experiments performed in the pseudogap regime can be understood. However, to today the direct

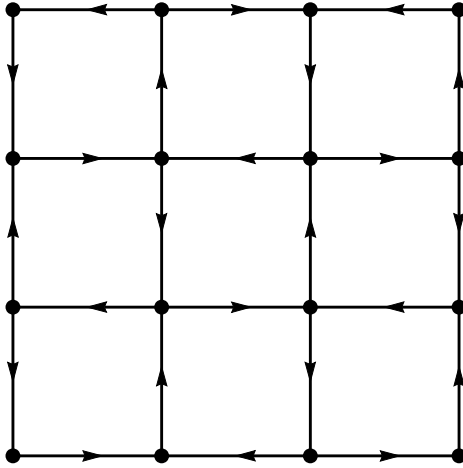


Figure 1.2: Schematic diagram of the current pattern of a two-fold DDW order parameter on a square lattice. The DDW order current is represented by the black arrows and defined on bonds.

experimental establishment of the DDW order is still controversial. This could be due to the d -wave current nature of the order parameter that makes it hidden from most experimental probes which typically couple to either electric or magnetic dipole moments. This point was emphasized in Ref. [10] as well.

Recently after the observation of quantum oscillations in the hole underdoped cuprates, the DDW order revives its interest because it can provide a nice explanation for the Fermi surface reconstruction inferred from the experiment. The two-fold DDW order was first adopted to do such an analysis. The reconstructed Fermi surface [63] consists of an electron pocket which can explain not only the fact that the oscillation frequency $F \sim 530T$ observed is small but also why the observed Hall coefficient [7] has a negative sign, although the system is doped with holes. Remember that the sign of the Hall coefficient is directly related to whether the underlying charge carriers are electron like or hole like. Coming along with the small electron pocket is a larger hole pocket whose area is about twice of that of the electron pocket. This kind of two band model can naturally explain why quantum oscillations have been observed in the Hall coefficient while a single band is difficult to give rise to quantum oscillations in Hall coefficient [63], if not impossible. There are some recent efforts [68] exploring the possibility of observing the Hall coefficient oscillation within a single band by using some nontrivial curvature effects of the Fermi surface contour. However their derivations for the quantum oscillations are not correct

and therefore the conclusions they obtained need to be further scrutinized. Although the two-fold DDW explanation is so attractive, there is a problem: the predicted large hole pocket oscillation has not been observed experimentally. This has motivated us to consider a more exotic order—the period-8 DDW order [67], which can reconstruct the bare band structure in a more complicated yet much more interesting way. This order can provide a nice resolution to the dilemma with the two-fold DDW order explanation. Detail analysis of the problem will be given in Chapter 2. In the following we only briefly introduce the period-8 DDW order parameter.

1.1.3.3 The period-8 DDW order

The period-8 DDW order parameter in real space can be written as follows

$$\begin{aligned} \langle c_{\mathbf{r}}^\dagger c_{\mathbf{r}'} \rangle &= \sum_{\mathbf{r}, \mathbf{r}'} i \frac{W_0}{2} \sin \frac{\mathbf{Q} \cdot (\mathbf{r} - \mathbf{r}')}{2} \sin \frac{\mathbf{Q} \cdot (\mathbf{r} + \mathbf{r}')}{2} \\ &\quad \times \{ \delta_{\mathbf{r}, \mathbf{r}'+a\hat{x}} + \delta_{\mathbf{r}, \mathbf{r}'-a\hat{x}} - \delta_{\mathbf{r}, \mathbf{r}'+a\hat{y}} - \delta_{\mathbf{r}, \mathbf{r}'-a\hat{y}} \}, \end{aligned} \quad (1.19)$$

where the ordering wavevector is $\mathbf{Q} = (\frac{3\pi}{4a}, \frac{\pi}{a})$ and W_0 is a constant controlling the overall magnitude of the order parameter. Similar to the two-fold DDW order case the factor $i \sin \frac{\mathbf{Q} \cdot (\mathbf{r} - \mathbf{r}')}{2}$ in the above indicates that the order is a current and the last factor in the curly bracket $\{ \dots \}$ explicitly exhibits its local d -wave symmetry. The major difference from the two-fold DDW order comes from the $\sin \frac{\mathbf{Q} \cdot (\mathbf{r} + \mathbf{r}')}{2}$ factor, which shows that the order parameter magnitude is modulated with a wavevector \mathbf{Q} , unlike the two-fold DDW order case where the order parameter magnitude is a spatial independent constant. This is most clearly illustrated by the current pattern diagram in Fig. 1.3. The current pattern has a period of 8 lattice spacings in one direction and has a period of 2 lattice spacings in the other direction. Locally at each site the current direction still has a d -wave symmetry. This is why we name it period-8 DDW order. This order parameter can reconstruct the bare band structure and give a much more complicated, yet much more interesting, Fermi surface structure than the two-fold DDW order. Detail discussion will be deferred to Chapter 2.

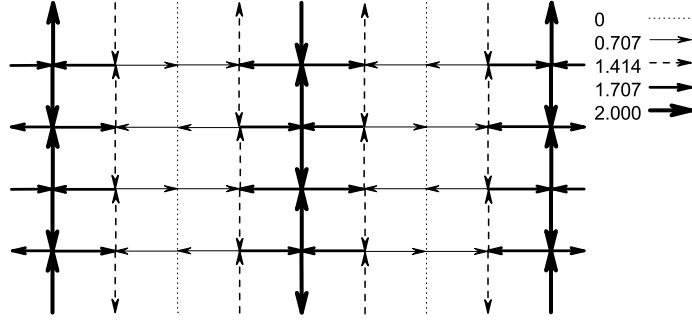


Figure 1.3: Current pattern of a period-8 DDW order. The ordering wavevector is $\mathbf{Q} = (\frac{3\pi}{4a}, \frac{\pi}{a})$. The relative magnitudes of the currents are depicted by the arrows in the legend. Note the antiphase domain wall structure.

1.1.4 Superconductivity fluctuations in the mixed vortex state

In the previous discussions, we have left out one piece of ingredient in the entire picture of quantum oscillation experiments of hole doped cuprates. That is the superconductivity fluctuation. The quantum oscillation experiments are typically carried out along a trajectory represented by the blue dashed arrow in the mean field $H - T$ ¹ phase diagram in Fig. 1.4.

The cuprate is a strong type II superconductor with an upper critical field H_{c2} widely believed to be much higher [70, 71] than the typical magnetic fields applied in the quantum oscillation experiments (in most experiments oscillations start to develop at $H \sim 30$ T while the H_{c2} is believed to be typically ~ 100 T or even higher). However, the value of H_{c2} for the hole doped cuprate is still controversial. Counter claims have also been made in, for example, Ref. [72]. The question we are interested in is that if the experimentally applied H field is indeed less than H_{c2} , what is the effect of the superconductivity fluctuations on normal state quasiparticles quantum oscillation.

In the mixed state phase of the mean field phase diagram in Fig. 1.4, the superconductivity vortex orders into an Abrikosov vortex lattice, which we will call a vortex solid state. However, this mean field picture only holds within a finite regime below the $H_{c2}(T)$ line in the $H - T$ phase diagram, if the superconductivity order parameter fluctuations are

¹In this thesis we use B to denote magnetic fields most of the time, but in this section we use H instead, conforming to the notation used in most literatures that discuss the magnetic field-temperature phase diagram for a superconductor.

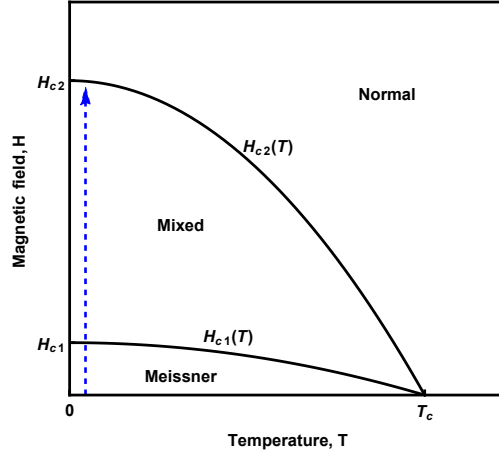


Figure 1.4: Schematic mean field $H - T$ phase diagram of a type II superconductor [69]. The horizontal axis is the temperature T , and the vertical axis is the applied magnetic field H . T_c is the zero field superconductivity transition temperature. $H_{c1}(T)$ and $H_{c2}(T)$ are the temperature dependent lower and upper critical magnetic fields respectively. H_{c1} and H_{c2} are their zero temperature values. The two lines of $H_{c1}(T)$ and $H_{c2}(T)$ divide the phase diagram into three different regimes: Meissner, Mixed, and Normal phases. In the Meissner phase the magnetic field is completely expelled out from the superconductor; in the Mixed state phase the magnetic field can penetrate into the superconductor in the form of quantized flux tubes and produces vortices in the superconductivity order parameter; above $H_{c2}(T)$ the superconductivity order parameter is completely destroyed and the system evolves into its normal state. The blue dashed arrow represents a typical trajectory along which the quantum oscillation experiment is carried out. Notice that for cuprates H_{c1} is very small so that the Meissner phase regime in this diagram should be very narrow.

taken into account. As either the temperature or the magnetic field is increased towards the $H_{c2}(T)$ line the vortex solid will melt into a vortex liquid state, due to either thermal fluctuations or quantum fluctuations [69]. Because the quantum oscillation experiments are performed at very low temperature, the quantum fluctuations are mainly responsible for this melting process. The delineation between the vortex solid and vortex liquid state can be pinned down by measuring the resistivity. In the vortex liquid state the magnetic flux tubes are free to move and lead to finite dissipation of energy [73]. Therefore it is a resistive state. The vortex solid state, on the contrary, is dissipationless because the vortices are frozen. Experimentally the quantum oscillations are observed in a resistive state and therefore the system must have entered into a vortex liquid state. In this state the superconductivity order parameter can fluctuate in both space and time. In Chapter 3 we model the vortex liquid state as a collection of quenched random superconductivity order parameter vortices. This could be viewed as a snapshot of the vortex liquid state. The spatial fluctuations of the superconductivity order parameter are taken into account by averaging the computed quantity over many different random vortex configurations. However, dynamic fluctuations in time are ignored in our treatment but are believed not to alter our conclusion, as indicated by Ref. [74]. The detail discussions will be given in detail in Chapter 3.

1.2 Pairing in half filled Landau level

The observations of the integer quantum Hall effect (IQHE) by Klitzing [75] in 1980 and the fractional quantum Hall effect (FQHE) in 1982 by Tsui, Stormer, and Gossard [4] have opened a new chapter in modern condensed matter physics. Before the discovery of QHE, different states of matter can be classified and understood by the concept of spontaneous symmetry broken (local) order parameter within the framework of Ginzburg-Landau theory. However, to understand the QHE a completely new paradigm and a new concept of topological order [76] is needed, which have recently evolved into the center stage of condensed matter research due to the rise of topological insulators [77, 78].

Although the IQHE can be well understood within a single particle picture [79, 13], with the help of the concept of Anderson localization [80], the FQHE is inherently a

many-particle problem due to the absence of a small energy scale and the massive degeneracy of a partially filled Landau level. To attack this problem different approaches have been adopted such as Laughlin's variational wavefunctions [11], Haldane's hierarchy construction [12], Jain's composite fermions theory [81], and the Hamiltonian theory [82]. These approaches have been very fruitful in understanding the odd denominator fractional quantum Hall states and have generated many fascinating ideas such as fractional charges, fractional statistics, etc.

Among these approaches the composite fermion theory is unique in the sense that it provides a simple unification of the IQHE and FQHE. In this theory the emergent fundamental quasiparticle is not electron anymore but a composite object of an electron and some even integer number $2n$ of magnetic field flux quanta ($\Phi_0 = \frac{2\pi\hbar c}{e}$)². The mutual braiding statistic angle [76] between the composite fermions, which characterizes the statistics of these quasiparticles, is given by

$$\pi + \frac{1}{2} \times 1 \times 2n(2\pi) = (2n + 1)\pi. \quad (1.20)$$

In this equation on the left hand side the first π factor comes from the Fermi statistics inherited from the original electrons; the second factor comes from the Aharonov-Bohm phase picked up by a composite fermion when it traverses around the magnetic fluxes carried by another composite fermion. The $1/2$ factor is needed because adiabatically moving one particle around another is equivalent to adiabatically exchanging the two particles twice. Then because $e^{i(2n+1)\pi} = -1$, exchanging two composite fermion coordinates produces a minus sign in their total wavefunction. In other words the composite fermions still carry Fermi-Dirac statistics and are therefore fermions. Because the fluxes bound to the composite fermions are in a direction opposite to the external magnetic field \mathbf{B} , the composite fermions feel an effective magnetic field $B^* = B - 2n\rho\Phi_0$, whose strength is weaker than the original external magnetic field B . Here ρ is the electron density. Due to the field B^* the composite fermions will execute cyclotron motion and their orbits are quantized into Landau levels. However, the filling fraction of the composite fermions' Landau levels is different from that of the original bare electrons' Landau levels. If the

²Notice that this magnetic flux quanta Φ_0 is different from the definition of the fundamental magnetic flux quanta $\Phi_s = 2\pi\hbar c/2e$ carried by superconductivity vortex. The difference lies in the fact that a Cooper pair carries a charge of $-2e$ while an electron carries a charge of $-e$.

original electron Landau level has a filling fraction $\nu = p/(2np + 1)$ with $n, p \in \mathbb{N}$, then the composite fermions Landau level, whose spacing is determined by the effective field B^* , has an integral filling fraction $\nu^* = p$ [13]. In this way an odd denominator FQHE of the original electrons can be understood as an IQHE of the composite fermions.

However, if the electron filling fraction is $\nu = 1/2n$, which has an even denominator, then $B^* = 0$. In this case the composite fermions can form a Fermi sea (composite fermion Fermi sea) if there is no Cooper pairing instability and the state should be gapless. From the above IQHE picture of composite fermions, it seems a FQHE state at these even denominator filling fractions is impossible since $B^* = 0$. However, experimentally both gapless and gapped states have been observed at even denominator filling fractions. The most well-known even integer denominator Hall plateau is observed at the $\nu = 2 + 1/2 = 5/2$ filling fraction, which has been well established since its first discovery by Willett *et al* [16]. Other even denominator FQHE at $\nu = 7/2$ and $\nu = 19/8$ [83, 84, 85] have also been observed but have received much less attention because of their more stringent experimental requirements. In contrast to the $\nu = 5/2$ filling fraction, the $\nu = 1/2$ state has been found to be gapless [16] in early experiments. Recently some experimental claims of Hall plateaus at $\nu = 1/2$ in wide quantum wells [86] have also appeared. However, these are still controversial. But in principle we do not see any general rule excluding a Hall plateau at $\nu = 1/2$. In this thesis, we consider that both a compressible gapless state and an incompressible state are possible at $\nu = 1/2$. In the following by half filled Landau level we mean $\nu = 1/2$ filling fraction; but the discussions could be equally applied to $\nu = 5/2$ if we take the fully filled first Landau level to be completely inert.

To date, a full comprehension of both the gapless state and the gapped state in half filled Landau level remains illusive. In the following we give a brief account of the current understanding of these states from a theoretical perspective.

1.2.1 Half filled Landau level problem: a brief overview

1.2.1.1 Compressible states

The attention to the $\nu = 1/2$ compressible state problem was first drawn by the anomalies observed in transport by Jiang *et al* [14] and in the surface acoustic wave propagation

by Willett *et al* [15]. The theoretical investigations of the gapless state start with the pioneering work by Halperin, Lee, and Read (HLR) [23] and another work by Kalmeyer and Zhang [87]. In the HLR paper, the authors applied the Chern-Simons gauge field theory, which mathematically implements the flux attachment for composite fermions, to the half filled Landau level. They proposed that the gapless state in the half-filled Landau level has a sharp Fermi surface but do not have well-defined Landau quasiparticles. In this theory within the mean field approximation the composite fermions feel zero magnetic field and the state is described by a Fermi sea of free composite fermions. However, when both the composite fermion-fermion (repulsive) interaction and the Chern-Simons gauge field fluctuations are turned on, the composite fermions pick up a self-energy $\Sigma(k, \omega)$, where k is the momentum and ω is the frequency. The derivative of $\Sigma(k, \omega)$ with respect to the frequency ω diverges at the Fermi surface. Therefore the composite fermion quasiparticle residue, which in the Landau Fermi liquid theory [8] is given by $Z(k, \omega) = (1 - \partial\Sigma(k, \omega)/\partial\omega)^{-1}$, vanishes at the Fermi surface³. The divergence of $\partial\Sigma(k, \omega)/\partial\omega$ also leads to a divergent effective mass m^* . The specific form of the divergence depends on the nature of the composite fermion-fermion interaction $v(q)$. If it is a Coulomb interaction $v(q) \propto 1/q$, then the divergence is logarithmic and the compressible state is a marginal Fermi liquid [32]; whereas if it is a short-range interaction $v(q) \equiv v(0) = \text{const.}$, then the divergence takes a power law form.

The HLR theory has explained the surface acoustic wave propagation experiments [15, 88, 89] very well. Its prediction of a diverging effective mass of the composite fermions at $\nu = 1/2$ was also supported by the magnetoresistance oscillation experiments by Du *et al* [90]. Other experimental findings supporting the HLR picture can be found in Ref. [91, 92, 93, 13].

Despite its great success the HLR theory has long suffered from the lacking of a particle-hole symmetry defined for a single Landau level. This issue was first pointed out in Ref. [94, 95] but did not get a satisfactory resolution. Very recently it was brought to the focus of researches again by an ingenious proposal by Son [2]. In this proposal the composite fermions are particle-hole symmetric. These new composite fermions are quite

³This limit is achieved by first setting $\omega = \xi_k$ in the expression of $Z(k, \omega)$, where $\xi_k = \epsilon_k - \mu$ is the noninteracting particle energy dispersion measured from the chemical potential μ . This is called the on-shell limit. Then sending $\xi_k \rightarrow 0$ gives the quasiparticle residue on the Fermi surface.

different from the old composite fermions used in the HLR theory. To distinguish the two we will call the old composite fermions “HLR composite fermions”. We leave further discussions of the particle-hole symmetry issue to the Section 1.2.3 and turn to discuss the incompressible state in half filled Landau level within the HLR composite fermion picture.

1.2.1.2 Incompressible states

As intriguing as the compressible state is, the half-integral incompressible fractional quantum Hall state is even more mysterious. Its theoretical understanding has experienced several twists and even up till now remain unsettled.

The first theoretical attempt is the Haldane-Rezayi wavefunction proposed by Haldane and Rezayi [96]. This wavefunction can be interpreted as a spin singlet d -wave Cooper pairing state of the HLR composite fermions. The spin-singlet nature of the Haldane-Rezayi state is consistent with the experimental observations that the observed $5/2$ plateau can be destroyed by a parallel(to the 2d electron gas plane) component of magnetic field [97] and makes it an attractive candidate. However, as later argued by Read and Green in Ref. [22], the Haldane-Rezayi state corresponds to a critical point between a weak pairing phase and a strong pairing phase and therefore has gapless excitations in its bulk spectrum. Hence it is not a good candidate for the half-integral FQHE state whose bulk spectrum needs to be gapped.

Later on Moore and Read [17, 18] proposed another wavefunction—the Moore-Read Pfaffian wavefunction, which can be viewed as a p -wave pairing state of spinless(or spin-polarized) HLR composite fermions [20, 21]. This proposal was supported by later numerical work by Morf [98] and Rezayi *et al* [99]. In the work by Morf [98] it was shown that the ground state is spin polarized and therefore in favor of the Moore-Read state rather than the singlet Haldane-Rezayi state. Recently in 2007 a new candidate, the so-called anti-Pfaffian state which is the particle-hole symmetry conjugate of the Moore-Read Pfaffian state, has also been put forward by Lee *et al* [100] and Levin *et al* [101].

Other states [102, 103, 104, 105, 106, 107], such as the 331 state by Halperin [103],

have also been suggested to explain the $5/2$ gapped state.

Among these different theoretical proposals some of them are abelian; while others are non-abelian [19]. Whether a state is abelian or non-abelian is determined by the braiding statistics [108, 109] of its quasiparticle excitations above the ground state. In the abelian case, when two indistinguishable quasiparticles are adiabatically exchanged the total wavefunction picks up a phase factor: $\psi(\mathbf{r}_1, \mathbf{r}_2) \rightarrow e^{i\theta} \psi(\mathbf{r}_2, \mathbf{r}_1)$. When there are more than two particles, each braiding (adiabatically exchanging) of two particles produces an additional phase factor. Because multiplication of the phase factors in different order gives identical final results, the different braiding operations commute with each other. Therefore the corresponding braiding statistics is called abelian. Examples of abelian particles include our familiar $\theta = 0$ bosons such as photons, and $\theta = \pi$ fermions such as electrons. However, emergent quasiparticles with $\theta \neq 0, \pi$ can be also realized in odd denominator fractional quantum Hall states.

More exotically the statistics between quasiparticles can be non-abelian. This can happen when there is a set of degenerate ortho-normal N indistinguishable particle ground states $\psi_\alpha(\mathbf{r}_1, \mathbf{r}_2, \dots, \mathbf{r}_N)$, $\alpha = 1, 2, \dots, g$. Then if two particles are interchanged: $\mathbf{r}_i \leftrightarrow \mathbf{r}_j$, the resultant new wavefunction ψ_β can be different from ψ_α not just by a phase factor but by a unitary rotation in the degenerate ground state subspace: $\psi_\beta = T_{\beta\alpha}^{ij} \psi_\alpha$, where $T_{\beta\alpha}^{ij}$ is a $g \times g$ rotation matrix and it depends on the ground state pair (α, β) . Since different matrices $T_{\beta\alpha}^{ij}$ typically do not commute with each other, exchanging pairs of particles in different orders can lead to different final wavefunctions and therefore does not commute with each other. Then the corresponding braiding statistics is called non-abelian. Braiding non-abelian quasiparticles is a topological manipulation, which is immune to any weak local perturbations. This makes the non-abelian particles very useful for building a fault-tolerant topological quantum computer. Therefore establishing the existence of non-abelian quasiparticles has been a tremendously interesting endeavor in condensed matter physics. In this regard the $\nu = 5/2$ FQHE state is especially interesting because it is believed to have provided a concrete realization of non-abelian quasiparticles [19], although experimentally its non-abelian nature is still not established yet [13, 110].

Among the different candidate wavefunctions proposed, the Moore-Read Pfaffian wavefunction, as well as its particle-hole conjugate —the anti-Pfaffian wavefunction, is

one such kind of wavefunctions that support non-abelian quasiparticles. The Moore-Read wavefunction for N particles is [17]

$$\Psi_{\text{MR}}(z_1, \dots, z_N) = \mathcal{A} \left\{ \frac{1}{z_1 - z_2} \frac{1}{z_3 - z_4} \dots \frac{1}{z_{N-1} - z_N} \right\} \prod_{i < j} (z_i - z_j)^2 e^{-|z_i|^2/4\ell_B}, \quad (1.21)$$

where the subscript ‘‘MR’’ in Ψ_{MR} is a short hand notation for Moore-Read, $z_i = x_i + iy_i$ is the complex spatial coordinate of the i th particle. $\ell_B = \sqrt{\hbar c/eB}$ is the magnetic length. In this wavefunction the Jastrow factor $\prod_{i < j} (z_i - z_j)^2 e^{-|z_i|^2/4\ell_B}$ contains the information of attaching two magnetic flux quanta to each electron to form a composite fermion; while the rest factor $\mathcal{A}\{\dots\}$ encodes the Pfaffian correlation between these composite fermions. The Pfaffian of an anti-symmetrical $N \times N$ (N needs to be an even integer number) dimensional matrix M_{ij} is defined as

$$\text{Pf}(M) = \mathcal{A} \{ M_{12} M_{34} \dots M_{N-1, N} \} \quad (1.22)$$

$$\equiv \frac{1}{2^{N/2} (N/2)!} \sum_{\sigma \in S_N} \text{sgn}(\sigma) \prod_{i=1,3,\dots}^{N-1} M_{\sigma_i, \sigma_{i+1}}, \quad (1.23)$$

where S_N is the permutation group of degree N , σ is an element of the group S_N , and the $\text{sgn}(\sigma)$ is ± 1 depending on whether σ is different from the set $\{1, 2, \dots, N\}$ by an even number of permutations(+1) or odd number of permutations(-1). Mathematically it can be easily shown that a Pfaffian of an antisymmetric matrix is equal to the square root of the corresponding determinant of that matrix: $\text{Pf}(M) = \sqrt{\det(M)}$.

The connection between the Moore-Read wavefunction Ψ_{MR} and a Cooper pairing state of composite fermions can be immediately established once we realize that the real space BCS ground state wavefunction of a definite number of particles is also a Pfaffian, as was first pointed out by Freeman Dyson [111]. To see this clearly we consider a mean field superconductivity Hamiltonian in momentum space

$$H = \sum_{\mathbf{k}} \xi_{\mathbf{k}} c_{\mathbf{k}}^\dagger c_{\mathbf{k}} + \frac{1}{2} \sum_{\mathbf{k}} [\Delta_{\mathbf{k}} c_{\mathbf{k}}^\dagger c_{-\mathbf{k}} + \text{h.c.}], \quad (1.24)$$

where $\xi_{\mathbf{k}} = \epsilon_{\mathbf{k}} - \mu$ and $\Delta_{\mathbf{k}}$ is the pairing order parameter. This quadratic Hamiltonian can be diagonalized directly by Bogoliubov transformation [111]. The excitation energy dispersion is $E_{\mathbf{k}} = \sqrt{\xi_{\mathbf{k}}^2 + |\Delta_{\mathbf{k}}|^2}$ and the ground state is a coherent superposition of single particle empty states and occupied states given by

$$|\Psi_{\text{BCS}}\rangle = \prod_{\mathbf{k}} (u_{\mathbf{k}} + v_{\mathbf{k}} c_{\mathbf{k}}^\dagger c_{-\mathbf{k}}^\dagger) |0\rangle, \quad (1.25)$$

where $|u_{\mathbf{k}}|^2, |v_{\mathbf{k}}|^2$ are the BCS coherent factors that satisfy the condition $|u_{\mathbf{k}}|^2 + |v_{\mathbf{k}}|^2 = 1$. The absolute phases of $u_{\mathbf{k}}$ and $v_{\mathbf{k}}$ are not important, but their relative phase needs to be chosen in accordance with the phase of the pairing order parameter so that the relation $v_{\mathbf{k}}/u_{\mathbf{k}} = -(E_{\mathbf{k}} - \xi_{\mathbf{k}})/\Delta_{\mathbf{k}}^*$ holds. From $|\Psi_{\text{BCS}}\rangle$ the real space BCS wavefunction of N fermions (N even) can be obtained by projecting $|\Psi_{\text{BCS}}\rangle$ onto the N -fermion state $c_{\mathbf{r}_1}^\dagger c_{\mathbf{r}_2}^\dagger \cdots c_{\mathbf{r}_N}^\dagger |0\rangle$. This gives the real space BCS wavefunction in its first quantization form as follows [111]

$$\Psi_{\text{BCS}}(\mathbf{r}_1, \cdots, \mathbf{r}_N) = \mathcal{A} \{g(\mathbf{r}_1 - \mathbf{r}_2) g(\mathbf{r}_3 - \mathbf{r}_4) \cdots g(\mathbf{r}_{N-1} - \mathbf{r}_N)\}, \quad (1.26)$$

where $g(\mathbf{r}) = \int \frac{d\mathbf{k}}{(2\pi)^2} e^{i\mathbf{k}\cdot\mathbf{r}} g_{\mathbf{k}}$ and $g_{\mathbf{k}} \equiv v_{\mathbf{k}}/u_{\mathbf{k}}$. As shown in Ref. [22], if the pairing order parameter⁴ is in the chiral $\ell = -1$ angular momentum channel: $\Delta_{\mathbf{k}} \simeq \Delta (k_x - ik_y) \propto e^{i\ell\theta}$, where $\ell = -1$ and θ is the azimuthal angle of the vector \mathbf{k} , then $g_{\mathbf{k}} \sim 1/(k_x + ik_y)$ as $k_x, k_y \rightarrow 0$. Correspondingly $g(\mathbf{r})$ has an asymptotic behavior $g(\mathbf{r}) \sim 1/z$ as $|\mathbf{r}| \rightarrow \infty$ in real space. Here $z = x + iy$ is the complex $2D$ space coordinate. The power law decay of $g(\mathbf{r})$ indicates that the state is in a weak pairing state, in contrast to the strong pairing phase where $g(\mathbf{r})$ decays exponentially [22]. If we take $g(\mathbf{r})$ to be $1/z$ in Ψ_{BCS} for all distances (not just the asymptotical large distance), then $\Psi_{\text{BCS}}(\mathbf{r}_1, \cdots, \mathbf{r}_N)$ in Equation (1.26) becomes exactly the Pfaffian factor appeared in the Ψ_{MR} in Equation (1.23). Therefore as long as the low energy long distance behavior is concerned, the Moore-Read wavefunction can be viewed as a chiral $\ell = -1$ pairing state of composite fermions. Especially their topological nature, which only depends on the global correlations encoded in these two states, should be identical.

If we view Ψ_{MR} as a $p_x - ip_y$ ⁵ (chiral $\ell = -1$ channel) pairing state of composite

⁴We will try to avoid using “superconductivity order parameter” when we talk about the pairing state of composite fermions, because the composite fermions are neutral to external magnetic field at half filling and there is no true superconductivity for composite fermions. Instead the defining Meissner effect of a regular superconductor for the composite fermions pairing condensate will be translated to an incompressibility of FQHE states in terms of original electrons [22].

⁵In the literature, such as Ref. [19], it is often said Ψ_{MR} corresponds to $p_x + ip_y$ pairing state. The convention here needs some clarifications. If we solve the Landau level problem with a Hamiltonian $\mathcal{H} = \frac{1}{2m}(\mathbf{p} + e\mathbf{A}/c)^2$, where e is the magnitude of the charge of an electron and is therefore positive, the lowest Landau level wavefunction will be an analytical function of $z = x + iy$ complex variable only if the external magnetic field direction is chosen to be in the negative \hat{z} direction: $\mathbf{B} = -B\hat{z}$ with $B > 0$. Therefore with respect to the $+\hat{z}$ direction, Ψ_{MR} corresponds to a chiral $\ell = -1$ pairing channel, or equivalently $p_x - ip_y$ channel; however, were the applied external magnetic field $\mathbf{B} = -B\hat{z}$ direction chosen to be the positive direction, Ψ_{MR} would correspond to a $p_x + ip_y$ pairing state, which is the one used a lot in literature. Here we are trying to be consistent by using the $+\hat{z}$ as the single reference direction when we talk about pairing channels.

fermions, as argued in the previous paragraph, then there can be vortex excitations in the pairing order parameter. As shown in Ref. [22], each single vortex supports one zero energy Majorana mode (bound state) centered at that vortex. If there are several well separated vortices, we can consider the braiding statistics between them. It turns out that because of the Majorana zero mode captured by each vortex, the braiding statistics between these vortices is non-abelian [19]. In the Moore-Read wavefunction case, the corresponding elementary excitations are quasiholes [13] which carry a charge of $e/4$. The braiding statistics of these quasiholes are argued by Moore and Read [17, 18] to be non-abelian by identifying the Ψ_{MR} wavefunction as conformal blocks of two-dimensional conformal field theory. That both Ψ_{MR} and the $p_x - ip_y$ pairing state of composite fermions support non-abelian quasiparticles strongly support that they can be identified with each other, at least if only the asymptotically large distance behavior is concerned.

1.2.1.3 Pairing transition from the composite fermion liquid state to a composite fermions pairing state

Although the non-abelian statistics of a pairing state of composite fermions discussed above is extremely interesting in its own, it is not our focus. Instead we are more interested in understanding how a pairing state of composite fermions develops from the compressible composite fermion liquid state. In other words we want to explore the possible pairing mechanism behind this transition.

This problem is not trivial for at least the following several reasons:

1. The bare composite fermion-fermion interaction $v(q)$, which does not incorporate the screening effects from the fluctuations of the emergent gauge fields, is repulsive and therefore does not naturally lead to pairing.
2. Systematically studying the effects of the fluctuations of the emergent gauge fields by perturbation is not well controlled at all. This is because the perturbation expansion parameter in this problem is given by the number of flux quanta attached to the electron and for half filling is equal to $\frac{1}{\nu} = 2$ [21], which is by no means small. This is in stark contrast to the (3+1)d QED, where the coupling of electrons to the electro-magnetic gauge field is governed by the fine structure constant $\alpha \approx 1/137$,

which is so small such that the perturbation calculations developed by Feynman, Schwinger, and Tomonaga agree with experimental observations incredibly well.

3. When the interaction $v(q)$ and the coupling to the emergent gauge fields are both present, the pairing problem is even more complicated because, as is discussed previously and shown in Ref. [23], the conspiring effect of interaction and gauge field fluctuations tends to destroy the low energy quasiparticles which are supposed to form a Cooper pair in the pairing state. Therefore there is a competition between the non-Fermi liquid behavior (Landau quasiparticle residue vanishing) [23, 112, 113] and the pairing instability in such a problem [114]. This makes a complete solution to the problem even more challenging.

Despite of all these difficulties, attempts to explain the pairing instability have been made before, albeit based on some uncontrolled approximations. Greiter, Wen and Wilczek [21] first considered a bare interaction⁶ between one composite fermion and the current carried by another composite fermion. Because the interaction depends on both the number density and the current density of composite fermions, it is called density-current interaction. This interaction is nothing but a Lorentz force between the magnetic flux tubes carried by one composite fermion and a current of the electron carried by another composite fermion. Remember that the composite fermions are bound states of an electron and an even number of magnetic flux quanta. This interaction is attractive in the chiral $\ell = 1, 3, \dots$ pairing channels⁷. The pairing gap has its largest value in the $\ell = 1$ channel, which is the correct pairing channel that the Moore-Read Pfaffian state corresponds to.

However, if both the interaction $v(q)$ and the coupling to the gauge fields are taken into account, then apart from the density-current interaction, another current-current interaction can be generated between composite fermions. This interaction can be un-

⁶“Bare” in the sense that the screening effects of the finite density CFs on the gauge fields are not included. In the field theoretical language, the interaction considered is a tree level interaction. Also this interaction should not be confused with the interaction $v(q)$ (which may be a Coulomb interaction or a short range interaction) mentioned previously, which is present even in the absence of gauge field fluctuations.

⁷The pairing angular momentum channel here is defined with respect to the external magnetic field direction and therefore it is not $\ell = -1$. We stick to the convention used in Ref. [21] here for the convenience of discussion. This convention will be also used in Chapter 4.

derstood by the following picture: a current of composite fermion can interact with the density of another composite fermion by the above density-current interaction (a Lorentz force); then the second composite fermion can interact with the third composite fermion via the interaction $v(q)$, which only depends on the density but not the current of composite fermions; then the third composite fermion can interact again with a current of the fourth composite fermion again by a Lorentz force. This kind of chain processes generate a net current-current interaction between composite fermions. From this picture we see that the current-current interaction appears only if we go to the second order perturbation or even higher order in the couplings to the emergent gauge field. Therefore normally we might think that these terms are small and can be discarded. However, as emphasized previously this does not need to be the case as the gauge field coupling constant is not small in the current problem and the perturbation expansion is not trustworthy. In fact, if we carry out the previous chain process of generating current-current interaction all the way to infinite order and sum up all these terms, which in the language of Feynmann diagrams is equivalent to summing up all the so called bubble diagrams only and is often called random phase approximation (RPA) [115, 116, 117, 118, 119], we end up with a current-current interaction which depends on the frequency transfer and is divergent in the zero frequency limit ⁸. This has been shown by Bonesteel in Ref. [120]. Furthermore, this current-current interaction is repulsive in the BCS channel ⁹. This is easy to understand: because the Cooper pairs are formed by two composite fermions with opposite momentum, then the electron charge current carried by them are also in opposite directions. The current-current interaction is nothing but an emergent Ampere force between these two composite fermion currents. It is well known that the Ampere force between opposite static currents repel each other. Therefore the current-current interaction should be repulsive in the zero frequency limit. This repulsive and singular low frequency limit current-current interaction, together with the attractive density-current interaction, has been used to solve the BCS gap equation in Ref. [120]. It was shown that

⁸ The generated current-current interaction depends on the frequency because of the energy exchange between the composite fermions and the gauge fields. Throughout this whole thesis when analyzing the half-filled Landau level problem, we work with Matsubara frequencies only. This is enough if we only care about the thermodynamic properties. Working out the real frequency dynamics is a much harder problem.

⁹BCS channel [121] means that the interaction scatters electron pair from $\{\mathbf{k}, -\mathbf{k}\} \rightarrow \{\mathbf{k}', -\mathbf{k}'\}$ with the momentum transfer $\mathbf{q} = \mathbf{k} - \mathbf{k}'$.

the gap equation can either have no solution or have a finite gap solution(at least when the interaction $v(q)$ is a short range interaction) depending on the relative strengths of the two interaction. Therefore the transition from the composite fermion liquid state to a pairing state is concluded to be of first order given that the gap function has a jump at the transition point as a function of relevant tuning parameter.

In Chapter 4, we make a twist to this whole story by considering the full frequency dependence of the current-current interaction, not just its small frequency limit. It turns out that although the current-current interaction is repulsive and singular in the zero Matsubara frequency limit, it has a considerable portion of attraction at higher frequencies in certain angular momentum channels. Therefore if these attractions are included, even the current-current interaction itself may result in a net pairing. If that is the case this gives an example of pairing from repulsive forces in the sense that although the static force is repulsive, the dynamic screened interaction can in fact give attraction and lead to pairing. This alter some conclusions obtained in Ref. [120]. In the following we give a short introduction to this new pairing mechanism and compare it with other similar ideas.

1.2.2 New pairing mechanism from repulsive forces

The idea of pairing from repulsive forces is not new. Long time ago Kohn-Luttinger [122] proposed a pairing mechanism from repulsive forces. Their idea is based on the observation that in a finite density fermion system, due to the Pauli exclusion, the Coulomb interaction between particles is screened and has a long tail Friedel oscillation in real space. Due to the oscillation there are attractions in some regime of the real space. If somehow we can take advantage of attraction and avoid the repulsive portions, there can be a chance of getting a net pairing. This obviously can not happen in the $\ell = 0$ pairing channel because of the divergent repulsion at zero distance. As shown in [122], indeed there can be pairing at higher angular momentum channels. However, the pairing gap energy scale is extremely small [122] so that it is irrelevant to most of experiments(including our half-filled Landau level problem). The key ingredient of this mechanism is a static screening of the electron electron interaction from finite density fermions.

Recently Chung *et al.* [123] have came up with a new paring mechanism from a

repulsive force. The idea is to consider the *dynamic* screening of a repulsive interaction due to the finite density of fermions. To the lowest order, this screening is given by the Landau damping. It turns out that the screened interaction can have significant attractions at higher frequencies in some pairing angular momentum channels although it is repulsive in the zero frequency limit. This is similar to the Kohn-Luttinger case except that now the attraction is in the frequency domain. Typically the $\ell = 0$ channel is completely repulsive in the whole frequency range and therefore can not give any pairing. In contrast to the Kohn-Luttinger case, the pairing gap energy can be some fraction of the Fermi energy of composite fermions and is therefore not small and can be relevant to half-filled Landau level experiments.

The other difference of this new mechanism from the Kohn-Luttinger's idea is that the new mechanism always needs a finite interaction coupling strength to trigger the pairing instability; while in the Kohn-Luttinger case an infinitesimal coupling can result in a pairing.

We have applied this new mechanism to the pairing problem of HLR composite fermions in Chapter 4, as mentioned previously. In Chapter 5 this idea is further extended to a new particle-hole symmetric composite fermion theory for the half-filled Landau level. In the following we introduce this particle-hole symmetric composite fermion theory.

1.2.3 Particle-hole symmetric composite fermion theory of the half filled Landau level

Although the HLR theory has been very successful in explaining many experiments of half-filled Landau level, there is a conflict of this theory with an emergent particle-hole symmetry defined for a half filled single Landau level.

1.2.3.1 Definition of the particle-hole symmetry

The emergent particle-hole symmetry is defined in the vanishing Landau level mixing limit. In this limit the lowest Landau level with an electron filling fraction ν can be

equally well viewed as a full ¹⁰ Landau level filled with holes, with a corresponding hole filling fraction $1 - \nu$. Then a particle-hole transformation (\mathcal{PH}) [124, 2, 125, 126, 127, 128] can be defined for a single Landau level as follows

$$|\nu = 0\rangle \xrightarrow{\mathcal{PH}} |\nu = 1\rangle \quad (1.27)$$

$$c_m^\dagger \xrightarrow{\mathcal{PH}} c_m, \quad (1.28)$$

where $|\nu = 0\rangle, |\nu = 1\rangle$ stand for a completely empty and a completely full Landau level respectively and c_m^\dagger, c_m are the creation operator and annihilation operators of the m th degenerate orbit of the lowest Landau level. From this definition we see that the \mathcal{PH} transformation differs from the single charge conjugation operation as defined by Equation (1.28). Instead it also requires that the external magnetic field direction to be reversed so that the ground state of an empty Landau level is properly transformed into a ground state of completely filled Landau level for holes as shown in Equation (1.27)(ignoring all other Landau levels). Therefore the \mathcal{PH} transformation involves a simultaneous physical charge conjugation and physical time reverse.

1.2.3.2 Conflict of the \mathcal{PH} symmetry with the HLR theory

If the electron filling fraction $\nu = 1/2$, then the hole filling fraction of a full Landau level is $1 - \nu = \nu = 1/2$. In other words the system are equally well described by particles and holes with the same filling fraction. In other words \mathcal{PH} is a symmetry at half filling. This symmetry puts a severe constraint on the possible value of composite fermion Hall conductivity: $\sigma_{xy}^{cf} = -\frac{1}{2} \frac{e^2}{h}$ ¹¹, where $h = 2\pi\hbar$. However, this apparently contradicts the HLR picture, as explicitly pointed out in Ref. [94]. Here we recapitulate some results from Ref. [94] to exhibit the contradiction. Because a single Landau level with an electron filling fraction ν can be equally described by a full Landau level filled with holes at a hole filling fraction $1 - \nu$, the electron Hall conductivity $\sigma_{xy}^e(\nu)$ and the hole Hall conductivity $\sigma_{xy}^h(1 - \nu)$ are connected by

$$\sigma_{xy}^e(\nu) = \frac{e^2}{h} + \sigma_{xy}^h(1 - \nu). \quad (1.29)$$

¹⁰ By ‘‘Full’’ we mean that the lowest Landau level is fully occupied by electrons.

¹¹The minus sign here is defined with respect to the Hall conductivity σ_{xy}^e of the original electrons. In other words the sign of σ_{xy}^{cf} is opposite to that of σ_{xy}^e .

On the right hand side the first term comes from the contribution of the completely electron filled Landau level. Because electrons and holes carry opposite charges we have the following relation

$$\sigma_{xy}^e(\nu) = -\sigma_{xy}^h(\nu). \quad (1.30)$$

Combining Equation (1.29) with Equation (1.30) leads to

$$\sigma_{xy}^e(\nu = \frac{1}{2}) = \frac{1}{2} \frac{e^2}{h}. \quad (1.31)$$

To find out the value of σ_{xy}^{cf} we use the following relation between the electron and composite fermion resistivity [129]

$$\rho_{xx}^e = \rho_{xx}^{cf}, \quad \rho_{yx}^e = \rho_{yx}^{cf} + 2\frac{h}{e^2}, \quad (1.32)$$

where the superscript “ e ” and “ cf ” are used to denote the quantities defined for electrons and composite fermions respectively. In the equation of Hall resistivity the second term on the right hand side comes from the contribution from the two magnetic flux quanta carried by each composite fermion. Then the composite fermion Hall conductivity can be computed as follows

$$\sigma_{xy}^{cf} = \frac{\rho_{yx}^{cf}}{(\rho_{xx}^{cf})^2 + (\rho_{yx}^{cf})^2} = \frac{\rho_{yx}^e - 2h/e^2}{(\rho_{xx}^e)^2 + (\rho_{yx}^e - 2h/e^2)^2} = -\frac{1}{2} \frac{e^2}{h}. \quad (1.33)$$

¹² This large value of σ_{xy}^{cf} implied from the \mathcal{PH} symmetry is in a sharp contrast to the HLR picture. In the HLR theory the composite fermions on average feels zero magnetic field and therefore the Hall conductivity should vanish: $\sigma_{xy}^{cf} = 0$, because at the mean field level the external magnetic field is exactly cancelled out by the fluxes bounded to composite fermions. Beyond the mean field approximation there can be fluctuations of the emergent gauge fields, either due to thermal fluctuations, quantum fluctuations, or disorder. However, including these fluctuations can only lead to a small correction and can not explain the big value of $\sigma_{xy}^{cf} = -\frac{1}{2} \frac{e^2}{h}$. Experimentally the measured σ_{xy} magnitude is very close to $\frac{1}{2} \frac{e^2}{h}$ [130] and the emergent \mathcal{PH} symmetry has also been supported by the self duality found in the non-linear transport measurements [131, 132] and by the more

¹²In deriving this equation we have used $\sigma_{xy}^e = -\rho_{xy}^e/[(\rho_{xx}^e)^2 + (\rho_{xy}^e)^2] = e^2/2h$, and $\sigma_{xx}^e = \rho_{xx}^e/[(\rho_{xx}^e)^2 + (\rho_{xy}^e)^2]$. Also $\sigma_{xx}^e \neq 0$ is needed. This requires breaking of the Galilean invariance by disorder, which is not a bad assumption given that in real experiments disorder is always unavoidable. In Ref. [94] the zero disorder limit of σ_{xy}^{cf} is inconclusive.

recent composite fermion Fermi wavevector measurements at half filling [133, 134]. These measurements contradict the HLR picture, which apparently breaks the \mathcal{PH} symmetry. Early attempt to resolve this contradiction can be found in Ref. [95].

1.2.3.3 \mathcal{PH} symmetric Dirac composite fermion theory

Very recently Son [2] has revisited this issue and proposed an ingenious new \mathcal{PH} symmetric composite fermion theory for the half-filled Landau level problem. In this proposal the original non-relativistic electron Landau level at half filling is first mapped to a Dirac fermion(which still carries electric charge) Landau level problem with the chemical potential sitting at the neutrality point(Dirac point). Then the low energy physics of the Dirac fermion Landau level problem is proposed to be described by a finite density Dirac composite fermion. The Dirac composite fermion carries an emergent two component pseudo-spin degrees of freedom and its dynamics is described by a Rashba pseudospin-orbital coupling Hamiltonian. Therefore its energy dispersion is given by a single Dirac cone with two branches. The lower negative energy branch is inert and completely filled with the composite fermions. The Dirac composite fermions density in the upper positive energy branch is fixed by the external magnetic field such that one composite fermion corresponds to two external magnetic flux quanta, similar to the HLR picture. Furthermore, the particle hole symmetric composite fermions are electrically neutral. Therefore the \mathcal{PH} symmetric composite fermions are essentially the double flux quanta object in the original electron theory and enjoys an electro-magnetic duality to the original electron theory. This point is further discussed and elucidated in the following up works [135, 136, 137, 125].

Because the new composite fermions are Dirac, there is a nontrivial $\phi_F = \pi$ Berry phase picked up by composite fermions as they are traversed around the Fermi surface. According to Ref [138] this Berry phase contributes an additional Hall conductivity to the composite fermi liquid by an amount $|\sigma_{xy}^{cf}| = \frac{\phi_F}{2\pi} \frac{e^2}{h} = \frac{1}{2} \frac{e^2}{h}$. This can reconcile the constraint on σ_{xy}^{cf} from the \mathcal{PH} symmetry with the fact that the Dirac composite fermions feel both zero external magnetic field and on average zero emergent magnetic field(see following discussions).

Similar to the HLR theory the \mathcal{PH} symmetric composite fermions also couple to an

emergent gauge field a_μ . However, there is a crucial difference. In the new theory the Chern-Simons(CS) term of the gauge fields: $\int d^2x dt \epsilon^{\mu\nu\sigma} a_\mu \partial_\nu a_\sigma$, which is present in the HLR theory, is absent. As shown in Ref. [2], in the HLR theory it is precisely the CS term that breaks the \mathcal{PH} symmetry. Therefore the absence of this term rescues the \mathcal{PH} symmetry in the new theory.

As another manifestation of the electro-magnetic duality, the strength of the emergent magnetic field: $b = \hat{z} \cdot \nabla \times \mathbf{a}$, where \mathbf{a} is the spatial vector part of the gauge fields a_μ , is completely dictated by the deviation of the original electron charge density from its value at a half-filled Landau level. Therefore if the original electron Landau level filling fraction is right at $\nu = 1/2$, then on average b is zero.

As argued in Ref. [2, 125], most of the phenomenology of the old HLR theory can be carried over to the new particle hole symmetric Dirac composite fermion theory. These include the small q linear dependence of the composite fermion conductivity $\sigma_{xx}^{cf} \propto q$ for $q \gg l^{-1}$, where l is the disorder induced mean free path. This point is crucial to explain the surface acoustic wave propagation experiments [88]. Also the new theory has similar infrared logarithmic divergence as in the old HLR theory in the presence of a Coulomb interaction. Some differences between the \mathcal{PH} symmetric theory and the HLR theory have been predicted for transport measurements [2, 125, 137]. However, these are still waiting for experimental verification or falsification. So far, the most direct support of this new \mathcal{PH} symmetric theory comes from a density matrix renormalization group numerical study by Geraedts *et al* [126], where a suppression of $2k_F$ backscattering, which is a characteristic of Dirac fermions, has been observed.

After Son's proposal many works followed up [139, 140, 126, 136, 128, 125, 135, 137, 127, 141, 142]. In Ref. [125] the authors tried to develop an intuitive dipolar picture for the Dirac composite fermions and also connect the Dirac composite fermions theory to other seemingly completely unrelated fields such as the surface theory of strongly correlated topological insulator, and spin liquid theory. There are also other particle-hole symmetric theories proposed for the half filled Landau level that are different from Son's idea, such as those in Ref. [140, 141]. In these theories the particle hole symmetry is assumed to be spontaneously broken on the two sides of half filling. The exact $\nu = 1/2$ point corresponds to a critical transition point between the two symmetry broken states.

Whether these theories describe the half-filled Landau level problem better than Son's proposal or vice versa needs much further investigation and can only be determined by experiments. There are also criticisms from Haldane [143] on the Dirac character of the composite fermions in Son's proposal. He has argued that only the nontrivial π Berry phase around the composite fermion Fermi surface is essential for a resolution to the particle-hole symmetry problem in the half filled Landau level; while the Dirac character itself of the composite fermions is unnecessary and inappropriate. To what extent the Dirac nature of composite fermions is needed to describe the low energy physics of the half filled Landau level is a debatable question and is beyond the scope of this thesis.

1.2.3.4 The focus and scope of Chapter 5

Instead of getting involved into any controversy mentioned above, we take Son's proposal as a good low energy effective field theory for the half filled Landau level, and based on it we consider the pairing problem of the \mathcal{PH} symmetric composite fermions. Specifically we apply the new pairing mechanism discussed in Section 1.2.2 to the \mathcal{PH} symmetric composite fermions and consider the pairing phase transition. Detail discussions are given in Chapter 5. Given that the essential ingredient in the new pairing mechanism is a Landau damping given by the finite density Fermi sea of composite fermions and the pairing angular momentum channels classification (such as which channel corresponds to the Moore-Read Pfaffian state) only essentially depends on the π Berry phase around the Fermi surface, we would expect that the conclusions obtained in Chapter 5 still hold even if the Dirac nature (the singularity at the Dirac point far from the Fermi surface) is not there, as long as the two essential ingredients mentioned are still present.

1.3 Outline of this thesis

In this thesis we study two sets of problems: the quantum oscillations observed in hole underdoped cuprates and the pairing of composite fermions in half-filled Landau level. For the quantum oscillation we focus on how to explain the observed oscillation frequencies by Fermi surface reconstruction from a d -density wave perspective and the effects of superconductivity fluctuations on the quantum oscillations; as to the half filled Landau

level problem our primary interest is to understand the pairing mechanism behind the transition from a composite fermion liquid state to different kinds of pairing states.

In Chapter 2 we address a question raised in previous explanations of the quantum oscillation frequencies by a two-fold d -density wave order. In that explanation the reconstructed Fermi surface consists of a small electron pocket Fermi surface, whose area can explain the experimentally observed frequency $F \sim 530T$ well, and a large hole pocket, which has not been observed in experiments. We show that the absence of the large hole pocket oscillation frequency in experiments can be resolved if a period-8 stripe DDW order is behind the scene of the Fermi surface reconstruction. The new reconstructed Fermi surface also contains an electron pocket and a hole pocket. However, the hole pocket is much smaller than the electron pocket. Correspondingly the hole pocket oscillation is very slow such that its experimental establishment requires a much larger field range. We suggest this might explain its absence in previous experimental observations. We demonstrate these oscillations in the presence of disorders explicitly by analyzing the field dependent conductance, which is computed by using the Pichard-Landauer formula and the transfer matrix method.

In Chapter 3 we investigate the effects of the superconductivity fluctuations on the quantum oscillation of normal state quasiparticles. We consider a mixed-vortex state where randomly distributed quenched superconductivity vortices coexist with normal state quasiparticles. The model considered for the normal state consists of one of various kinds of density wave orders. We show that the Onsager rule that connects the normal state quasiparticle Fermi surface area to the quantum oscillation frequency remains intact to an excellent approximation even in the mixed-vortex state of the underdoped cuprates. We establish this conclusion by calculating the magnetic field dependent density of states within the Bogoliubov-de Gennes Hamiltonian formalism, using the recursive Green's function method. We also show that the oscillations ride on top of a field independent density of states, $\rho(B)$, for higher fields. This feature appears to be consistent with recent specific heat measurements [C. Marcenat, *et al.* Nature Comm. **6**, 7927 (2015)]. At lower fields we model the system as an ordered vortex lattice, and show that its density of states follows a dependence $\rho(B) \propto \sqrt{B}$ in agreement with the semiclassical results [G. E. Volovik, JETP Lett. **58**, 469 (1993)].

In Chapter 4 we turn to the pairing problem in the half-filled Landau level. We apply the new pairing mechanism discussed in Section 1.2.2 to the composite fermion liquid state described by the HLR picture. Both an emergent density-current and current-current interaction have been included within the random phase approximation to pair up the composite fermions. By numerically and self-consistently solving the pairing gap equation we show that there can be a continuous transition from the Halperin-Lee-Read state to a chiral odd angular momentum Cooper pair state regardless of whether the bare interaction between composite fermions is a short-range contact interaction or a Coulomb interaction. This is at odds with the previously established conclusion of first order pairing transition for the bare short range interaction case. We construct the phase diagrams and show that $\ell = 1$ angular momentum channel is quite different from higher angular momentum $\ell \geq 3$. Similar analysis has been carried out for the bilayer Hall system with a total filling fraction $\nu = \frac{1}{2} + \frac{1}{2}$. We found that the qualitative features of the previously established results remain unchanged.

In Chapter 5 the new pairing mechanism discussed in Section 1.2.2 is further applied to the particle-hole symmetric Dirac composite fermion theory proposed very recently by Son [2]. We consider a repulsive bare interaction and the dynamical screening of it from the finite density Dirac composite fermions. Using the screened interaction we again solve the self-consistent pairing gap equation as in Chapter 4. We show that there can be nonzero pairing in angular momentum channels $|\ell| \geq 1$ depending on the magnitude of a coupling constant. These include the well known Moore-Read Pfaffian and anti-Pfaffian states. There is a quantum phase transition from the Dirac composite fermi liquid state to Cooper pairing states in angular momentum channels $|\ell| \geq 1$ as the coupling constant is tuned across its critical point value. Surprisingly the particle-hole symmetric $\ell = 0$ channel pairing turns out to be energetically impossible irrespective of the size of the coupling constant within the current pairing mechanism.

CHAPTER 2

Quantum oscillations in $\text{YBa}_2\text{Cu}_3\text{O}_{6+\delta}$ from period-8 d -density wave order

2.1 Introduction

The problem of pseudogap in high-temperature superconductors is one of the most challenging problems in condensed matter physics; see Ref. [5] and references therein. At present there are two views: (*i*) it is either a form of particle-hole condensate reflecting a density wave order, or (*ii*) it is a remnant of the fundamental superconducting order, a particle-particle condensate, that occurs at a lower temperature. As mentioned in the Chapter 1 we adopt the former view.

The discovery of quantum oscillations [7] in the Hall coefficient (R_H) of hole-doped high temperature superconductor $\text{YBa}_2\text{Cu}_3\text{O}_{6+\delta}$ (YBCO) in high magnetic fields approximately between 35T and 62T was an important event that is likely to shed light on the origin of the pseudogap [53]. Although the original measurements were performed in the underdoped regime, close to 10% hole doping, later measurements have also revealed clear oscillations for $\text{YBa}_2\text{Cu}_4\text{O}_8$ (Y248), which corresponds to about 14% doping [144, 145]. Fermi surface reconstruction due to a density wave order that could arise if superconductivity is effectively destroyed by high magnetic fields has been a promising focus of attention [65, 63, 67, 146, 1, 66]. Similar quantum oscillations in the c -axis resistivity in $\text{Nd}_{2-x}\text{Ce}_x\text{CuO}_4$ (NCCO) [147, 148, 149] have been easier to interpret in terms of a two-fold commensurate density wave order, even quantitatively, including magnetic breakdown effects [150, 151].

At this time, in YBCO, there appears to be no general agreement about the precise nature of the translational symmetry breaking. A pioneering idea invoked an order corresponding to period-8 anti-phase spin stripes [65]. The emphasis there was to show

how, over a reasonable range of parameters, the dominant Fermi pockets are electron pockets, thus explaining the observed negative Hall coefficient. At around the same time a two-fold commensurate d -density wave (DDW) order was suggested to be able to explain the observations as well [53]. There are several reasons for such a choice. One of them is that the presence of both hole and electron pockets with differing scattering rates leads to a natural explanation [53] of oscillations of R_H . A period-8 DDW was also considered [67]. Fermi surfaces resulting from this order are very similar to those due to spin stripes. The lack of Luttinger sum rule and a multitude of possible reconstructed Fermi surfaces appeared to have little constraining power in a Hartree-Fock mean field theory. However, since then many experiments that indicate the importance of stripe physics [152] and even possible unidirectional charge order have led us to reconsider the period-8 DDW.

Whereas commensurate models can explain measurements in NCCO, it appears to fail to explain the measurements in YBCO. Luttinger sum rule leads to a concomitant hole pocket with an oscillation frequency roughly about twice the frequency of the electron pocket (~ 500 T). Despite a motivated search no such frequency has been detected. In contrast, for period-8 DDW the hole pockets can be quite small for a range of parameters. To convincingly detect such an oscillation, it is necessary to perform experiments in much higher fields than is currently practiced, which may have bearing on the absence of the hole pocket in previous measurements. However, a tantalizing evidence of a frequency (270 ± 20 T) has been reported in a recent 85 T measurement [153]. There is also a more recent experimental work [154] showing that a small hole pocket oscillation with a frequency ~ 100 T has been found. However, further experiments are still required to firmly establish the small hole pocket. Another consequence of our work is that, depending on disorder, one may even have a situation in which the slower frequency arising from the hole pocket can be more prominent than the faster frequency from the electron pocket.

A number of further considerations suggest that singlet DDW order is a good candidate. Tilted field measurements have revealed spin zeros in quantum oscillations, which are indicative of a symmetry breaking order parameter that is a spin singlet rather than a triplet [155, 156]. Also, NMR experiments in high fields indicate that there is no spin

order but a period-4 charge order that develops at low temperatures [45]¹. This fact can be easily incorporated in our theory because in Landau theory period-8 DDW order of the wave vector \mathbf{Q} can result in a period-4 $2\mathbf{Q}$ charge order. It is important to note that DDW order is very effectively hidden [9, 10]. As long as the CuO-plane is square planar, the currents induced by the DDW cannot induce net magnetic moment to couple to the nuclei in a NMR measurement. Any deviation from the square planar character could give rise to a NMR signal [157]. To the extent these deviations are small the effects will be also small.

First, in Sec. 2.2, we describe our model. Second, in Sec. 2.3, we outline the transfer matrix calculation of the conductivity. Third, in Sec. 2.4, we describe our results, most importantly the quantum oscillation spectra. The final Section 2.5 contains a discussion and an overall outlook.

2.2 The Model

2.2.1 Band structure

The parametrization of the single particle band structure for YBCO from angle resolved photoemission spectroscopy (ARPES) is not entirely straightforward because cleaving at any nominal doping leads to an overdoped surface. Nonetheless an interesting attempt was made to reduce the doping by a potassium overlayer [158]. Further complications arise from bilayer splitting and chain bands. Nonetheless, the inferred band structure appears to be similar to other cuprates where ARPES is a more controlled probe [159]. Here we shall adopt a dispersion that has become common and has its origin in a local density approximation (LDA) based calculation [160], which is as follows:

$$\begin{aligned} \epsilon_{\mathbf{k}} = & -2t(\cos k_x + \cos k_y) + 4t' \cos k_x \cos k_y \\ & - 2t''(\cos 2k_x + \cos 2k_y). \end{aligned} \tag{2.1}$$

¹ Since the time we wrote our paper in 2012 many more experiments have been conducted to reveal the nature of this charge order and most experiments [46, 47, 48, 49] seem to suggest that the charge order is incommensurate and bi-directional with a local d -wave symmetry, unlike the unidirectional commensurate charge order proposed in Ref. [45]. However, the nature of this charge order is still under debate. Our prediction of a small hole pocket in this chapter does not depend on the nature of this charge order, which is much weaker than the dominant period-8 DDW order.

The band parameters are chosen to be $t = 0.15eV$, $t' = 0.32t$, and $t'' = 0.5t'$ [160]. The only difference with the conventional LDA band structure is a rough renormalization of t (from $0.38eV$ to $0.15eV$), which is supported by many ARPES experiments that find that LDA overestimates the bandwidth. A more recent ARPES measurement on thin films paints a somewhat more complex picture. [161]

2.2.2 Incommensurate DDW without disorder

An ansatz for period-eight incommensurate DDW [67] involves the wave vector $\mathbf{Q} = (\frac{\pi}{a}, \frac{\pi}{a}) - \frac{\pi}{a}(2\eta, 0) = \frac{\pi}{a}(\frac{3}{4}, 1)$ for $\eta = 1/8$. With the 8-component spinor defined by $\chi_{\mathbf{k}}^\dagger = (c_{\mathbf{k},\alpha}^\dagger, c_{\mathbf{k}+\mathbf{Q},\alpha}^\dagger, c_{\mathbf{k}+2\mathbf{Q},\alpha}^\dagger, \dots, c_{\mathbf{k}+7\mathbf{Q},\alpha}^\dagger)$, the Hamiltonian without disorder can be written as

$$\mathcal{H} = \sum_{\mathbf{k},\alpha} \chi_{\mathbf{k}\alpha}^\dagger Z_{\mathbf{k},\alpha} \chi_{\mathbf{k}\alpha} \quad (2.2)$$

The up and down spin sector eigenvalues merely duplicate each other, and we can consider simply one of them:

$$Z_{\mathbf{k}} = \begin{pmatrix} \epsilon_{\mathbf{k}} - \mu & iG_{\mathbf{k}} & V_c & 0 & 0 & 0 & V_c & -iG_{\mathbf{k}+7\mathbf{Q}} \\ \text{c.c} & \epsilon_{\mathbf{k}+\mathbf{Q}} - \mu & iG_{\mathbf{k}+\mathbf{Q}} & V_c & 0 & 0 & 0 & V_c \\ V_c & \text{c.c} & \epsilon_{\mathbf{k}+2\mathbf{Q}} - \mu & iG_{\mathbf{k}+2\mathbf{Q}} & V_c & 0 & 0 & 0 \\ 0 & V_c & \text{c.c} & \epsilon_{\mathbf{k}+3\mathbf{Q}} - \mu & iG_{\mathbf{k}+3\mathbf{Q}} & V_c & 0 & 0 \\ 0 & 0 & V_c & \text{c.c} & \epsilon_{\mathbf{k}+4\mathbf{Q}} - \mu & iG_{\mathbf{k}+4\mathbf{Q}} & V_c & 0 \\ 0 & 0 & 0 & V_c & \text{c.c} & \epsilon_{\mathbf{k}+5\mathbf{Q}} - \mu & iG_{\mathbf{k}+5\mathbf{Q}} & V_c \\ V_c & 0 & 0 & 0 & V_c & \text{c.c} & \epsilon_{\mathbf{k}+6\mathbf{Q}} - \mu & iG_{\mathbf{k}+6\mathbf{Q}} \\ iG_{\mathbf{k}+7\mathbf{Q}} & V_c & 0 & 0 & 0 & V_c & \text{c.c} & \epsilon_{\mathbf{k}+7\mathbf{Q}} - \mu \end{pmatrix}, \quad (2.3)$$

where $G_{\mathbf{k}} = (W_{\mathbf{k}} - W_{\mathbf{k}+\mathbf{Q}})/2$, and the DDW gap is $W_{\mathbf{k}} = \frac{W_0}{2}(\cos k_x - \cos k_y)$. On symmetry grounds, one can quite generally expect that an incommensurate DDW with wave vector \mathbf{Q} will induce a charge density wave (CDW) of wave vector $2\mathbf{Q}$ [9]. This fact is taken into account by explicitly incorporating a period-4 CDW by introducing the real matrix elements V_c . The chemical potential μ and the DDW gap amplitude W_0 can be adjusted to give the desired quantum oscillation frequency of the electron pocket as well as the doping level. The Fermi surfaces corresponding to the spectra of Eq. (2.2) (an example is shown in Fig. 2.1) are not essentially different from the mean field theory of $1/8$ magnetic antiphase stripe order [65]. This higher order commensuration generically produces complicated Fermi surfaces, involving open orbits, hole pockets, and electron pockets.

To picture the current modulation and to define the order parameter of period-8 DDW

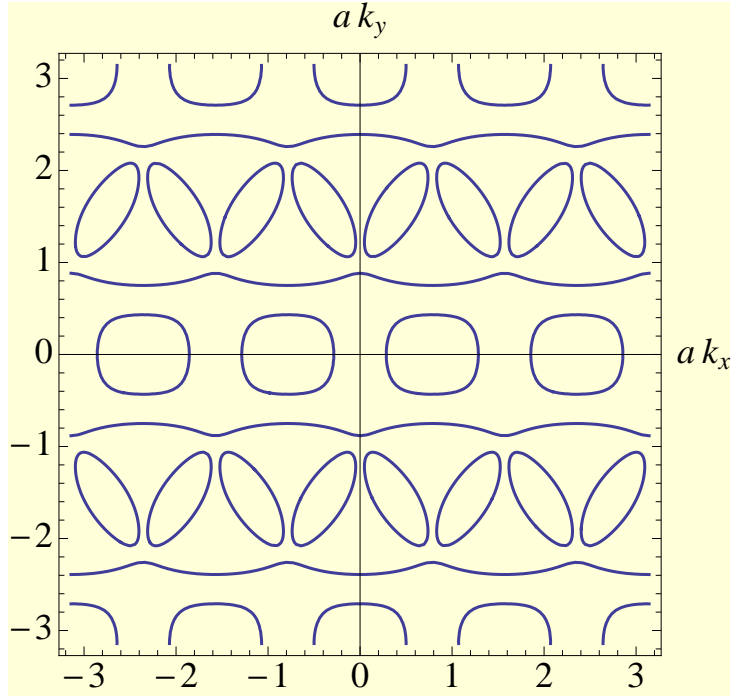


Figure 2.1: Reconstructed Fermi surfaces with $\mathbf{Q} = \frac{\pi}{a}(\frac{3}{4}, 1)$, $W_0 = 0.65t$, $V_c = 0.05t$, and $\mu = -0.83t$. There are electron pockets, hole pockets and open orbits. The electron pocket frequency corresponds to 530T and the hole pockets to 280T. The doping corresponds to 12.46%. Note that the figure is shown in the extended BZ for clarity.

in the real space Hamiltonian we need to calculate $\langle c_{\mathbf{r}'}^\dagger c_{\mathbf{r}} \rangle$ for $\mathbf{r}' \neq \mathbf{r}$. We get, correcting here a mistake in Ref. [67],

$$\begin{aligned}\langle c_{\mathbf{r}'}^\dagger c_{\mathbf{r}} \rangle &= \frac{1}{N} \sum_{\mathbf{k}'\mathbf{k}} \langle c_{\mathbf{k}'}^\dagger c_{\mathbf{k}} \rangle \exp[-i(\mathbf{k}' \cdot \mathbf{r}' - \mathbf{k} \cdot \mathbf{r})] \\ &= \pm \frac{iW_0}{2} (-1)^{n'+m'} \widetilde{V}_{\mathbf{r}',\mathbf{r}},\end{aligned}\tag{2.4}$$

where $\mathbf{r}' = (m'a, n'a)$, and $\widetilde{V}_{\mathbf{r}',\mathbf{r}}$ is

$$\widetilde{V}_{\mathbf{r}',\mathbf{r}} = \left[\frac{1 + \cos 2\pi\eta}{2} (\delta_{\mathbf{r}',\mathbf{r}+a\hat{x}} + \delta_{\mathbf{r}',\mathbf{r}-a\hat{x}}) - (\delta_{\mathbf{r}',\mathbf{r}+a\hat{y}} + \delta_{\mathbf{r}',\mathbf{r}-a\hat{y}}) \right] \cos 2m'\pi\eta\tag{2.5}$$

$$+ \frac{\sin 2\pi\eta \sin 2m'\pi\eta}{2} (\delta_{\mathbf{r}',\mathbf{r}+a\hat{x}} - \delta_{\mathbf{r}',\mathbf{r}-a\hat{x}}).\tag{2.6}$$

The current pattern is then

$$J_{\mathbf{r}',\mathbf{r}} = \frac{1}{2i} \left[\langle c_{\mathbf{r}'}^\dagger c_{\mathbf{r}'} \rangle - \langle c_{\mathbf{r}}^\dagger c_{\mathbf{r}} \rangle \right] = -\frac{W_0}{2} (-1)^{n'+m'} \widetilde{V}_{\mathbf{r}',\mathbf{r}},\tag{2.7}$$

which has already been shown previously in Fig. 1.3 of Section 1.1.3.3. The incommensurate d -density wave order parameter is proportional to

$$\widetilde{W}_{\mathbf{r}',\mathbf{r}} = \frac{iW_0}{2} (-1)^{n'+m'} \widetilde{V}_{\mathbf{r}',\mathbf{r}}.\tag{2.8}$$

Notice that although at first glance the expression of $\widetilde{W}_{\mathbf{r}',\mathbf{r}}$ looks quite different from the real space period-8 DDW order parameter given in Equation 1.19 of Section 1.1.3.3, they are in fact identical to each other.

2.2.3 The real space Hamiltonian including disorder

In real space, the Hamiltonian in the presence of both disorder and magnetic field is

$$\begin{aligned}H &= \sum_{\mathbf{r}} [V(\mathbf{r}) + 2V_c \cos(\pi m/2)] c_{\mathbf{r}}^\dagger c_{\mathbf{r}} \\ &+ \sum_{\mathbf{r}',\mathbf{r}} t_{\mathbf{r}',\mathbf{r}} e^{ia_{\mathbf{r}',\mathbf{r}}} c_{\mathbf{r}'}^\dagger c_{\mathbf{r}} \\ &+ \sum_{\mathbf{r}',\mathbf{r}} \widetilde{W}_{\mathbf{r}',\mathbf{r}} e^{ia_{\mathbf{r}',\mathbf{r}}} c_{\mathbf{r}'}^\dagger c_{\mathbf{r}} + h.c.\end{aligned}\tag{2.9}$$

Here $t_{\mathbf{r}',\mathbf{r}}$ defines the band structure. The nearest neighbor, the next nearest neighbor, and the third nearest neighbor hopping terms: t , t' , t'' . And $2V_c \cos(\frac{\pi}{2}m)$ is responsible

for the period-4 charge stripe order, where m is $\mathbf{r} \cdot \hat{x}/a$ and a is lattice spacing. We include correlated disorder in the form [162]

$$V(\mathbf{r}) = \frac{g_V}{2\pi l_D^2} \int d\mathbf{x} e^{-\frac{|\mathbf{r}-\mathbf{x}|^2}{2l_D^2}} u(\mathbf{x}), \quad (2.10)$$

where l_D is the disorder correlation length and the disorder averages are $\langle u(\mathbf{x}) \rangle = 0$ and $\langle u(\mathbf{x})u(\mathbf{y}) \rangle = \delta(\mathbf{x} - \mathbf{y})$; the disorder intensity is set by g_V .

Whereas white noise disorder seems to be more appropriate for NCCO with intrinsic disorder, correlated disorder may be more relevant to relatively cleaner YBCO samples in the range of well ordered chain compositions. Thus, here we shall focus on correlated disorder. A constant perpendicular magnetic field B is included via the Peierls phase factor $a_{\mathbf{r}',\mathbf{r}} = \frac{e}{\hbar c} \int_{\mathbf{r}}^{\mathbf{r}'} \mathbf{A} \cdot d\mathbf{l}$, where $\mathbf{A} = (0, -Bx, 0)$ is the vector potential in the Landau gauge; the lattice vector $\mathbf{r}' = (m'a, n'a)$ is defined by an arbitrary set of integers.

2.3 The transfer matrix method

The transfer matrix technique is a powerful method to compute conductance oscillations. It requires neither quasiclassical approximation nor *ad hoc* broadening of the Landau level to incorporate the effect of disorder. Various models of disorder, both long and short-ranged, can be studied *ab initio*. The mean field Hamiltonian, being a quadratic non-interacting Hamiltonian, leads to a Schrödinger equation for the site amplitudes, which is then recast in the form of a transfer matrix; the derivation has been discussed in detail previously [162, 150]. The conductance is then calculated by a formula that is well known in the area of mesoscopic physics, the Pichard-Landauer formula [163, 164]. This yields Shubnikov-de Haas oscillations of the *ab*-plane resistivity, ρ_{ab} .

We consider a quasi one-dimensional system, $N \gg M$, with a periodic boundary condition along *y*-direction. Here Na is the length in the *x*-direction and Ma is the length in the *y*-direction. Let $\Psi_n = (\psi_{n,1}, \psi_{n,2}, \dots, \psi_{n,M})^T$, $n = 1, \dots, N$, be the amplitudes on the slice n for an eigenstate with a given energy. Then the amplitudes between the successive slices depending on the Hamiltonian must form a given transfer matrix, \mathbb{T} .

The complete set of Lyapunov exponents, γ_i , of $\lim_{N \rightarrow \infty} (\mathcal{T}_N \mathcal{T}_N^\dagger)$, where $\mathcal{T}_N = \prod_{j=1}^{j=N} \mathbb{T}_j$

determine the conductance, $\sigma_{ab}(B)$ from the Pichard-Landauer formula:

$$\sigma_{ab}(B) = \frac{e^2}{h} \text{Tr} \sum_{j=1}^{2M} \frac{2}{(\mathcal{T}_N \mathcal{T}_N^\dagger) + (\mathcal{T}_N \mathcal{T}_N^\dagger)^{-1} + 2}. \quad (2.11)$$

In this work we have chosen $M = 30$ and N of the order of 10^5 . This guaranteed 4% accuracy of the smallest Lyapunov exponent. Note that at each step we have to invert a $4M \times 4M$ matrix and numerical errors prohibit much larger values of M .

2.4 Results

2.4.1 Specific heat without disorder

The coefficient of the linear specific heat is

$$\gamma = \frac{\pi^2}{3} k_B^2 \rho(0). \quad (2.12)$$

The density of states $\rho(\omega)$ measured with respect to the Fermi energy can be easily computed by taking into account all eight bands in the irreducible part of the Full Brillouin zone and a factor of 2 for spin. A Lorentzian broadening of the δ -functions was used in computing the density of states. Although Lorentzian broadening is useful for numerical computation, the smoothing is a rough way of incorporating the effect of disorder on the density of states.

For a single CuO-layer we get,

$$\gamma \approx 5.4 \frac{mJ}{\text{mole} \cdot K^2}, \quad (2.13)$$

where we have used the density of states at the Fermi energy from numerical calculation to be approximately 2.3 states/eV, as shown in the Figure 2.2. Including both layers $\gamma = 2 \times 5.4 = 10.8 \frac{mJ}{\text{mole} \cdot K^2}$, approximately a factor of 2 larger than the observed $5 \frac{mJ}{\text{mole} \cdot K^2}$ at $45T$ [165].

2.4.2 Charge modulation without disorder

Before we carry out an explicit calculation it is useful to make a qualitative estimate. For $V_c = 0.05t$, the total charge gap is $4V_c = 0.2t$. To convert to modulation of the charge-order parameter, we have to divide by a suitable coupling constant. In high temperature

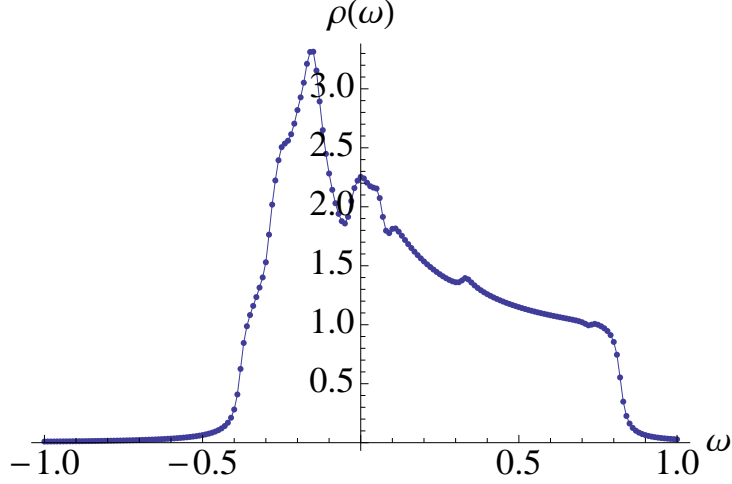


Figure 2.2: Total density of states, $t = 0.15$, including eight bands in the reduced Brillouin zone per layer. The horizontal axis is in terms of electron volts and the vertical axis is a pure number, that is, the number of states. The rounding at the tails is due to the Lorentzian broadening of the δ -functions by $\Gamma = 0.1t$. The remaining parameters are the same as in Fig. 2.1. Further smoothing will reduce the density of states at the Fermi energy and lower the value of γ .

superconductors, all important coupling constants are of the order bandwidth, which is $8t = 1.2eV$. Taking this as a rough estimate, we deduce that the charge modulation is $0.025e$, expressed in terms of electronic charge.

To explicitly calculate charge modulation at a site, we diagonalize the 8×8 Hamiltonian matrix $Z(k_x, k_y)$ for each \mathbf{k} in the reduced Brillouin zone (RBZ). We get 8 eigenvalues and the corresponding eigenvectors: E_{n,k_x,k_y} and ψ_{n,k_x,k_y} for $n = 1, 2, \dots, 8$. The eigenvector ψ_{n,k_x,k_y} has eight components of the form:

$$\psi_{n,k_x,k_y} = (\alpha_{n,k_x,k_y}(1), \alpha_{n,k_x,k_y}(2), \dots, \alpha_{n,k_x,k_y}(8)) \quad (2.14)$$

Then the wave function in the real space for each state $\{n, k_x, k_y\}$ is

$$\psi_{n,k_x,k_y}(\mathbf{r}) = \sum_{j=1}^8 \alpha_{n,k_x,k_y}(j) \frac{1}{\sqrt{N}} \exp i(\mathbf{k} + (j-1)\mathbf{Q}) \cdot \mathbf{r} \quad (2.15)$$

So, by definition, the local number density is

$$n(\mathbf{r}) = 2 \sum'_{n,k_x,k_y} |\psi_{n,k_x,k_y}(\mathbf{r})|^2 \quad (2.16)$$

Here the prime in the sum means that all occupied states with energy below the chemical potential are considered. The factor of 2 is for spin and the summation over k_x, k_y is performed in the RBZ. For different parameter sets the numerical results are, as follows:

- Parameter set 1

$$W_0 = 0.71t, V_c = 0.05t, \mu = -0.78t, x = 11.73\%$$

Averaged number density of electron is $n = 0.882$ per site, whereas the estimated deviation is about $\delta n = 0.029$ per site. So $\delta n/n = 3.2\%$. The cyclotron effective mass calculated are 0.567 for the hole pocket and 1.98 for the electron pocket in units of the free electron mass.

- Parameter set 2

$$W_0 = 0.65t, V_c = 0.05t, \mu = -0.83t, x = 12.46\%$$

Averaged number density of electron is $n = 0.877$ per site, whereas the estimated deviation is about $\delta n = 0.031$ per site. So $\delta n/n = 3.58\%$. The cyclotron effective masses calculated are 0.652 for the hole pocket and 2.04 for the electron pocket in units of the free electron mass.

Of course, for both cases, the period of the CDW modulation is $4a$, where a is the lattice spacing. It is also interesting to calculate the ratio of the modulation of the local density of states to the average density of states at the Fermi energy; we find $\delta\rho(\mu)/\rho(\mu) \approx 13 - 15\%$ depending on the parameters. As pointed out in Ref. [66], this leads to an estimate of the corresponding variation of the Knight shift.

2.4.3 Oscillation spectra in the presence of correlated disorder

Previously it was found from the consideration of $1/8$ magnetic antiphase stripe order that there is a remarkable variety of possible Fermi surface reconstructions depending on the choice of parameters [65]. This is also true for the incommensurate period-8 DDW. In contrast, two-fold commensurate DDW order leads to much lesser variety. While this is more satisfying, period-4 charge modulation observed in NMR measurements [45] and the non-existence of the larger hole pocket commensurate with the Luttinger sum rule have forced us to seriously consider the period-8 DDW.

Although we cannot constrain the parameters uniquely, we have used a number of guiding principles. First, disorder was chosen to be correlated with a length scale ℓ_D smaller than the transverse width of the strip, Ma . Because the YBCO samples studied appear to have lesser degree of disorder than the intrinsic disorder of NCCO, the white noise disorder did not appear sensible. Because the experimentally measured charge modulation in NMR is $0.03 \pm 0.01e$, it is necessary to keep V_c small enough to be consistent with experiments. A value of V_c in the neighborhood of $0.05t$ seemed reasonable. Of course, this could be adjusted to agree precisely with experiments, but this would not have been very meaningful.

The band structure parameter t was chosen to be 0.15 eV as opposed to LDA value of 0.38 eV. Although reliable ARPES measurements are not available for YBCO, measurements in other cuprates have indicated that the bandwidth is renormalized by at least a factor of 2. Had we chosen $t = 0.38$ eV, the agreement with specific heat measurements would have been essentially perfect, but we could not see any justification for adopting the bare band structure parameter. The parameters t'/t and t''/t' are the same as the commonly used LDA values, as the shape of the Fermi surface in most cases appear to be given correctly by LDA. We searched the remaining parameters, μ , g_V and W_0 , extensively. There are a number of issues worth noting. Oscillation spectra hardly ever show any substantial evidence of harmonics, which should be used as a constraining factor. Moreover, as we believe that it is the electron pocket that is dominant in producing negative R_H , it is necessary that we do not employ parameters that wipe out the electron pocket altogether. The coexistence of electron and hole pockets give a simple explanation of the oscillations of R_H as a function of the magnetic field. We generically found hole pocket frequencies in the range 150 – 300T. This is one of our crucial observations. It implies that to resolve clearly such a slow frequency, one must go to much higher fields than are currently possible. We argue that the absence of observations at higher magnetic fields may be a plausible reason why the hole pocket has not been observed previously except for one experiment which goes up to 85T; in this experiment some evidence of a 250T frequency is observed [153]. ²

²As mentioned previously, in a more recent work [154] a small hole pocket oscillation frequency ~ 100 T has been claimed to be observed.

The DDW gap and the disorder level are consistent with the observed data. Overall we find satisfactory consistency with doping levels between 11 – 12.5% within our calculational scheme. Lower doping levels produce less satisfactory agreement, but can be made better with further adjustment of parameters, but we have avoided fine-tuning as much as possible. The broad brush picture can already be seen in the oscillation spectra in Figs. 2.3, 2.4, 2.5, and 2.6. Two general trends are that electron pockets dominate at higher doping levels within the range we have checked, and an increase in disorder intensity reduces the intensity of the Fourier spectra of the electron pockets. A few harmonics are still present. Interestingly, depending on disorder one may have a situation in which the faster oscillations from the electron pocket can disappear leaving the slower frequency from the hole pocket intact; see, for example, Figs. 2.4 and 2.6.

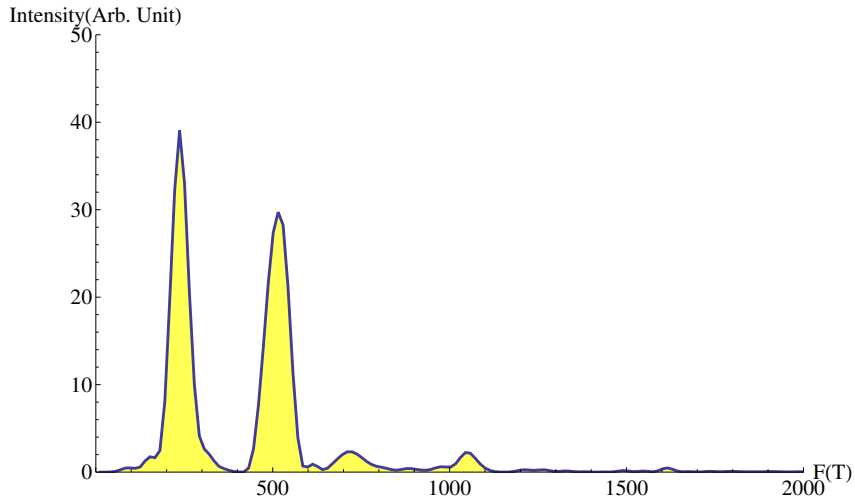


Figure 2.3: Fourier transform of the oscillation spectra after a background subtraction with a cubic polynomial. $W_0 = 0.71t$, $V_c = 0.05t$, $\mu = -0.78t$, $M = 30 a$, $N = 10^5 a$, $\ell_D = 8 a$, $g_V = 0.1t$. Doping is 11.73%.

2.5 Discussion

The complex materials physics of high temperature superconductors lead to a fairly large number of dimensionless parameters. Thus, it is not possible to frame a unique theory. Tuning these parameters can indeed lead to many different phases. However, there may be a general framework that could determine the overall picture. To be more specific, let

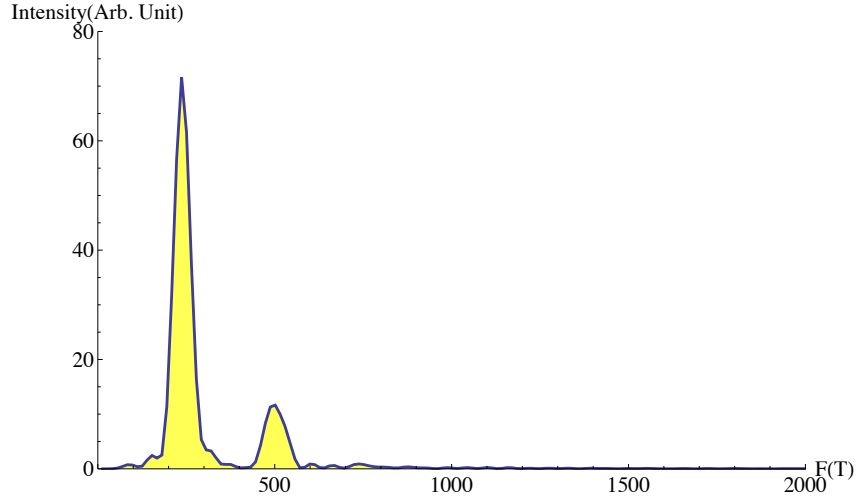


Figure 2.4: Fourier transform of the oscillation spectra after a background subtraction with a cubic polynomial. $W_0 = 0.71t$, $V_c = 0.05t$, $\mu = -0.78t$, $M = 30 a$, $N = 10^5 a$, $\ell_D = 8 a$, $g_V = 0.3t$. Doping is 11.73%.

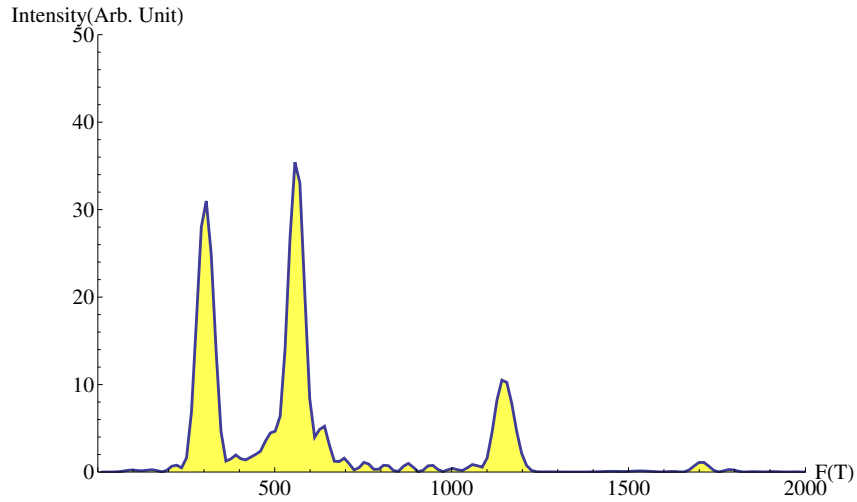


Figure 2.5: Fourier transform of the oscillation spectra after a background subtraction with a cubic polynomial. $W_0 = 0.65t$, $V_c = 0.05t$, $\mu = -0.83t$, $M = 30 a$, $N = 10^5 a$, $\ell_D = 8 a$, $g_V = 0.1t$. Doping is 12.46%.

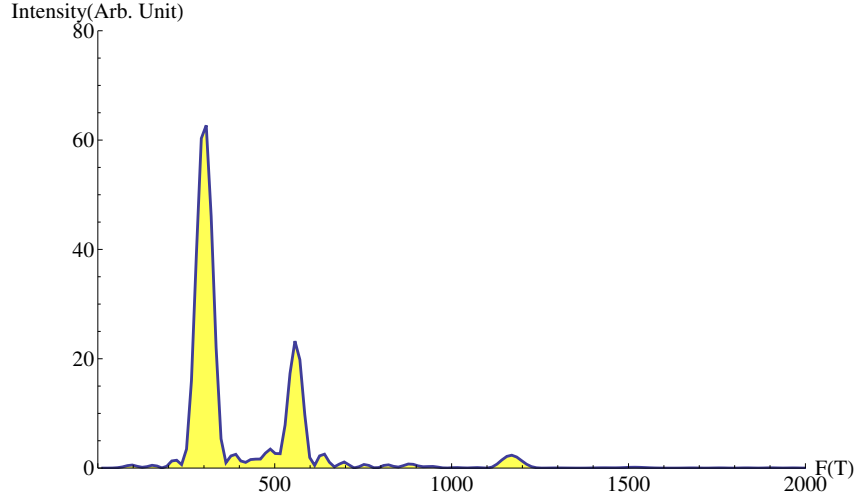


Figure 2.6: Fourier transform of the oscillation spectra after a background subtraction with a cubic polynomial. $W_0 = 0.65t$, $V_c = 0.05t$, $\mu = -0.83t$, $M = 30 a$, $N = 10^5 a$, $\ell_D = 8 a$, $g_V = 0.2t$. Doping is 12.46%.

us consider the quantum oscillation measurements that we have been discussing here.

- Are the applied magnetic fields sufficiently large to essentially destroy all traces of superconductivity and thereby reveal the underlying normal state from which superconductivity develops? Whereas for NCCO H_{c2} is less than 10T and the quantum oscillation measurements are carried out between 30 – 65T, far above H_{c2} , for YBCO lingering doubts remain. However, one may argue that the high field measurements are such that one may be in a vortex liquid state where the slower vortex degrees of freedom may simply act as quenched disorder to the nimble electrons. This is the picture we have adopted here. The effects of these slower vortex degrees of freedom on the quantum oscillations will be investigated in detail in the next Chapter 3.
- The emergent picture of Fermi pockets are seemingly at odds with ARPES, unless only half the pocket is visible in ARPES, as was previously argued [166]. On the other hand, reliable ARPES in YBCO is not available. For electron-doped NCCO the signature of pockets are quite strong [167].
- Quantum oscillations of R_H are easier to explain if there are at least two closed pockets in the Boltzmann picture [53]. Thus associated with the electron pocket

there must be a hole pocket or vice versa. This is not a problem with NCCO, as we have shown how magnetic breakdown [150], and a greater degree of intrinsic disorder, provides a simple resolution as to why only one pocket, in this case a small but prominent hole pocket is seen. In any case, oscillations of R_H in NCCO are yet to be measured. With respect to YBCO the apparent lack of two closed pockets becomes a serious problem. Any commensurate picture would lead to a hole pocket of frequency about twice that of the electron pocket frequency if the Luttinger sum rule is to be satisfied. Despite motivated effort no evidence in this regard has emerged. An escape from the dilemma discussed here is that the relevant electron pocket is accompanied by a much smaller hole pocket and some open orbits. To convincingly observe such small hole pockets, one would require extending these measurements to higher fields; see Ref. [153].

- All oscillation measurements to date have been convincingly interpreted in terms of the Lifshitz-Kosevich theory for which the validity of Fermi liquid theory and the associated Landau levels seem to be obligatory.
- The contrast between electron and hole doped cuprates is interesting. In NCCO the crystal structure consists of a single CuO plane per unit cell, and, in contrast to YBCO, there are no complicating chains, bilayers, ortho-II potential, stripes, etc. [167]. Thus, it would appear to be ideal for gleaning the mechanism of quantum oscillations. On the other hand, disorder in NCCO is significant. It is believed that well-ordered chain materials of YBCO contain much less disorder by comparison.
- In YBCO, studies involving tilted field seem to rule out triplet order parameter, hence SDW [155, 156]. Moreover, from NMR measurements at high fields, there appears to be no evidence of a static spin density wave order in YBCO [45]. Similarly there is no evidence of SDW order in fields as high as $23.2T$ in $\text{YBa}_2\text{Cu}_4\text{O}_8$ [168], whereas quantum oscillations are clearly observed in this material [144, 145]. Also no such evidence of SDW is found up to $44T$ in $\text{Bi}_2\text{Sr}_{2-x}\text{La}_x\text{CuO}_{6+\delta}$ [169]. Energetically a perturbation even as large as $45T$ field is weak [170].
- As to singlet order, relevant to quantum oscillations, [171, 172, 173] charge density wave is a possibility which has recently found some support in the high field NMR

measurements in YBCO [45]. But since the mechanism is helped by the oxygen chains, it is unlikely that the corresponding NMR measurements in NCCO will find such a charge order. Moreover, the observed charge order in YBCO sets in at a much lower temperature ($20 - 50K$) compared to the pseudogap. Thus the charge order may be secondary phenomenon because its scale is significantly different from the pseudogap scale, especially in the under doped regime. As to singlet DDW, there are two neutron scattering measurements that seem to provide evidence for it [174, 175]. However, these measurements have not been confirmed by further independent experiments. However, DDW order should be considerably hidden in NMR involving nuclei at high symmetry points, because the orbital currents should cancel.

As mentioned above, a mysterious feature of quantum oscillations in YBCO is the fact that only one type of Fermi pockets is observed. If two-fold commensurate density wave is the mechanism, this will violate the Luttinger sum rule [62, 176, 177, 53]. We had previously provided an explanation of this phenomenon in terms of disorder arising from both defects and vortex scattering in the vortex liquid phase [162]; however, the arguments are not unassailable. In contrast, for NCCO, the experimental results are quite consistent with a simple theory presented previously [150, 151]. The present work, based on incommensurate DDW, may provide another, if not a more plausible alternative in YBCO.

The basic question as to why Fermi liquid concepts should apply remains an important unsolved mystery [6]. It is possible that if the state revealed by applying a high magnetic field has a broken symmetry with an order parameter (hence a gap), the low energy excitations will be quasiparticle-like, not a spectra with a branch cut, as in variously proposed strange metal phases.

CHAPTER 3

Onsager rule, quantum oscillation frequencies, and the density of states in the mixed-vortex state of cuprates

3.1 Introduction

A breakthrough in the area of cuprate superconductivity is the observation of quantum oscillations in cuprates [7, 178]. In these experiments a strong magnetic field is applied to suppress the superconductivity, which most likely reveals the ground state [53] without superconductivity. However, the understanding of this “normal state” may be a crucial ingredient in the theory high temperature superconductivity. Standing in the way are at least two important issues: (1) Does the quantum oscillation frequencies substantially deviate from the classic Onsager rule for which the oscillation frequency $F = (\hbar c/2\pi e)A(\epsilon_F)$, where $A(\epsilon_F)$ is equal to the extremal Fermi surface area normal to the magnetic field? If so, it would lead to considerable uncertainty in the interpretation of the experiments. (2) Do the oscillations ride on top of a magnetic field dependence of the density of states(DOS) $\rho(B) \sim \sqrt{B}$? [165] If so, it might indicate the presence of superconducting fluctuations even in high magnetic fields at zero temperature, $T = 0$, from an extrapolation of a result of Volovik [179], which is supposed to be asymptotically true as $B \rightarrow 0$. Therefore high field behavior requires careful analyses. Quantum oscillations require the existence of Landau levels. If this is true, they might indicate the existence of normal Fermi liquid quasiparticles [6].

It has been argued from a theoretical analysis that the Onsager rule could be violated by as much as 30% [1]. We find that under reasonable set of parameters, to be defined below, the violation is miniscule, $\sim 10^{-4}$. Even for extreme situations discussed in Ref. [1],

it is less than 2%. If we are correct, one can use the Onsager rule to interpret the experiments with impunity. The second encouraging result is that $\rho(B)$ saturates in the regime where oscillations are present. We interpret this to mean that there are generically no superconducting fluctuations in high fields. A recent specific heat measurement [180] shows that the specific heat indeed saturates at high fields, signifying that the normal state is achieved.

To put our discussions in the context, note that in conventional s -wave superconductors, previous work has shown that for higher Landau level indices, and within coherent potential approximation, vortices mainly damp the oscillation amplitude, but the shift in the oscillation frequency [181, 182] is negligible; however, for d -wave underdoped cuprate superconductors with small coherence length and high fields with Landau level indices ~ 10 this calculation should not hold [1]. A more recent semi-classical analysis based on an ansatz of *gaussian phase fluctuations* of the d -wave pairing [74] indicates that the oscillation frequency is unchanged, as here. However, relatively undamped quantum oscillations riding on top of \sqrt{H} was found in this dynamic Gaussian ansatz that does not account for vortices, which must necessarily be present, as in Ref. [1], and the branch cuts introduced by the vortices must also be taken into account.

We consider the vortices explicitly in the Bogoliubov-de Gennes (BdG) Hamiltonian, as in Ref. [1], and model the vortex liquid state as quenched, randomly distributed vortices, paying special attention to branch cuts. There are other important differences as well, as we shall discuss below. To have a complete picture, we also consider the low field regime where the quantum oscillations disappear. In this regime the vortices arrange themselves into a vortex solid state and should be modeled as an ordered lattice instead. We compute the DOS of such vortex lattices explicitly and find that $\rho(B) \propto \sqrt{B}$ in the asymptotically low field limit, consistent with Volovik's semiclassical analysis [179].

In Section 3.2 we define the model Hamiltonian that includes d -wave superconducting order parameter as well as a variety of density wave states. Our numerical method, the recursive Green function method adapted for the present problem is discussed in Section 3.3. The results are discussed in Section 3.4 and Section 3.5 contains discussion. Appendices are included in Chapter A.

3.2 The Model Hamiltonians

The starting point is the Bogoliubov-de Gennes (BdG) Hamiltonian

$$\mathcal{H} = \begin{pmatrix} H - \mu & \Delta_{ij} \\ \Delta_{ij}^\dagger & -H + \mu \end{pmatrix} \quad (3.1)$$

defined on a square lattice. Here μ is the chemical potential. H is the Hamiltonian that describes the normal state electrons; while the off-diagonal pairing term Δ_{ij} defines the superconducting order parameter. For simplicity, we ignore self consistency, as we believe that it cannot change the major striking conclusions.

3.2.1 The diagonal component H

Besides the hopping parameters, the normal state Hamiltonian H contains a variety of mean field order parameters defined below. Although many different orders are suggested to explain the normal state of the high- T_c superconductivity, for our purposes it is sufficient to consider three different types: a period-2 d -density wave (DDW) [63, 6, 183], a bi-directional charge density wave (CDW), and a period-8 DDW model [183]. We believe that our major conclusions in this Chapter 3 do not depend on the nature of the density wave that is responsible for Fermi surface reconstruction. The DDW is argued to be able to account for many features of quantum oscillations, as well as the pseudogap state [184, 185] in the cuprates. Among the many different versions of density waves of higher angular momentum [9], the simplest period-2 singlet DDW, also the same as staggered flux state in Ref. [1], and also a period-8 DDW order, proposed by us previously to explain quantum oscillations[183], have been chosen here for illustration.

Recently a bi-directional CDW has been observed ubiquitously in the underdoped cuprates [45, 46, 47, 48, 49]. It has ordering wavevectors $\mathbf{Q}_1 \approx \frac{2\pi}{a}(0.31, 0)$ and $\mathbf{Q}_2 \approx \frac{2\pi}{a}(0, 0.31)$, which are incommensurate. This order has also been used to explain the Fermi surface reconstructions and quantum oscillation experiments [186, 64], although a recent numerical work [187] has demonstrated that the strict incommensurability of the CDW can destroy *strict* quantum oscillations completely. For the purpose of illustration we chose, instead, commensurate vectors $\mathbf{Q}_1 = \frac{2\pi}{a}(\frac{1}{3}, 0)$ and $\mathbf{Q}_2 = \frac{2\pi}{a}(0, \frac{1}{3})$.

Therefore without the magnetic field, B , H is given by

$$\begin{aligned}
H &= -t \sum_{\langle i,j \rangle} c_{\mathbf{r}_i}^\dagger c_{\mathbf{r}_j} + t' \sum_{\langle\langle i,j \rangle\rangle} c_{\mathbf{r}_i}^\dagger c_{\mathbf{r}_j} \\
&\quad - t'' \sum_{\langle\langle\langle i,j \rangle\rangle\rangle} c_{\mathbf{r}_i}^\dagger c_{\mathbf{r}_j} + \text{h.c.} + H_{\text{d.w.}},
\end{aligned} \tag{3.2}$$

where t, t' , and t'' are the 1st, 2nd and the 3rd nearest neighbor hopping parameters respectively. $H_{\text{d.w.}}$ is various density wave orders specified below. The external uniform magnetic field $\mathbf{B} = B\hat{z}$ is included into H via the Peierls substitution: $c_{\mathbf{r}_i}^\dagger c_{\mathbf{r}_j} \Rightarrow \exp[-i\frac{e}{\hbar c} \int_{\mathbf{r}_j}^{\mathbf{r}_i} \mathbf{A} \cdot d\mathbf{l}] c_{\mathbf{r}_i}^\dagger c_{\mathbf{r}_j}$ with the vector potential $\mathbf{A} = Bx\hat{y}$ chosen, for simplicity, in the Landau gauge.

1. Two-fold DDW order

$$H_{\text{d.w.}} = \sum_{\mathbf{r}_i, \delta} i \frac{W_0}{4} (-1)^{x_i + y_i} \eta_\delta c_{\mathbf{r}_i + \delta}^\dagger c_{\mathbf{r}_i}, \tag{3.3}$$

where $\delta = \hat{x}, \hat{y}$ denote the two nearest neighbors. $\eta_\delta = 1$ for $\delta = \hat{x}$ while $\eta_\delta = -1$ for $\delta = \hat{y}$ indicates the DDW order has a local d -wave symmetry.

2. Bi-directional CDW order

$$\begin{aligned}
H_{\text{d.w.}} &= V_c \sum_{\mathbf{r}_i, \delta} \eta_\delta \{ \cos[\mathbf{Q}_1 \cdot (\mathbf{r}_i + \delta/2)] \\
&\quad + \cos[\mathbf{Q}_2 \cdot (\mathbf{r}_i + \delta/2)] \} c_{\mathbf{r}_i + \delta}^\dagger c_{\mathbf{r}_i}.
\end{aligned} \tag{3.4}$$

Again $\eta_\delta = \pm 1$ is the local d -wave symmetry factor of the CDW order.

3. Period-8 DDW order

$$H_{\text{d.w.}} = \sum_{\mathbf{k}} iG_k c_{\mathbf{k}}^\dagger c_{\mathbf{k}+\mathbf{Q}} + V_c c_{\mathbf{k}}^\dagger c_{\mathbf{k}+2\mathbf{Q}} + \text{h.c.} . \tag{3.5}$$

where the iG_k term is the period-8 DDW order

$$\langle c_{\mathbf{k}'}^\dagger c_{\mathbf{k}} \rangle = iG_{\mathbf{k}} \delta_{\mathbf{k}', \mathbf{k}+\mathbf{Q}} - iG_{\mathbf{k}'} \delta_{\mathbf{k}, \mathbf{k}'+\mathbf{Q}} \tag{3.6}$$

Here $G_{\mathbf{k}} = (W_{\mathbf{k}} - W_{\mathbf{k}+\mathbf{Q}})/2$ with the DDW gap $W_{\mathbf{k}} = \frac{W_0}{2} (\cos k_x - \cos k_y)$, and the ordering wavevector is $\mathbf{Q} = (\frac{3\pi}{4a}, \frac{\pi}{a})$. The V_c term in Eq. (3.5) represents a period-4 unidirectional CDW with an ordering wavevector $2\mathbf{Q}$, which is consistent with the symmetry of the period-8 DDW order. Notice that this CDW is different from the

bi-directional CDW we considered in the previous section. Experimentally whether the observed CDW in cuprates is unidirectional or bi-directional is still not fully resolved.

Fourier transformed to the real space, the Hamiltonian $H_{\text{d.w.}}$ becomes

$$\begin{aligned}
H_{\text{d.w.}} = & \sum_{\mathbf{r}, \mathbf{r}'} i \frac{W_0}{2} \sin \frac{\mathbf{Q} \cdot (\mathbf{r} - \mathbf{r}')}{2} \sin \frac{\mathbf{Q} \cdot (\mathbf{r} + \mathbf{r}')}{2} \\
& \times \{ \delta_{\mathbf{r}, \mathbf{r}' + a\hat{x}} + \delta_{\mathbf{r}, \mathbf{r}' - a\hat{x}} - \delta_{\mathbf{r}, \mathbf{r}' + a\hat{y}} - \delta_{\mathbf{r}, \mathbf{r}' - a\hat{y}} \} c_{\mathbf{r}}^\dagger c_{\mathbf{r}'} \\
& + 2V_c \sum_{\mathbf{r}} \cos[2\mathbf{Q} \cdot \mathbf{r}] c_{\mathbf{r}}^\dagger c_{\mathbf{r}}.
\end{aligned} \tag{3.7}$$

On the right hand side the first term gives the period-8 DDW order in real space, of which the physical meaning of each factor has already been discussed in Section 1.1.3.3 of Chapter 1; while the second term is the $2\mathbf{Q}$ charge modulation. Note that this CDW is defined on sites, differing from the bi-directional CDW defined on bonds.

3.2.2 The off-diagonal component Δ_{ij}

The off-diagonal pairing term Δ_{ij} in the BdG Hamiltonian is defined on each bond connecting two nearest neighboring sites i and j . $\Delta_{ij} = |\Delta_{ij}| e^{i\theta_{ij}} \eta_{ij}$, where $\eta_{ij} = +1$ if the bond is along x -direction and $\eta_{ij} = -1$ if it is along y -direction so that Δ_{ij} has a local d -wave symmetry. The pairing amplitude is taken to be

$$|\Delta_{ij}| = \Delta \frac{r_{\text{eff}}}{\sqrt{r_{\text{eff}}^2 + \xi^2}} \tag{3.8}$$

where Δ is the pairing amplitude far away from any vortex center. ξ is the vortex core size. In our calculation $\xi = 5a$ is adopted, where a is the lattice spacing. In the presence of a single vortex, r_{eff} in the above is simply the distance from the center of our bond $\frac{\mathbf{r}_i + \mathbf{r}_j}{2}$ to the center of that vortex. While in the presence of multiple vortices, following the ansatz used in Ref. [1] we choose $(\frac{\xi}{r_{\text{eff}}})^q = \sum_n (\frac{\xi}{r_n})^q$ where r_n is the distance from the bond center to the n th vortex center and $q > 0$ is some real number.

In this ansatz, r_{eff} is a monotonic increasing function of the parameter q for a given vortex configuration. Therefore if q is large, the calculated r_{eff} as well as $|\Delta_{ij}|$ is also larger, which means the vortex scattering is stronger. However our conclusions do not

depend on the different choices of q (for more details see the Appendix A.3). Therefore in this Chapter 3, if not specified otherwise, $q = 2$ will be chosen.

The bond phase variable θ_{ij} contains the information of our quenched random vortex configuration, but for the purpose of our calculation we need the site phase variables. We use the ansatz for θ_{ij} given in Refs. [188, 189, 190]

$$e^{i\theta_{ij}} = e^{i\frac{\phi_i + \phi_j}{2}} \text{sgn}\left[\cos\frac{\phi_i - \phi_j}{2}\right] \quad (3.9)$$

where ϕ_i is the pairing order parameter phase field defined on a site. In the above, without the “sgn[...]” factor θ_{ij} is simply the arithmetic mean of ϕ_i and ϕ_j . However using $\theta_{ij} = \frac{\phi_i + \phi_j}{2}$ is not enough because whenever the bond \overline{ij} crosses a vortex branch cut, the phase factor $e^{i\theta_{ij}}$ will be incorrect and different from the correct one by a minus sign. This can be corrected by the additional “sgn[...]” factor (see the Appendix A.2).

Then ϕ_i can be further computed from the superfluid velocity field $\mathbf{v}_s(\mathbf{r}_i)$ by

$$\phi_i - \phi_0 = \int_{\mathbf{r}_0}^{\mathbf{r}_i} \left[\frac{m^* \mathbf{v}_s(\mathbf{r})}{\hbar} + \frac{e^*}{\hbar c} \mathbf{A}(\mathbf{r}) \right] \cdot d\mathbf{l} \quad (3.10)$$

with $m^* = 2m$ and $e^* = -2e$ are the mass and the charge of the Cooper pairs respectively. The path for this integral is chosen such as to avoid the branch cuts of all the vortices so that the phase field ϕ_i is single valued on every site, as illustrated in Fig. 3.1.

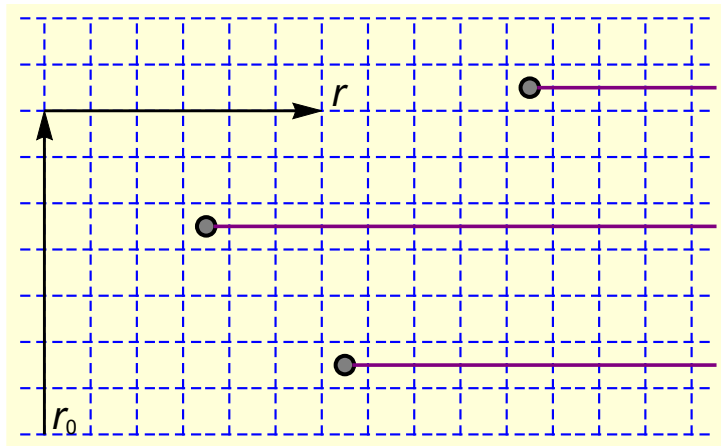


Figure 3.1: Illustrations of the vortices (circle) on the lattice (dashed lines). The arrows show the path of the integral we have chosen in defining our phase field $\phi(\mathbf{r})$. To make this phase definite, the branch cuts of all the vortices are chosen to extend from the vortex center to the positive infinity ($x = \infty$), represented by the magenta horizontal lines.

We still need to compute the superfluid velocity $\mathbf{v}_s(\mathbf{r})$. This can be done by following Ref. [73]

$$m\mathbf{v}_s(\mathbf{r}) = -i\pi\hbar \int \frac{d^2k}{(2\pi)^2} \frac{\mathbf{k} \times \hat{z}}{k^2 + \lambda^{-2}} \sum_n e^{i\mathbf{k}\cdot(\mathbf{r}-\mathbf{R}_n)}, \quad (3.11)$$

where m is the electron mass, λ is the penetration depth, and \mathbf{R}_n gives the n th random vortex position. In this integrand, because $\mathbf{k} \times \hat{z}$ is odd in \mathbf{k} , only the imaginary part of $e^{i\mathbf{k}\cdot(\mathbf{r}-\mathbf{R}_n)}$ will survive after the integration, so the whole expression on the right hand side becomes real. We also make an approximation $\lambda = \infty$ so that we can ignore the λ^{-2} term in the denominator. This is equivalent to replacing the magnetic field $\mathbf{B}(\mathbf{r})$ by its spatial average, which is equal to the external magnetic field $\mathbf{B} = B\hat{z}$. It is a good approximation when $B \gg H_{c1}$, where H_{c1} is the lower critical field. This condition is well satisfied in the quantum oscillation experiments of cuprates. Also this approximation is consistent with our initial choice of the vector potential $\mathbf{A} = Bx\hat{y}$, given completely by the applied external field \mathbf{B} .

For our square lattice calculation we discretize the above \mathbf{k} integral and choose $2\pi/\xi$ as its upper cutoff, since the vortex is only well defined over a length scale larger than the vortex core size ξ . Therefore in the limit $\lambda \gg \xi > a$, $\mathbf{v}_s(\mathbf{r})$ can be rewritten as follows

$$m\mathbf{v}_s(\mathbf{r}) = \frac{\pi\hbar}{LMa^2} \sum'_{(k_x, k_y)} \frac{\mathbf{k} \times \hat{z}}{k^2} \sum_n \sin[\mathbf{k} \cdot (\mathbf{r} - \mathbf{R}_n)]. \quad (3.12)$$

In this summation $k_x = -\frac{2\pi}{\xi}, -\frac{2\pi}{\xi} + \frac{2\pi}{La}, \dots, \frac{2\pi}{\xi} - \frac{2\pi}{La}, \frac{2\pi}{\xi}$, $k_y = -\frac{2\pi}{\xi}, -\frac{2\pi}{\xi} + \frac{2\pi}{Ma}, \dots, \frac{2\pi}{\xi} - \frac{2\pi}{Ma}, \frac{2\pi}{\xi}$. The prime superscript in the summation means the point $(k_x, k_y) = (0, 0)$ is excluded to be consistent with our approximation $\lambda = \infty$.

3.3 The recursive Green function

Given the BdG Hamiltonian \mathcal{H} defined above, we use the recursive Green's function method [191] to compute the local DOS(LDOS). We attach our central system, which has a lattice size $L \times M$, to two semi-infinite leads in the $\pm x$ directions. The leads are normal metals described by t, t', t'' only. Then we can compute the retarded Green's function $G_i(j, j'; E + i\delta)$ at an energy E for the i th principal layer (see the Appendix A.1). Here each i th principal layer contains two adjacent columns of the original square lattice

sites. So there are $L/2$ principal layers and each of them contains $2M$ number of sites. Therefore $G_i(j, j'; E + i\delta)$ is a $4M \times 4M$ matrix, with $j, j' = 1, 2, \dots, 4M$, because it has both an electron part and a hole part. In calculating the LDOS at the j th site of the i th layer only the imaginary part of the j th diagonal element in the electron part of G_i is included. This is equivalent to treating the random vortices as some off-diagonal scattering centers for the normal state electrons. To see smooth oscillations of the DOS we also average the calculated LDOS over different sites and realizations of uncorrelated vortices. In other words the quantity of our central interest is

$$\rho(B) = \left\langle \frac{1}{LM} \sum_{i=1}^{L/2} \sum_{j=1}^{2M} \left(-\frac{1}{\pi}\right) \text{Im} G_i(j, j; 0 + i\delta) \right\rangle, \quad (3.13)$$

where the angular brackets denote average over independent vortex realizations. In the Green's function we have already set the energy to the chemical potential $E = 0$. For all the numerical results presented in the following, an infinitesimal energy broadening $\delta = 0.005t$ will be chosen, if not specified otherwise, and the periodic boundary condition is imposed in the y -direction.

3.4 Results

3.4.1 The Onsager rule for quantum oscillation frequencies

3.4.1.1 The two-fold DDW order case

With the parameters: $t = 1, t' = 0.30t, t'' = t'/9.0, \mu = -0.8807t, W_0 = 0.26t, V_c = 0$, the hole doping level is $p \approx 11\%$. Without vortices we can diagonalize the Hamiltonian H in the momentum space and obtain the normal state Fermi surface. This Fermi surface consists of two closed orbits, see the inset of Fig. 3.2a. The bigger one centered around the node point $(\frac{\pi}{2}, \frac{\pi}{2})$ is hole like. It has an area $\frac{A_h}{(2\pi/a)^2} \approx 3.47\%$. This corresponds to an oscillation frequency $F_h = \frac{A_h}{(2\pi/a)^2} \frac{2\Phi_s}{a^2} = 966\text{T}$ from the Onsager relation, where $\Phi_s = hc/2e$ is the fundamental flux quanta and the two lattice spacings $a^2 = 3.82\text{\AA} \times 3.89\text{\AA}$ are chosen for YBCO. At the antinodal point $(0, \pi)$ there is an electron pocket with an area $\frac{A_e}{(2\pi/a)^2} \approx 1.9\%$, corresponding to a frequency $F_e = 525\text{T}$ (electron). We should notice that the fast oscillation F_h (hole) is not observed in the experiments in cuprates. This problem can be resolved if we consider a period-8 DDW model [183]; see below.

We compute the $\rho(B)$ as a function of the inverse of the magnetic field $1/B$ in the presence of various Δ . In these calculations, the number of vortices are chosen such that the total magnetic flux is equal to $\Phi = BLMa^2$. From the oscillatory part of $\rho(B)$ we perform Fast Fourier Transform(FFT) to get the spectrum. The result is shown in Fig. 3.2b. In this spectrum the two oscillation frequency $F_e = 525\text{T}$ and $F_h = 966\text{T}$ calculated from the normal state Fermi surface areas via the Onsager relation are also shown by the two vertical dashed lines. We see clearly that as we increase Δ the oscillation amplitudes are damped. However, remarkably, the oscillation frequencies remain the same within numerical errors. Thus, even in the presence of vortices, the Onsager rule still holds to an excellent approximation.

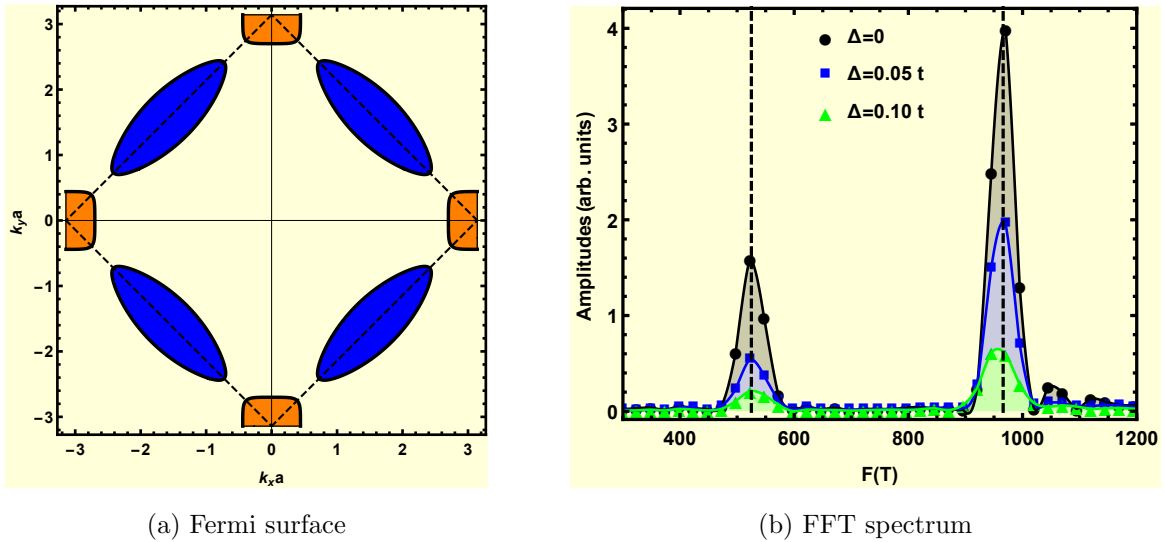


Figure 3.2: Plots of the Fermi surface(FS) and Fast Fourier transform(FFT) spectrum for the two-fold DDW order case. The two vertical dashed lines in the subfig (b) denote the two fundamental oscillation frequencies calculated from the Fermi surface area via the Onsager relation. They are $F_e = 525\text{T}$, $F_h = 966\text{T}$. Other parameters used are $L = 1000$, $M = 100$, $\delta = 0.005t$.

3.4.1.2 The bi-directional CDW order case

We choose the following parameters: $t = 1$, $t' = 0.2t$, $t'' = t'/8$, $V_c = 0.12t$, $\mu = -0.73t$ so that we can produce the right oscillation frequencies that are observed in experiments. The hole doping level is $p \approx 11\%$. The Fermi surface of the normal state is plotted in the inset of Fig. 3.3a (open orbits are not shown for clarity). There are two closed Fermi

surface sheets. Centered around the point $(\frac{\pi}{3}, \frac{\pi}{3})$ and other symmetry related positions there are diamond shaped electron pockets, highlighted in orange. This pocket has an area $\frac{A_e}{(2\pi/a)^2} = 1.9\%$. It corresponds to a frequency $F_e = 529\text{T}$ from the Onsager relation. Besides this electron pocket, there is an oval shaped hole pocket centered around $(\frac{\pi}{3}, \frac{2\pi}{3})$, highlighted in blue. The area of this hole pocket is $\frac{A_h}{(2\pi/a)^2} = 0.33\%$. This corresponds to an oscillation frequency $F_h = 92\text{T}$.

The oscillation spectrum of the $\rho(B)$ is shown in Fig. 3.3b. From the spectrum we see that when the vortex scattering is absent, $\Delta = 0$, the oscillation amplitudes peak at the two frequencies F_e, F_h , as denoted by the two vertical dashed lines. These results agree with our Fermi surface calculation, as we expected. When the vortices are included the oscillation amplitude is gradually damped as the vortex scattering strength is increased by increasing Δ . However whenever the oscillation frequency can be clearly resolved, we see that their positions do not change with Δ . Again this means that the Onsager rule survives in the presence of vortex scattering.

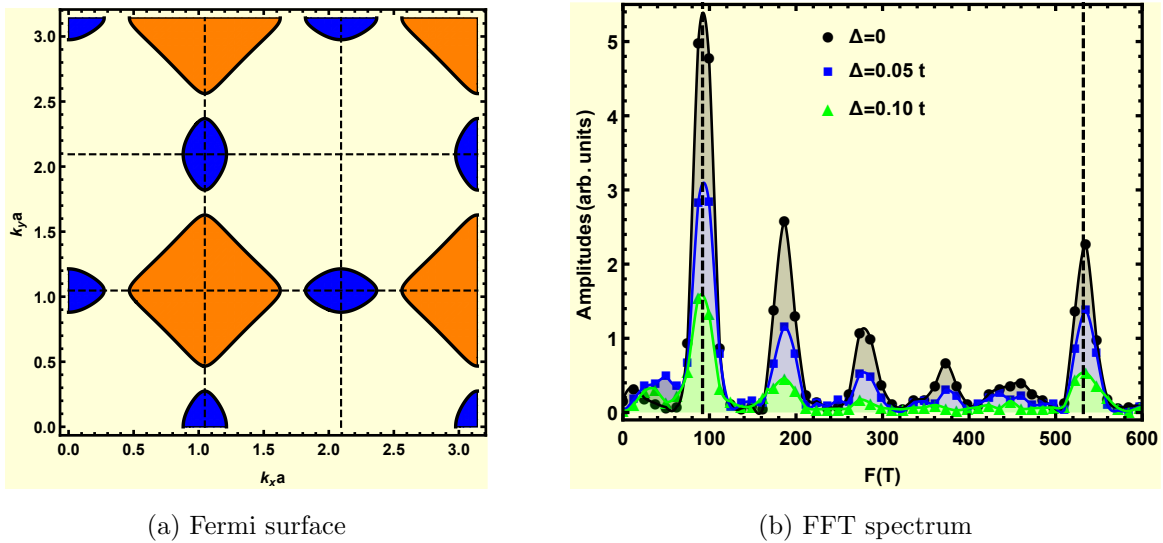


Figure 3.3: Plots of the Fermi surface and Fast Fourier transform spectrum for the bi-directional CDW order. The two fundamental oscillation frequencies calculated from the Fermi surface area via the Onsager relation are $F_e = 529\text{T}$, $F_h = 92\text{T}$. Other parameters used are $L = 1000$, $M = 102$, $\delta = 0.005t$.

3.4.1.3 The period-8 DDW order case

In this subsection we present our quantum oscillation results for the period-8 DDW model. In this model the period-8 stripe DDW order is considered as the major driving force behind the Fermi surface reconstructions; while a much weaker unidirectional period-4 CDW is included as a subsidiary order.

We choose the parameter set $t' = 0.3t$, $t'' = t'/2.0$, $W_0 = 0.70t$, $V_c = 0.05t$, $\mu = -0.70t$ and estimate the hole doping level to be $p \approx 11.2\%$. We also obtain a Fermi surface similar to the one we had in Ref.[183]. It has a large pocket of electron like with a frequency $F_e = 523\text{T}$, a smaller pocket of hole like with a frequency $F_h = 159\text{T}$, and also some open orbits which do not contribute to quantum oscillations.

The corresponding oscillation spectrum is presented in Fig. 3.4b, where we see the oscillation amplitude decreases as we increase Δ , however, the frequencies do not change with Δ . In other words the presence of vortex scattering does not alter the oscillation frequencies.

The observations here, combined with the other two cases, strongly suggest that the Onsager's relation being intact in the presence of vortex scattering is generic and independent of the order parameters that reconstruct the Fermi surface.

3.4.2 The Density of states at high fields

In the above we have examined the effects of random vortex scattering on the quantum oscillations. Now we give an overview of the B dependence of the DOS for fields $B \gtrsim 10\text{T}$, at a representative value of $\Delta = 0.1t$. At lower fields, the vortex liquid model is not valid any more, since vortices should order into a solid instead. Therefore we should use a vortex lattice to model such a state. In the following we focus on the high field regime first and defer our vortex lattice discussions for the low field regime to the later Section 3.4.3.

3.4.2.1 The period-2 DDW order case

In Fig. 3.5 we plot $\rho(B)/\rho_n(0)$ as a function of the field B for the two-fold DDW order case, where $\rho_n(0)$ is the normal state DOS at zero field. In the following, the normal

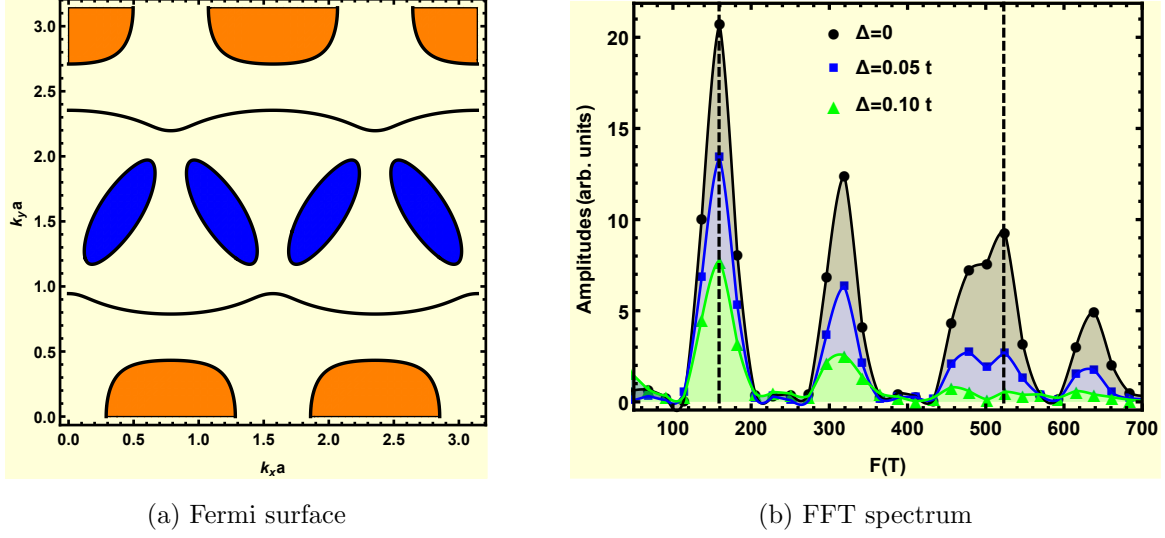


Figure 3.4: Plots of the Fermi surface and Fast Fourier transform spectrum for the period-8 DDW order. The two fundamental oscillation frequencies calculated from the Fermi surface area via the Onsager relation are $F_e = 523T$, $F_h = 159T$. There are also other oscillation peaks in the spectrum, which are higher order harmonics of the two frequencies F_e and F_h . They do not represent new pieces of Fermi surface. Other parameters used are $L = 1000$, $M = 200$, $\delta = 0.002t$.

state should be understood as a state, which does not have any superconductivity but can have a particle-hole density wave order. And all the DOS value calculated is for one electron in a single CuO plane, without including the spin degeneracy. From Fig. 3.5 we see that as B decreases, the DOS oscillation gets suppressed gradually. This is because the orbital quantization of electrons becomes dominated by the vortex scattering.

A noticeable feature of this plot is that when the field becomes large, the oscillation of $\rho(B)$ in $1/B$ gradually develops on top of a constant background. This constant background of $\rho(B)$ is different from the previous results obtained in Fig. 3(b) of the Ref. [74] in the absence of vortices. We notice that this constant background value of $\rho(B)$ is still suppressed from the normal state DOS $\rho_n(0)$. Recall that $\rho_n(0)$ is calculated for a state at $B = 0$ with the density wave order but without any superconductivity. Presumably this suppression is due to the remaining superconductivity fluctuations which are not completely killed by the applied magnetic field considered here. We expect this suppression to vanish when the field becomes high enough. The size of this suppression depends on the superconductivity order parameter Δ value. For the parameters used in

Fig. 3.5 it is $\sim 15\%$.

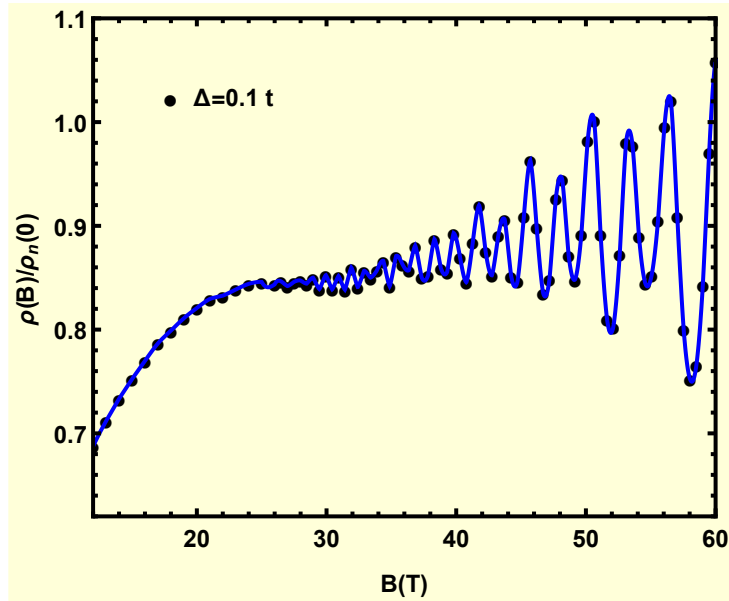


Figure 3.5: The DOS $\rho(B)$, normalized to the normal state DOS $\rho_n(0)$ at zero field $B = 0$ for the two-fold DDW order. The estimated values of the normal state DOS is $\rho_n(0) \approx 0.23$ states/ t , where t is the nearest neighboring hopping. The data is averaged over 108 different vortices configuration realizations.

3.4.2.2 The bi-directional CDW order case

The constant background of the DOS oscillation is not restricted to the two-fold DDW order case. As we can see in Fig. 3.6, for the bi-directional CDW order, the $\rho(B)$ oscillation background is again a constant at high fields.

3.4.2.3 The period-8 DDW order case

We also confirm this constant $\rho(B)$ background feature in the oscillation regime for the period-8 DDW order case in Fig. 3.7.

Therefore we can conclude that the high field $\rho(B)$ oscillation background being a constant is generic.

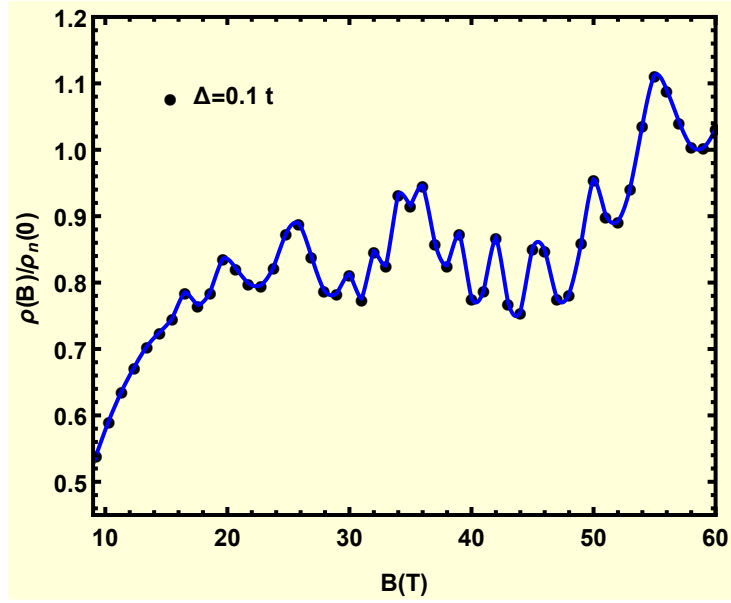


Figure 3.6: The DOS $\rho(B)$, normalized to the normal state DOS $\rho_n(0)$ at zero field $B = 0$ for the bi-directional CDW order. The estimated values of the normal state DOS is $\rho_n(0) \approx 0.25$ states/ t . The data is averaged over 120 different vortices configuration.

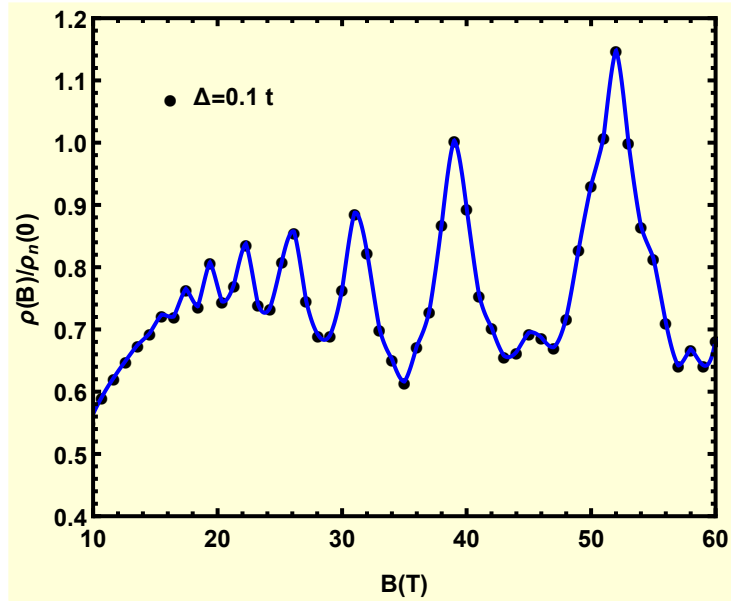


Figure 3.7: The DOS $\rho(B)$, normalized to the normal state DOS $\rho_n(0)$ at zero field $B = 0$ for the period-8 DDW order. The estimated values of the normal state DOS is $\rho_n(0) \approx 0.18$ states/ t . The data is averaged over 40 different vortices configuration.

3.4.3 Vortex solid at low fields

Now we move on to the low field regime. In this regime when the field is low enough, the vortices order into a lattice. Whether the lattice is square or triangular requires a self-consistent computation of the system's free energy, which is far beyond the scope of this thesis. Instead we simply take a square lattice for illustration. But none of the following qualitative features should depend on the vortex lattice type.

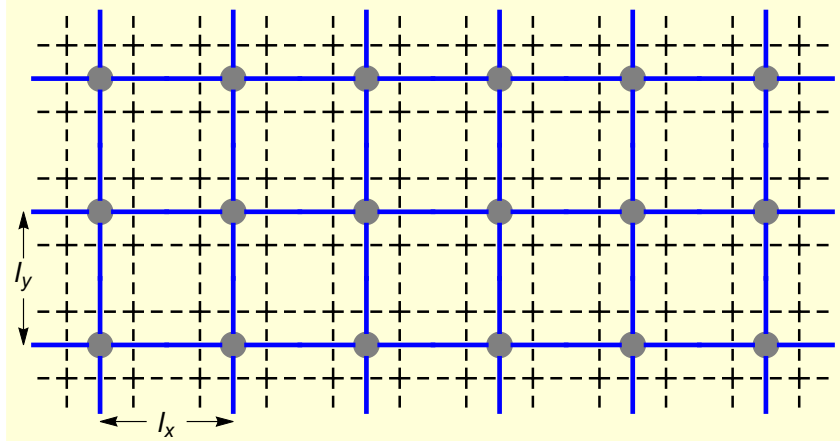


Figure 3.8: Schematic diagram of a square vortex lattice. The dashed lines represent the original CuO lattice; while the full lines stand for the vortex lattice, with each vortex, represented by the grey disks, sitting at the CuO plaquette center. And (l_x, l_y) are the vortex lattice spacings, in units of the original CuO square lattice spacing a .

3.4.3.1 Implementation of the square vortex lattice

To put the square vortex lattice onto our original CuO lattice so that each vortex sits at the CuO lattice plaquette center and the periodic boundary condition is still preserved along the transverse direction, we require the vortex lattice to be commensurate with our original CuO lattice, as schematically shown in Fig. 3.8. Namely, if the vortex lattice spacings are (l_x, l_y) , and the corresponding vortex lattice size is (N_x, N_y) , we require that the original CuO lattice size (L, M) satisfies $L = N_x l_x, M = N_y l_y$. For a particular value of (L, M) , this restricts the possible values of (l_x, l_y) and also the possible values of the magnetic field, because the vortex lattice spacings (l_x, l_y) are connected to the magnetic flux density via $B = \Phi_s / (l_x l_y a^2)$, where $\Phi_s = hc/2e$ is the fundamental flux quanta. In our following calculation we pick a particular value of the system size (L, M) , find all

the possible compatible values of the vortex lattice spacings $l_x = l_y$, and then for each of them calculate the magnetic field B as well as the corresponding DOS.

However, we should calculate the DOS of the Bogoliubov quasiparticles instead of the electrons, because the system is far from being in a normal state in such a low field regime. Therefore now $\rho(B)$ is computed from the following formula instead

$$\rho(B) = \frac{1}{2} \frac{1}{LM} \sum_{i=1}^{L/2} \sum_{j=1}^{4M} \left(-\frac{1}{\pi}\right) \text{Im} G_i(j, j; 0 + i\delta). \quad (3.14)$$

The major differences here from the one we used in our quantum oscillation calculations are: (1) the summation of the Green's function's diagonal matrix elements includes both the electron part and the hole part: j runs from $j = 1$ to $j = 4M$ instead of $j = 2M$; (2) there is no averaging over different vortices configurations because the vortex lattice is ordered; (3) an additional prefactor of $1/2$ is added to avoid double counting of degrees of freedoms.

For such a vortex lattice calculation, the summation over different vortex positions in the superfluid velocity calculation in Eq. (3.12) can be done exactly by using

$$\sum_n e^{i\mathbf{k}(\mathbf{r}-\mathbf{R}_n)} = N_x N_y \sum_{(n_1, n_2)} e^{i\mathbf{G}_{n_1, n_2} \cdot \mathbf{r}}, \quad (3.15)$$

where $\mathbf{G}_{n_1, n_2} = \left(\frac{2n_1\pi}{l_x a}, \frac{2n_2\pi}{l_y a}\right)$ is a reciprocal Bragg vector of the square vortex lattice, with $n_1, n_2 \in \mathbb{Z}$. Then the Eq. (3.12) of \mathbf{v}_s becomes

$$m\mathbf{v}_s = \pi\hbar \frac{1}{l_x l_y a^2} \sum_{(n_1, n_2)}' \frac{\mathbf{G}_{n_1, n_2} \times \hat{z}}{|\mathbf{G}_{n_1, n_2}|^2} \sin[\mathbf{G}_{n_1, n_2} \cdot \mathbf{r}] \quad (3.16)$$

The summations of (n_1, n_2) are restricted to those values that satisfy $0 \leq \frac{2n_1\pi}{l_x a} < \frac{2\pi}{a}$, $0 \leq \frac{2n_2\pi}{l_y a} < \frac{2\pi}{a}$. Again the prime superscript in the summation means the point $(n_1, n_2) = (0, 0)$ is excluded.

3.4.3.2 DOS numerical results

According to Volovik [179], for a $d_{x^2-y^2}$ -wave vortex, the major contribution to the low energy DOS comes from the extended states along the nodal direction. In his semiclassical analysis this contribution is computed from the Doppler shift of the quasiparticle energy. The conclusion is that the DOS for a single vortex is $\rho(B) \propto 1/\sqrt{B}$. In the limit

that the number of vortices is proportional to B , which is not valid if B is near the lower critical field H_{c1} , multiplying it by the number of vortices gives $\rho(B) \propto \sqrt{B}$. Extrapolating this result to the high field regime and using the fact that near the upper critical field H_{c2} , $\rho(B)$ should roughly recover the normal state DOS $\rho_n(0)$, he concluded that $\rho(B)/\rho_n(0) = \kappa\sqrt{B/H_{c2}}$, with κ some constant of order unity. This type of analysis is applicable only in the small field limit in the sense that $B \ll H_{c2}$ so that each vortex is far apart from any others. This is exactly the field regime where the vortex solid state develops. In the following we compute the DOS for a d -wave vortex lattice, for the cases both with and without an additional particle-hole density wave order, and test them against Volovik's results. For our following comparisons we slightly rewrite the above field dependence of $\rho(B)$ as follows

$$\frac{\rho(B)}{\rho_n(0)} = \kappa \frac{\sqrt{B}}{\sqrt{H_{c2}}} = \kappa \sqrt{\frac{2\pi\xi^2}{\Phi_s}} \sqrt{B} \approx 0.1\kappa\sqrt{B}, \quad (3.17)$$

where $\frac{\Phi_s}{2\pi\xi^2} \approx 90\text{T}$, if $\xi = 5a$ and $a \approx 3.83\text{\AA}$ are used.

1. First we consider a square vortex lattice without any other additional density wave order. We choose the band structure parameters to be $t'/t = 0.3$, $t'' = t'/9.0$, $\mu = -1.01t$ so that the estimated normal state hole doping level $p \approx 15\%$ is at the optimal doping. The computed DOS is shown in Fig. 3.9. At low enough fields, all the data points follow the $\rho(B)/\rho_n(0) = 0.3\sqrt{B}$ line, although there is some small scatter in the data, which comes from the finite size effects of our vortex lattice. This $0.3\sqrt{B}$ corresponds to $\kappa \approx 3$ in Eq. (3.17). To make a comparison with the specific heat measurements on YBCO123 at the optimal doping [192], we estimate the field dependent electronic specific heat $\gamma(B)$ from our DOS $\rho(B)$ as follows

$$\frac{\gamma(B)}{\gamma_n} = \frac{\rho(B)}{\rho_n(0)} \approx 0.1\kappa\sqrt{B}. \quad (3.18)$$

The normal state specific heat can be estimated as $\gamma_n = 4 \frac{\pi^2}{3} k_B^2 \rho_n(0)$. Here the additional prefactor of 4 comes from the spin degeneracy and the fact that one unit cell of YBCO123 contains two CuO planes. If we take $t = 0.15\text{eV}$, then $\gamma_n \approx 15.7\text{mJ/mol} \cdot \text{K}^2$ and $\gamma(B) = A\sqrt{B}$ with the coefficient $A \approx 4.7\text{mJ/mol} \cdot \text{K}^2 \cdot \text{T}^{1/2}$. Compared with the experimental value of $A \approx 0.9\text{mJ/mol} \cdot \text{K}^2 \cdot \text{T}^{1/2}$ from Ref. [192], our numerical value is greater by a factor of about 5. This quantitative

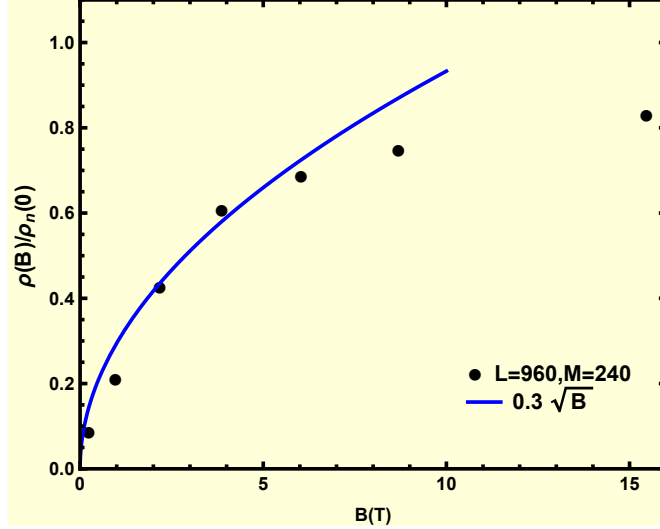


Figure 3.9: The density of states of a pure d -wave vortex solid without any particle-hole density wave order coexisting. The parameter $\Delta = 0.1t$. The estimated normal state DOS is $\rho_n(0) \approx 0.25$ states/ t .

discrepancy is not significant given our approximations. In fact, it is quite reasonably consistent.

- Next we consider the coexistence of a square vortex lattice and an additional two-fold DDW order in the underdoped regime. The parameters are the same as those in our high field quantum oscillation calculations: $t'/t = 0.3, t'' = t'/9.0, \mu = -0.8807t, W_0 = 0.26t$, so the estimated normal state, with the DDW order but no superconductivity, hole doping level is $p \approx 11\%$. Fig. 3.10 shows the corresponding DOS results. The small field data follows $\rho(B)/\rho_n(0) = 0.4\sqrt{B}$, corresponding to a value of $\kappa \approx 4$ in Eq. (3.17).

The above two values of κ are consistent with the fact that in Volovik's formula κ is of order unity. Of course its precise value depends on the vortex lattice structure, on the slope of the gap near the gap node (in the current case both the parameters Δ and q), and also on the normal state band structure.

From the above two scenarios we can conclude that irrespective of the existence of an additional density wave order, the DOS of a clean vortex lattice always scales as $\rho(B) \propto \sqrt{B}$ in the low field limit.

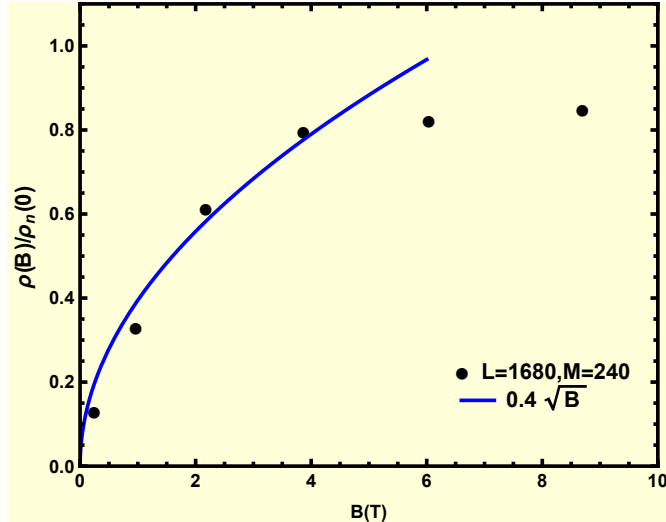


Figure 3.10: The density of states of a d -wave vortex solid coexisting with a two-fold DDW order. The parameter $\Delta = 0.1t$. The estimated normal state DOS is $\rho_n(0) \approx 0.23$ states/ t .

3.5 Conclusion

In summary we have shown that in the quenched vortex liquid state the quantum oscillations in cuprates can survive at large magnetic fields. Although the oscillation amplitude can be heavily damped if the vortex scattering is strong, the oscillation frequency is given by the Onsager rule to an excellent approximation. Of course, when the field is small the quantum oscillations are destroyed by the vortices and $\rho(B)$ gets heavily suppressed due to the formation of Bogoliubov quasiparticles. When the field is small enough, a vortex solid state forms instead and it can be modeled by an ordered vortex lattice. We show the field dependence of the vortex lattice's density of states follows $\rho(B) \propto \sqrt{B}$ in the asymptotically low field limit, in agreement with Volovik's semiclassical predictions. However in contrast to the previous suggestion our results show that this small field limit does not extend to the high field oscillatory regime of the vortex liquid state. Instead when the oscillations can be resolved, the non-oscillatory background of $\rho(B)$ flattens out, and becomes field independent consistent with the more recent specific heat measurements [180].

CHAPTER 4

Pairing in half-filled Landau level within the HLR picture

4.1 Introduction

The concept of composite fermions was introduced to understand quantum Hall states. [81, 13] Using this concept, Halperin, Lee and Reed [23] (HLR) further developed the Composite Fermi Liquid (CFL) theory to understand the gapless single layer half-filled Landau level problem. In the mean field approximation, this theory predicts a compressible “metal” with a sharp Fermi surface, which has received some support from experiments [90, 14, 15, 91, 92, 93]. However, in such a gapless system, the emergent Chern-Simons (CS) gauge field fluctuations can play an important role. In fact, these fluctuations can mediate an attractive density-current interaction between the fluxes attached to a composite fermion and the current associated with another composite fermion. As was shown by Greiter, Wen and Wilczek [21] (GWW), the mean field Fermi surface is always unstable to the formation of Cooper pairs in odd angular momentum channels. Thus at low temperatures, the system ends up in a superconducting state with an order parameter that is most likely a chiral p -wave.

However, Bonesteel [120] showed that if we go beyond GWW analysis and consider the random phase approximation (RPA) [23] corrections, there will be an induced current-current interaction mediated by the transverse CS gauge field. The current-current interaction is repulsive and divergent in the small Matsubara frequency limit for all angular momentum channels. Using this small frequency limit for the entire range of Matsubara frequencies, and assuming the gap to be weakly dependent on Matsubara frequencies, the zero temperature ($T = 0$) BCS gap equation was solved analytically. The conclusion was that with a bare short-range contact interaction, the repulsive current-current interaction

always dominates over other interactions when the BCS gap is small. Therefore there is no GWW pairing instability. However the gap equation was found to have a solution when the gap was finite. Thus the zero temperature pairing transition was conjectured to be first order for short-range interaction, while for a long-range Coulomb interaction, a continuous pairing transition was considered to be a possibility because of weaker gauge field fluctuations.

The above analysis, based on the small frequency limit of the current-current interaction needs to be reexamined. As mentioned and discussed in Section 1.2.2 of Chapter 1, in a recent work [123] by Chung *et al* a new pairing mechanism has been proposed. In the original work of Ref. [123] the authors considered a problem of non-relativistic fermions coupled to a transverse gauge field. They suggest that although the current-current interaction is repulsive and singular in the small frequency limit, at higher frequencies it can be attractive for angular momentum channels $\ell \geq 2$. This attractive part can outweigh the repulsive part, thus changing the solution to the BCS equation completely. Therefore it is crucial to consider the full Matsubara frequency dependence of the current-current interaction and solve the BCS gap equation in a self-consistent manner.

In addition to the single layer case, we also consider the full frequency dependent analysis of the double layer Hall system with a total filling fraction $\nu = \frac{1}{2} + \frac{1}{2}$. This system is decoupled into two separate composite fermion metals with $\nu = \frac{1}{2}$ in each layer if there are no disorder or inter-layer tunneling. If we include the most singular interaction, namely the inter-layer current-current interaction, the interaction can be attractive or repulsive depending on whether it is mediated by the out-of-phase or the in-phase mode of the CS gauge field fluctuations. [193] The competition between these two will determine the final fate of the double layer system. Bonesteel *et al* [194] showed that this interaction always drives the system into a inter-layer paired state for any large separation d between the two layers. However, this conclusion was also obtained from the previously mentioned small frequency analysis. Therefore, for similar reasons, it must be reexamined if only to put it on a firmer basis.

The major results of this Chapter 4 are as follows: (1) For the single layer system with either short-range contact interaction or long-range Coulomb interaction, there can be a *continuous* transition from the HLR state to a chiral odd ℓ -wave Cooper pair state.

(2) For the double layer system, there is always a non-zero pairing between inter-layer composite fermions if the inter-layer spacing d is much greater than the magnetic length ℓ_B . Thus, the small frequency analysis [194] does not qualitatively differ from the full frequency dependent analysis, except for significant quantitative differences.

The structure of this Chapter 4 is as follows: in Section 4.2 we derive the BCS gap equation for the $\nu = \frac{1}{2}$ single layer system; in Section 4.3 we present our numerical results for the single layer system with short-range contact interaction and also briefly discuss the results for the long-range Coulomb interaction; in Section 4.4 we write down the BCS gap equation for the double layer system and present our numerical results; in Section 4.5 we summarize our conclusion and provide some further discussions.

4.2 The Effective action and the BCS gap equation for a single layer system

Consider a two-dimensional ($2D$) electron gas with a perpendicular magnetic field B at a filling fraction $\nu = 1/\tilde{\phi}$. For half-filling $\tilde{\phi} = 2$. In the CFL picture, $\tilde{\phi}$, the emergent flux is described by the CS gauge fields (a_0, \mathbf{a}) attached to an electron to form a composite fermion. To describe this flux attachment, we need to add a CS term to the free electron action. Thus, without interactions, the total Euclidian Lagrangian density is given by [23] $\mathcal{L} = \mathcal{L}_0 + \mathcal{L}_{CS}$ with ($\hbar = c = e = 1$)

$$\mathcal{L}_0 = \psi^*(\partial_\tau - a_0 - \mu)\psi - \frac{1}{2m^*}\psi^*(\partial_i - i\mathbf{a}_i + i\mathbf{A}_i)^2\psi, \quad (4.1)$$

$$\mathcal{L}_{CS} = \frac{a_0}{2\pi\tilde{\phi}}\epsilon^{ij}\partial_i a_j, \quad (4.2)$$

where ψ is the composite fermion field, m^* is the composite fermion effective mass, and $\nabla \times \mathbf{A} = B\hat{\mathbf{z}}$, the physical magnetic field. At the mean field level, $\epsilon^{ij}\partial_i \bar{a}_j = 2\pi\tilde{\phi} \langle \psi^*\psi \rangle = B\hat{\mathbf{z}}$, B being the applied magnetic field. Then the CS gauge field exactly cancels the external magnetic field. Therefore the system is a composite fermion metal with the Fermi wave vector $k_F = \sqrt{\frac{2}{\tilde{\phi}}}\frac{1}{\ell_B}$, where ℓ_B is the magnetic length. At half filling, $k_F = \frac{1}{\ell_B}$.

Beyond this mean field approximation, there will be fluctuations of the composite fermion density, which also implies fluctuations of the CS gauge fields. These gauge field fluctuations can in turn couple to the composite fermion currents, mediating a density-

current interaction. Such an interaction is attractive in odd angular momentum channels, leading to the GWW instability. In addition, we have additional four fermion interaction term in the Lagrangian density,

$$\mathcal{L}_{int} = \frac{1}{2} \int d^2\mathbf{x}' \psi^*(\tau, \mathbf{x}) \psi(\tau, \mathbf{x}) v(r) \psi^*(\tau, \mathbf{x}') \psi(\tau, \mathbf{x}'), \quad (4.3)$$

where $r = |\mathbf{x} - \mathbf{x}'|$ and the interaction is: $v(r) = \frac{e^2}{\epsilon r}$ for a Coulomb interaction, ϵ being the dielectric constant, while $v(r) \propto \delta(r)$ for a short-range contact interaction.

Redefining (a_0, \mathbf{a}) as deviations from their mean field values, choosing the Coulomb gauge[23], and using the constraint $\psi^* \psi = (1/2\pi\tilde{\phi}) \epsilon^{ij} \partial_i a_j$, we can rewrite the total action in the momentum space as

$$S = S_0 + S_{CS}, \quad (4.4)$$

$$S_0 = \int d\tau d^2\mathbf{x} \left[\psi^* (\partial_\tau - ia_0) \psi - \frac{1}{2m^*} \psi^* (\partial_i - i\mathbf{a}_i)^2 \psi - \mu \psi^* \psi \right], \quad (4.5)$$

$$\begin{aligned} S_{CS} &= \int d\tau d^2\mathbf{x} (\mathcal{L}_{CS} + \mathcal{L}_{int}) \\ &= \frac{1}{2\beta} \sum_{n,\mu,\nu} \int \frac{d^2\mathbf{q}}{(2\pi)^2} a_\mu^*(i\omega_n, \mathbf{q}) \mathcal{D}_{\mu,\nu}^0(i\omega_n, \mathbf{q})^{-1} a_\nu(i\omega_n, \mathbf{q}). \end{aligned} \quad (4.6)$$

Here $\mu, \nu = \{0, 1\}$, $\omega_n = 2n\pi/\beta$ is a bosonic Matsubara frequency, and a_0, a_1 are the time and transverse components of the CS gauge fields with the convention $a_1(i\omega_n, \mathbf{q}) = \hat{\mathbf{z}} \cdot (\mathbf{q} \times \mathbf{a})$. The CS gauge field action term S_{CS} defines the bare CS gauge field propagator to be

$$\mathcal{D}^0(i\omega_n, \mathbf{q}) = \begin{pmatrix} v(q) & i\frac{2\pi\tilde{\phi}}{q} \\ -i\frac{2\pi\tilde{\phi}}{q} & 0 \end{pmatrix}, \quad (4.7)$$

where $v(q)$ is the bare density-density interaction expressed in the momentum space. Hence, $v(q) = 2\pi e^2/\epsilon q$ for long-range Coulomb interaction, and $v(q) = const.$ for short-range contact interaction. After RPA correction, the inverse gauge field propagator is given by

$$[\mathcal{D}(i\omega_n, \mathbf{q})]^{-1} = [\mathcal{D}^0(i\omega_n, \mathbf{q})]^{-1} + \mathcal{K}^0(i\omega_n, \mathbf{q}), \quad (4.8)$$

where $\mathcal{K}^0(i\omega_n, \mathbf{q})$ is the electromagnetic response function of the non-interacting fermions in 2D and has diagonal components only. In the limit $q < 2k_F$ and $|\omega_n| \ll \frac{k_F q}{m}$, we $\mathcal{K}_{00}^0 = N(\epsilon_F) = \frac{m^*}{2\pi}$ and $\mathcal{K}_{11}^0 = -\chi_d q^2 - \frac{k_F |\omega_n|}{2\pi q}$, where $\chi_d = \frac{1}{12\pi m^*}$ is the free fermion diamagnetic susceptibility. Inverting the matrix \mathcal{D}^{-1} , the RPA corrected gauge field

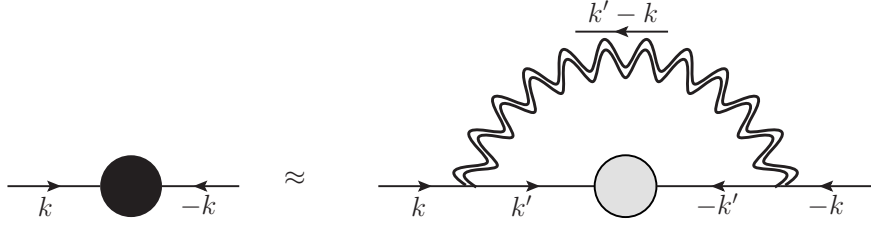


Figure 4.1: Diagrammatic representation of the Dyson equation for the off-diagonal components of the anomalous self-energy $\Delta(i\omega_n, \mathbf{k})$. The black blob denotes the proper anomalous self-energy, and the gray blob (along with the associated fermion lines) denotes the corresponding component of the exact propagator of the fermions. The wiggly line is the RPA corrected gauge field propagator. For compactness, we have used the Euclidean vector notation: $k \equiv (k_0, \mathbf{k}) = (\omega_n, \mathbf{k})$.

propagator is [23]

$$\mathcal{D}(i\omega_n, \mathbf{q}) = \frac{1}{\mathcal{K}_{00}^0 \left[\mathcal{K}_{11}^0 - \frac{q^2 v(q)}{(2\pi\phi)^2} \right] - \left(\frac{q}{2\pi\phi} \right)^2} \begin{pmatrix} \mathcal{K}_{11}^0 - \frac{q^2 v(q)}{(2\pi\phi)^2} & -i \frac{q}{2\pi\phi} \\ i \frac{q}{2\pi\phi} & \mathcal{K}_{00}^0 \end{pmatrix}. \quad (4.9)$$

Therefore, the RPA correction not only renormalizes the density-density and density-current interactions, but also generates a new current-current interaction, which turns out to be repulsive and divergent at small frequencies but attractive at high frequencies.

Let ϕ_1 and ϕ_2 be the real and the imaginary parts of the anomalous self-energy respectively, and $Z(i\omega_n, \mathbf{k})$ denote the mass renormalization. For our single layer problem we will ignore the mass renormalization equation by simply taking $Z(i\omega_n, \mathbf{k}) \simeq 1$. This can be safely done in the pairing state if the superconductivity forms at an energy scale higher than the characteristic energy scale of the onset of the non-Fermi liquid behaviour. [195] Therefore the complex anomalous self energy $\phi(i\omega_n, \mathbf{k}) = \phi_1(i\omega_n, \mathbf{k}) + i\phi_2(i\omega_n, \mathbf{k})$ is simply the gap function $\Delta(i\omega_n, \mathbf{k})$

Written out explicitly in terms of $\Delta(i\omega_n, \mathbf{k})$, the anomalous self-energy equation in Matsubara frequency is [111]

$$\Delta(i\omega_n, \mathbf{k}) = -\frac{1}{\beta} \sum_m \int \frac{d^2\mathbf{k}'}{(2\pi)^2} \frac{\Delta(i\omega_m, \mathbf{k}')}{|\omega_m|^2 + \bar{\epsilon}_{\mathbf{k}'}^2 + |\Delta(i\omega_m, \mathbf{k}')|^2} V_{\text{eff}}(i\omega_m - i\omega_n; \mathbf{k}', \mathbf{k}), \quad (4.10)$$

as shown diagrammatically in Fig. 4.1. Here $\bar{\epsilon}_{\mathbf{k}} = \epsilon_{\mathbf{k}} - \mu$ is the reduced kinetic energy.

Now let us write $\Delta(i\omega_n, \mathbf{k}) = \sum_{\ell} \Delta_{\ell}(i\omega_n, \mathbf{k}) e^{i\ell\theta_{\mathbf{k}}}$, where only odd ℓ angular momentum channels will be considered since the $\nu = 1/2$ single layer system is spin-polarized. Being a nonlinear integral equation involving the gap, we cannot strictly speaking decouple the various angular momentum channels. However, we shall assume approximate decoupling. Such decoupled gap equations for different channels can be considered as local minima of the free energy. We will use the Fermi surface approximation $|\mathbf{k}| = k_F$, ignoring the dependence on the magnitude of \mathbf{k} , so that $\Delta_{\ell}(i\omega_n, \mathbf{k}) \simeq \Delta_{\ell}(i\omega_n)$. We will also consider the zero temperature limit when the Matsubara frequencies become continuous: $\omega_n \rightarrow \omega$. For the ℓ -wave channel, we get

$$\begin{aligned} \Delta_{\ell}(i\omega) = & - \int \frac{d^2\mathbf{k}'}{(2\pi)^2} \frac{d\omega'}{2\pi} \frac{\Delta_{\ell}(i\omega') e^{i\ell\theta}}{|\omega'|^2 + \bar{\epsilon}_{\mathbf{k}'}^2 + |\Delta_{\ell}(i\omega')|^2} \\ & \times V_{\text{eff}}(i\omega' - i\omega; \mathbf{k}', \mathbf{k}) \Big|_{|\mathbf{k}|, |\mathbf{k}'|=k_F}, \end{aligned} \quad (4.11)$$

where θ is defined as $\hat{\mathbf{z}} \cdot (\hat{\mathbf{k}} \times \hat{\mathbf{k}}') = \sin \theta$.

At the Fermi surface, $\int \frac{d^2\mathbf{k}'}{(2\pi)^2} \approx N(\epsilon_F) \int_{-\infty}^{\infty} d\bar{\epsilon}_{\mathbf{k}'} \int \frac{d\theta}{2\pi}$, where $N(\epsilon_F) = \frac{m^*}{2\pi}$ is the 2D density of states of spin-polarized fermions at the Fermi energy ϵ_F . Performing the integration over $\bar{\epsilon}_{\mathbf{k}'}$ by the contour integral method, the BCS gap equation takes the form:

$$\Delta_{\ell}(i\omega) = \int d\omega' \frac{\Delta_{\ell}(i\omega')}{2\sqrt{|\omega'|^2 + |\Delta_{\ell}(\omega')|^2}} \tilde{V}_{\text{eff},\ell}(|\omega - \omega'|), \quad (4.12)$$

$$\tilde{V}_{\text{eff},\ell}(|\omega - \omega'|) = -\frac{m^*}{2\pi} \int \frac{d\theta}{2\pi} e^{i\ell\theta} V_{\text{eff}}(i\omega' - i\omega; \mathbf{k}', \mathbf{k}) \Big|_{|\mathbf{k}|, |\mathbf{k}'|=k_F}. \quad (4.13)$$

The Fermi surface approximation is good in the BCS case, because the Debye frequency ω_D is much smaller than the typical Fermi energy. But in the present problem, there is no similar small energy scale. There is, however, a rough high energy scale $\omega_0 \sim \frac{e^2}{\epsilon \ell_B}$, where ℓ_B is the magnetic length. On a length scale smaller than ℓ_B , the concept of composite fermion is not well-defined. But this energy scale is not small compared with ϵ_F ; in fact, $\frac{\omega_0}{\epsilon_F} = \frac{2m^*e^2\ell_B}{\epsilon} \simeq \frac{20}{3}$. [120, 23] It has the same order of magnitude as the Fermi energy of the free composite fermions. We assume that our Fermi surface approximation to be qualitatively correct. To get the explicit form of V_{eff} , we need to multiply $\mathcal{D}_{\mu,\nu}$ by the appropriate vertex factors, as shown in the Feynman diagram in Fig. 4.1. As we mentioned before, there will be density-density (associated with \mathcal{D}_{00}), density-current (involving \mathcal{D}_{01} and \mathcal{D}_{10}), and current-current interactions (involving \mathcal{D}_{11}).

Correspondingly $\tilde{V}_{\text{eff},\ell}(i\omega)$, which characterizes the interaction, can be separated into three pieces: the density-density interaction term $\lambda_{\ell,00}(i\omega)$, the density-current interaction term $\lambda_{\ell,10}(i\omega)$, and the current-current interaction term $\gamma_\ell(i\omega)$:

$$\tilde{V}_{\text{eff},\ell}(|\omega|) = \lambda_{\ell,00}(i\omega) + \lambda_{\ell,10}(i\omega) - \gamma_\ell(i\omega) \quad (4.14)$$

with $\lambda_{\ell,00}$, $\lambda_{\ell,10}$ and γ_ℓ are defined by

$$\lambda_{\ell,00}(i\omega) \equiv -\frac{m^*}{2\pi} \int_0^{2\pi} \frac{d\theta}{2\pi} e^{i\ell\theta} \mathcal{D}_{00}(i\omega, |\mathbf{k}' - \mathbf{k}|) \Big|_{|\mathbf{k}|, |\mathbf{k}'|=k_F}, \quad (4.15)$$

$$\lambda_{\ell,10}(i\omega) \equiv -\frac{m^*}{2\pi} \int_0^{2\pi} \frac{d\theta}{2\pi} e^{i\ell\theta} \left\{ 2 \frac{\hat{\mathbf{z}} \cdot (\mathbf{k}' \times \mathbf{k})}{m^* |\mathbf{k}' - \mathbf{k}|} \mathcal{D}_{01}(i\omega, |\mathbf{k}' - \mathbf{k}|) \right\} \Big|_{|\mathbf{k}|, |\mathbf{k}'|=k_F}, \quad (4.16)$$

$$\gamma_\ell(i\omega) \equiv \frac{m^*}{2\pi} \int_0^{2\pi} \frac{d\theta}{2\pi} e^{i\ell\theta} \left\{ \frac{|\hat{\mathbf{z}} \cdot (\mathbf{k}' \times \mathbf{k})|^2}{m^{*2} |\mathbf{k}' - \mathbf{k}|^2} \mathcal{D}_{11}(i\omega, |\mathbf{k}' - \mathbf{k}|) \right\} \Big|_{|\mathbf{k}|, |\mathbf{k}'|=k_F}. \quad (4.17)$$

In the density-current interaction term $\lambda_{\ell,10}(i\omega)$, there is a pre-factor of 2 inside the curly brackets. This is because the two off-diagonal CS gauge field propagators \mathcal{D}_{01} and \mathcal{D}_{10} contribute identically to the density-current interaction.

It can be shown that for the short-range interaction $v(q) = \text{const}$

$$\lambda_{\ell,00}(i\omega = 0) = 0 \quad (4.18)$$

$$\lambda_{\ell,10}(i\omega = 0) = \xi_\ell \text{sgn}(\ell) \quad (4.19)$$

with ξ_ℓ some positive constant [120]. From the expression of $\lambda_{\ell,10}(i\omega = 0)$ we see that it is attractive in the positive ℓ -wave channel while repulsive in the negative ℓ -wave channel, indicating the chirality of pairing if superconductivity is stabilized. Notice that because of the Fermi surface approximation ξ_ℓ is independent of angular momentum channel ℓ . However as this approximation is relaxed, in general it should pick up an ℓ dependence. In the following we are going to group the density-density and density-current interaction together and use $\xi_\ell = \lambda_{\ell,00}(i\omega = 0) + \lambda_{\ell,10}(i\omega = 0)$ (for $\ell > 0$) as a generic coupling constant to characterize them.

The transverse component gauge field propagator is given by [120]:

$$\mathcal{D}_{11}(i\omega, q = |\mathbf{k}' - \mathbf{k}|) \simeq \frac{1}{\tilde{\chi}(q)q^2 + \frac{k_F|\omega|}{2\pi q}} \quad (4.20)$$

where $\tilde{\chi}(q) = v(q)/(2\pi\tilde{\phi})^2 + (1 + 6/\tilde{\phi}^2)/(12\pi m^*)$. With short-range interaction $v(q) \simeq v(0) = \text{const}$, $\tilde{\chi}(q) \simeq \tilde{\chi}(0)$ is a constant. Then $\gamma_\ell(i\omega)$ of Eq. (4.17) can be expressed as:

$$\gamma_\ell(i\omega) = \zeta_\ell \int_0^{2\pi} \frac{d\theta}{2\pi} \frac{|\sin \frac{\theta}{2}| \cos^2 \frac{\theta}{2} \cos(\ell\theta)}{2|\sin^3 \frac{\theta}{2}| + \zeta_\ell \frac{|\omega|}{4\epsilon_F}}. \quad (4.21)$$

with the dimensionless constant ζ_ℓ defined by

$$\zeta_\ell \equiv \frac{1}{4\pi m^* \tilde{\chi}(0)} \quad (4.22)$$

Similarly to ξ_ℓ , ζ_ℓ will be also treated as a generic coupling constant for the current-current interaction.

In the small frequency limit

$$\gamma_\ell(i\omega) \propto \left(\frac{\epsilon_F}{|\omega|}\right)^{1/3} \quad (4.23)$$

with a frequency independent prefactor. Bonesteel [120] used this small frequency expression for the whole frequency range and solved the BCS gap equation. However, according to our previous experience [123] the behavior of $\gamma_\ell(i\omega)$ at high frequency is qualitatively very different from that in the small frequency limit. In fact it changes sign at high frequencies. Therefore, the full frequency dependence of $\gamma_\ell(i\omega)$ will be very important for the final result. In other words, we will use Eq. 4.21 for $\gamma_\ell(i\omega)$.

Fig. 4.2 shows the dependence of $\gamma_\ell(i\omega)$ on frequency ω . From these plots it is transparent that the current-current interaction term becomes attractive at high frequencies for angular momentum channel $\ell > 1$. Furthermore the attractive parts are considerable.

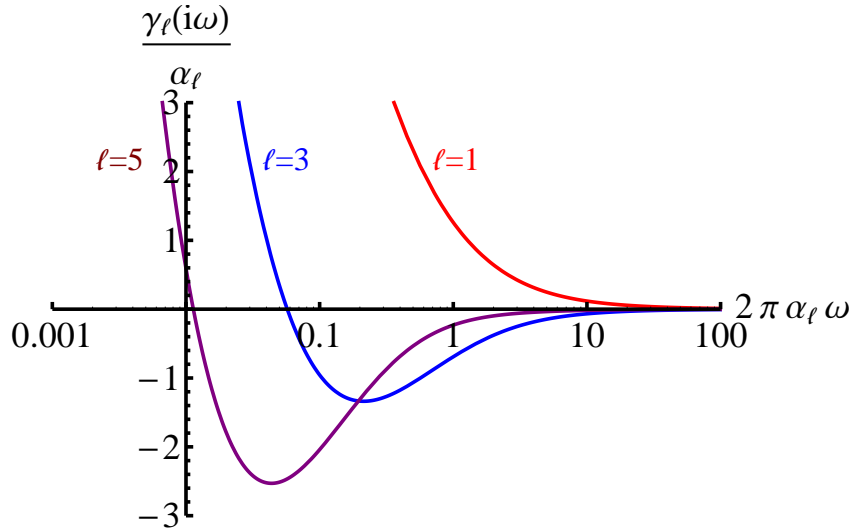


Figure 4.2: $\frac{\gamma_\ell(i\omega)}{\alpha_\ell}$ versus $2\pi\alpha_\ell\omega$ for the short-range interaction case, where $\alpha_\ell \equiv \frac{\zeta_\ell}{4\pi} > 0$. The frequency ω has been expressed in units of ϵ_F .

In summary, the equation to be solved is

$$\Delta_\ell(\omega) = \xi_\ell \int_{-\omega_{c1}}^{\omega_{c1}} d\omega' \frac{\Delta_\ell(\omega')}{2\sqrt{\omega'^2 + |\Delta_\ell(\omega')|^2}} - \int_{-\omega_{c2}}^{\omega_{c2}} d\omega' \frac{\Delta_\ell(\omega')}{2\sqrt{\omega'^2 + |\Delta_\ell(\omega')|^2}} \gamma_\ell(i\omega) \quad (4.24)$$

where the full frequency dependence, Eq. 4.21 of $\gamma_\ell(i\omega)$, is used.

In the above gap equation we have set a frequency cut-off ω_{c1} for the term involving ξ_ℓ . Using different values of ω_{c1} can in general change the non-universal critical constants ξ_ℓ and ζ_ℓ of the phase transition. However, as far as the nature of the phase transition is concerned, which is what we are interested in, the conclusions obtained here will be independent of these specific values. For simplicity we will choose $\omega_{c1} = \epsilon_F$. As for the current-current interaction term, we are going to choose the frequency integration cutoff ω_{c2} to be large enough to include all significant contributions of $\gamma_\ell(i\omega)$. Typical value of this cutoff for the displayed numerical results is $\omega_{c2} = 10 \epsilon_F$.

4.3 Numerical results for single layer system

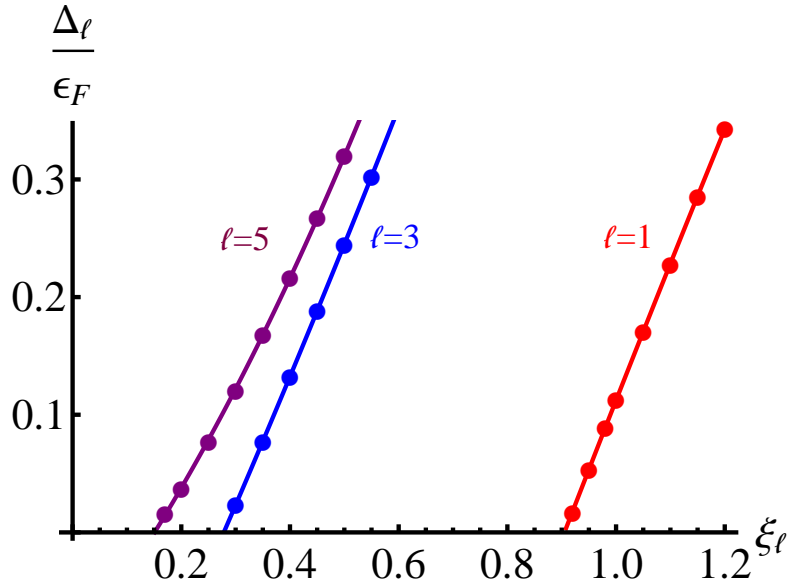


Figure 4.3: Zero frequency gap Δ_ℓ versus ξ_ℓ for the short-range interaction, plotted for $\ell = 1, 3, 5$. The other coupling constant $\zeta_\ell = 1$.

Fig. 4.3 shows the zero frequency gap $\Delta_\ell \equiv \Delta_\ell(i\omega = 0)$ versus ξ_ℓ for different ℓ 's, with $\zeta_\ell = 1$ (fixed). There are several noticeable features in this graph: (1) When ξ_ℓ is large enough, superconductivity exists. (2) The phase transition is continuous for all odd values of ℓ . (3) For $\ell = 1$, pairing requires a larger value of ξ_ℓ , because in this case, $\gamma_\ell(i\omega)$ is repulsive for all frequencies and a larger attraction from ξ_ℓ is required to produce pairing, as is shown previously in Fig. 4.2.

We have solved the gap equation for different values of ζ_ℓ to find the corresponding critical values of ξ_ℓ and constructed the phase diagram in the $\xi_\ell - \zeta_\ell$ space. The phase diagram for $\ell = 3$ is shown in Fig. 4.4. The generic features for $\ell > 1$ are as follows:

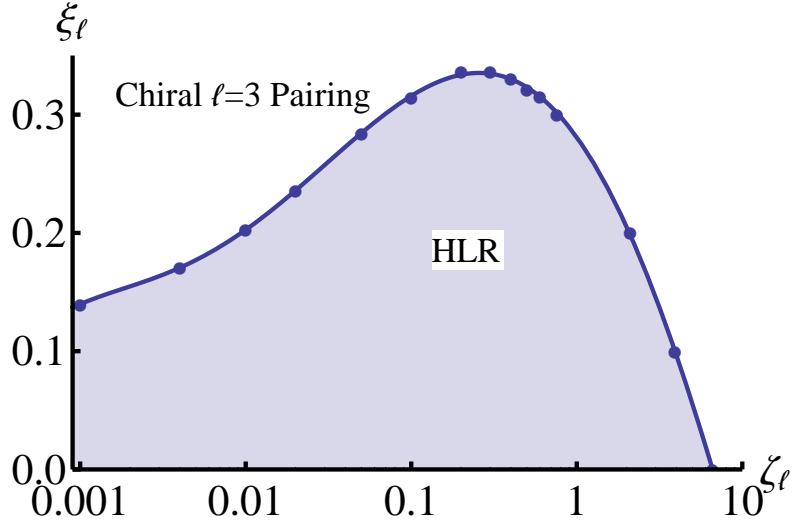


Figure 4.4: Phase diagram for $\ell = 3$ in the $\xi_\ell - \zeta_\ell$ plane, for the case of short-range interaction. In the shaded region, we have an *HLR* state. In the other regions, the system is unstable to a *chiral $\ell = 3$ pairing state*. The transition from the pairing state to the HLR state is *continuous*. We note that when ζ_ℓ is very small, the phase boundary curve should be extrapolated to the origin point.

1. Pairing exists when ζ_ℓ is large, since each individual term of the gap equation leads to pairing. The threshold value of ξ_ℓ for pairing increases as ζ_ℓ decreases.
2. When ζ_ℓ is small and ξ_ℓ is not large enough, the current-current interaction term is pair breaking¹, while the density-current term is not powerful enough to overcome this effect. Hence HLR state is stable against pairing in this region.
3. If ζ_ℓ is very small, we can ignore the current-current interaction term. Then even small ξ_ℓ can give us a pairing state. This is because in the limit $\zeta_\ell \rightarrow 0$, even infinitesimal attraction, characterized by ξ_ℓ , will produce a pairing state. This is

¹By “pair breaking” we simply mean that the net effect of that interaction is repulsive. It is different from its traditional usage in the case of scattering of electrons in Cooper pairs from either impurities or some bosonic modes, whose effect is to break Cooper pairs and reduce the superconductivity temperature. Thanks to Elihu Abrahams for pointing out the difference.

why in Fig. 4.4 when ζ_ℓ is very small, the phase boundary could be extrapolated to the origin.

As the frequency dependence of $\gamma_\ell(i\omega)$ is similar for all $\ell \geq 3$, seen in Fig. 4.2, the phase diagrams for different $\ell \geq 3$ should also be similar. The $\ell = 1$ phase diagram can be quite different since the current-current interaction term for this channel is repulsive over the entire frequency range. Only when the attractive term ξ_ℓ is large enough, overcoming the repulsive current-current interaction, a chiral $\ell = 1$ pairing state can exist. This is explicitly shown in the $\ell = 1$ phase diagram in Fig. 4.5.

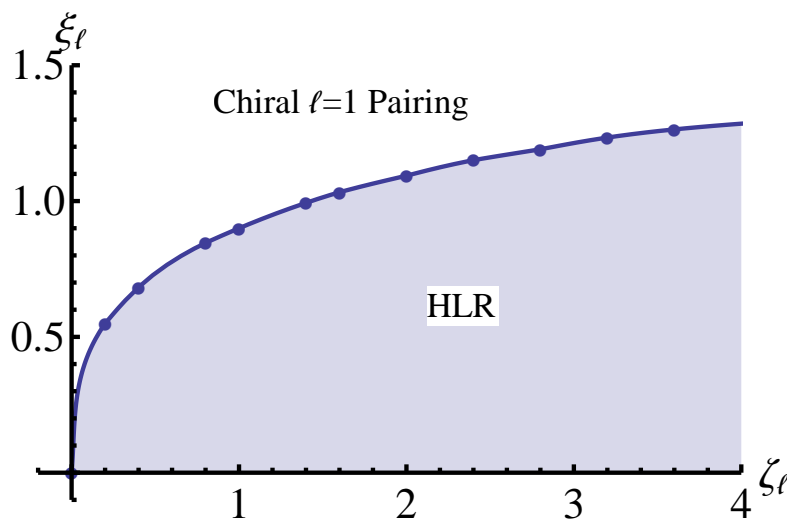


Figure 4.5: Phase diagram for $\ell = 1$ in the ξ_ℓ - ζ_ℓ plane, for the case of short-range interaction. The phase transition across the phase boundary is continuous.

Although all the above calculations are done with short-range contact interaction, we have also checked the Coulomb interaction case. In this case, the attractive part from the current-current interaction at high frequency is very small. So the current-current interaction mostly serves as a pair breaking term. Therefore the conclusion is similar to what Bonesteel [120] had in his paper: only when the density-current interaction dominates over other interactions will we have the GWW instability and the system be in a chiral odd ℓ pairing state; also the transition from the HLR state to the chiral pairing state is continuous. We should remind the reader that in reality the long-range interaction may take some different form, such as $1/q^x$, with $x \leq 2$, some positive constant [23, 112]. Although we did not do explicit calculations for these cases, we expect that the general

conclusions will be the same as that obtained for the Coulomb interaction.

4.4 BCS gap equation for the double layer system

The full frequency dependent analysis can also be applied to the double layered Landau level system with a total filling fraction $\nu = \frac{1}{2} + \frac{1}{2}$ without inter-layer tunneling. Originally Bonesteel *et al* [194] used full Eliashberg equations in their analysis. But it turns out that, as far as whether there is a BCS pairing state at zero temperature or not, the single BCS gap equation is enough. Since this will be a qualitative discussion, to simplify our numerical task, we are going to ignore the second Eliashberg equation. The numerical solution of the coupled Eliashberg equations with the full frequency dependence is quite complex.

In the zero temperature limit, the BCS gap equation for *s*-wave pairing in the Matsubara frequency space is [194]

$$\Delta(\omega) = \int_{-\omega_c}^{\omega_c} d\omega' \frac{\Delta(\omega')}{2\sqrt{\omega'^2 + |\Delta(\omega')|^2}} \tilde{V}_{\text{eff}}(|\omega' - \omega|) \quad (4.25)$$

where the effective interaction V_{eff} has two terms

$$\tilde{V}_{\text{eff}}(|\omega|) = \lambda^{(-)}(i\omega) - \lambda^{(+)}(i\omega) \quad (4.26)$$

Here the two dimensionless coupling constants $\lambda^{(\pm)}(i\omega)$ are defined as the average of two inter-layer current-current interactions in the Cooper channel over the Fermi surface

$$\lambda^{(\pm)}(i\omega) = \frac{m^*}{2\pi} \int_0^{2\pi} \frac{d\theta}{2\pi} \left(\frac{\mathbf{k} \times \hat{\mathbf{q}}}{m^*} \right)^2 \mathcal{D}^{\pm}(i\omega, q) \quad (4.27)$$

with $\mathbf{q} = \mathbf{k} - \mathbf{k}'$, $q = |\mathbf{q}|$. The scattering angle θ is defined via $\hat{\mathbf{z}} \cdot (\hat{\mathbf{k}} \times \hat{\mathbf{k}}') = \sin \theta$, same as before.

Here the superscript \pm means that the interaction is mediated either by the inter-layer in-phase ('+' sign) or the out-of-phase ('-' sign) modes of the gauge field fluctuations. And $\mathcal{D}^{\pm}(i\omega, q)$ are the two corresponding gauge field fluctuation propagators. Within RPA and in the limit that the inter-layer spacing $d \gg \ell_B$, they are given by

$$\mathcal{D}^+(i\omega, q) \simeq \left(\frac{e^2 q}{4\pi\epsilon} + \frac{|\omega| k_F}{4\pi q} \right)^{-1}, \quad (4.28)$$

and

$$\mathcal{D}^-(i\omega, q) \simeq \begin{cases} \left(\frac{e^2 dq^2}{4\pi\epsilon} + \frac{|\omega| k_F}{4\pi q} \right)^{-1}, & \text{for } q \lesssim d^{-1}, \\ \left(\frac{e^2 q}{4\pi\epsilon} + \frac{|\omega| k_F}{4\pi q} \right)^{-1}, & \text{for } q \gtrsim d^{-1}. \end{cases} \quad (4.29)$$

where ϵ is the dielectric constant. Now we can substitute these expressions into our definitions of $\lambda^{(\pm)}(i\omega)$ in Eq. (4.27). Writing everything out in terms of the scattering angle θ and making the Fermi surface approximation yields (with $k_F = \ell_B^{-1}$ at half-filling)

$$\lambda^{(+)}(i\omega) = \int_0^{2\pi} \frac{d\theta}{2\pi} \frac{4 \sin \theta}{\beta(2 - 2 \cos \theta) + \frac{|\omega|}{\epsilon_F}} \quad (4.30)$$

$$\begin{aligned} \lambda^{(-)}(i\omega) = & \left[\int_0^{\theta_c} + \int_{2\pi-\theta_c}^{2\pi} \right] \frac{d\theta}{2\pi} \frac{4 \sin \theta}{\beta \frac{d}{\ell_B} (2 - 2 \cos \theta)^{3/2} + \frac{|\omega|}{\epsilon_F}} \\ & + \int_{\theta_c}^{2\pi-\theta_c} \frac{d\theta}{2\pi} \frac{4 \sin \theta}{\beta(2 - 2 \cos \theta) + \frac{|\omega|}{\epsilon_F}}, \end{aligned} \quad (4.31)$$

where $\theta_c = 2 \arcsin(\frac{1}{2d/\ell_B})$. In the expression of $\lambda^{(-)}$ above, the first term comes from the propagator $\mathcal{D}^-(i\omega, q)$ with $q \lesssim d^{-1}$. We have also introduced the dimensionless parameter of $\beta \equiv \frac{e^2/(\epsilon\ell_B)}{\epsilon_F} = \frac{e^2 m^*}{\epsilon k_F}$. Direct inspections show that the $\int_{\theta_c}^{2\pi-\theta_c}$ part of integral contribution is the same in both $\lambda^{(\pm)}$. Therefore they cancel out each other in the effective interaction \tilde{V}_{eff} . This cancellation is vital to the explanations to our final numerical results. After this cancellation $\tilde{V}_{\text{eff}} = \lambda^{(-)} - \lambda^{(+)}$ is simply

$$\tilde{V}_{\text{eff}}(i\omega) = \int_0^{\theta_c} \frac{d\theta}{\pi} \left\{ \frac{4 \sin \theta}{\beta \frac{d}{\ell_B} (2 - 2 \cos \theta)^{3/2} + \frac{|\omega|}{\epsilon_F}} - \frac{4 \sin \theta}{\beta(2 - 2 \cos \theta) + \frac{|\omega|}{\epsilon_F}} \right\}. \quad (4.32)$$

This gives the full-frequency dependent $\tilde{V}_{\text{eff}}(i\omega)$. In the original analysis of Ref.[194], the zero frequency limit $\omega \rightarrow 0$ expression of $\tilde{V}_{\text{eff}}(i\omega)$ is used. Since we are going to make a comparison between the solutions using these two different expressions of $\tilde{V}_{\text{eff}}(i\omega)$, we also give the small frequency limit expression of $\tilde{V}_{\text{eff}}(i\omega)$ here. Taking the $\omega \rightarrow 0$ limit of Eq. (4.32) and keeping the most singular part only in each term we obtain

$$\tilde{V}_{\text{eff}}(i\omega) \simeq \frac{8}{3\sqrt{3}} \left(\frac{1}{\beta d/\ell_B} \right)^{2/3} \left(\frac{\epsilon_F}{|\omega|} \right)^{1/3} - \frac{2}{\pi} \frac{1}{\beta} \ln \frac{\epsilon_F}{|\omega|} \quad (4.33)$$

From this expression it is obvious that the out-of-phase attraction $\sim (\frac{\epsilon_F}{|\omega|})^{1/3}$ is more singular than, therefore dominates over, the in-phase repulsion $\ln \frac{\epsilon_F}{|\omega|}$ in the zero frequency limit. Hence using this \tilde{V}_{eff} always gives us pairing. What we want to see here is whether including the full frequency dependence of $\tilde{V}_{\text{eff}}(i\omega)$ is going to change the conclusions or not.

The specific value of d does not change our conclusion as long as it satisfies $d \gg \ell_B$, which is the domain of validity for all the above discussions. As for the frequency cutoff ω_c in the BCS equation (4.25), $\omega_c = 10\epsilon_F$ is taken when the full frequency dependent \tilde{V}_{eff} (4.32) is used. This value should be large enough to include all significant high frequency contributions. When using the small frequency limit expression of \tilde{V}_{eff} (4.33) we can still use a large frequency cutoff $\omega_c = 10\epsilon_F$ for the first term involving $|\omega|^{-1/3}$, as it decays fast enough at high frequencies. However, the second term involving $\ln \frac{\epsilon_F}{|\omega|}$ does not converge at high frequencies. Therefore we will set $\omega_c = \epsilon_F$ for it.

Numerical results for double layer Hall system

Fig. 4.6 shows the zero frequency gap $\Delta \equiv \Delta(i\omega = 0)$ as a function of β . Clearly, we always get non-zero pairing, irrespective of whether the full frequency dependence is considered or not. The explanation is as follows. As we mentioned before, the two gauge

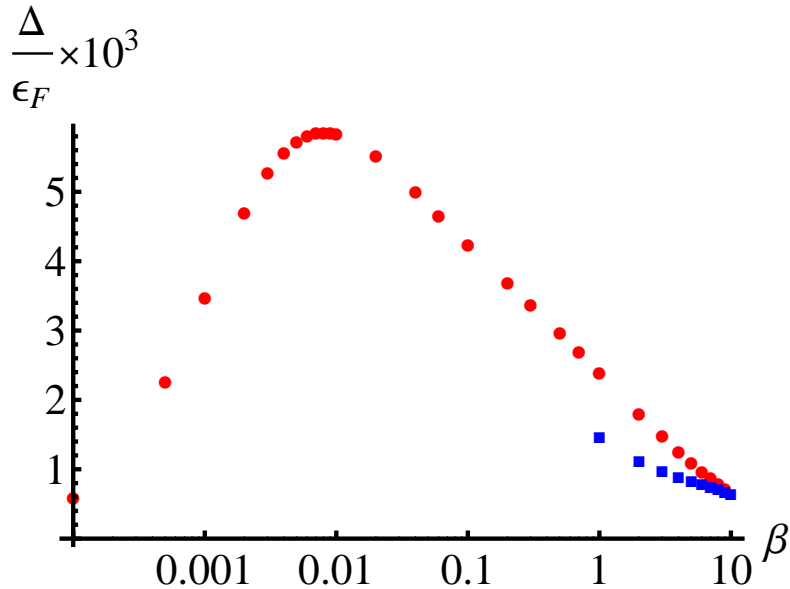


Figure 4.6: Pairing gap Δ for different values of $\beta \equiv \frac{e^2/(\epsilon\ell_B)}{\epsilon_F}$, in the s -wave channel. The circles denote the data obtained by using full frequency dependent \tilde{V}_{eff} , Eq. (4.32), while the squares denote the data obtained by using its small frequency limit expression, Eq. (4.33). Inter-layer distance $dk_F = \frac{d}{\ell_B} = 10$.

field propagators $\mathcal{D}^\pm(i\omega, q)$ differ from each other only when $q \lesssim d^{-1}$. This corresponds to a small frequency range $|\omega| \lesssim \omega_c$, with ω_c estimated by equating the Coulomb interaction

energy term with the Landau damping term in the denominator of $\mathcal{D}^+(i\omega_c, q = d^{-1})$

$$\frac{e^2 q}{4\pi\epsilon} \simeq \frac{\omega_c k_F}{4\pi q} \Rightarrow \frac{\omega_c}{\epsilon_F} \simeq \frac{e^2/(\epsilon \ell_B)}{\epsilon_F} (q \ell_B)^2 \simeq \beta \left(\frac{\ell_B}{d}\right)^2 \ll 1. \quad (4.34)$$

Therefore, $\lambda^{(+)}(i\omega)$ is significantly different from $\lambda^{(-)}(i\omega)$ only when $|\omega|/\epsilon_F \ll 1$. This implies that $\tilde{V}_{\text{eff},\ell}(i\omega)$ is basically non-vanishing only in the range $|\omega|/\epsilon_F \lesssim \omega_c/\epsilon_F \ll 1$. Hence including the high frequency part of $\tilde{V}_{\text{eff}}(i\omega)$ does not qualitatively change the conclusion. Of course quantitatively there will be differences as we see in Fig. 4.6. In fact this difference is bigger when β is smaller. This is because β comes into $\tilde{V}_{\text{eff}}(i\omega)$ in the form of $(\frac{1}{\beta})^x$ with $x = 2/3, 1$ in the prefactors. Therefore when β is smaller, the quantitative difference is enhanced. Notice that we only present our numerical gap data for $\beta \geq 1$ when using the small frequency limit expression of the effective interaction Eq. (4.33). This is because when $\beta \ll 1$, taking the frequency cutoff $\omega_c = \epsilon_F$ in the BCS gap equation for the repulsive term $\propto \ln \frac{\epsilon_F}{|\omega|}$ in Eq. (4.33) introduces considerable net repulsive effective interactions. However these net repulsive effective interactions are absent in the full frequency dependent expression of Eq. (4.32) and therefore unphysical.

In Fig. 4.6 we also see that when β is either very large or very small, the gap tends to vanish. These two limiting cases can be understood as follows

- When β is very large, in the denominators of both \mathcal{D}^\pm , the Coulomb energy, dominating over the Landau damping, controls the gauge field fluctuations. Then in the effective interaction Eq. (4.32) both terms are proportional to $\frac{1}{\beta}$, vanishing in the large β limit. Therefore the net effective interaction is very small and the pairing gap tends to vanish in this limit.
- When β is very small, the Landau damping term dominates over the Coulomb energy term and controls the gauge field fluctuations. However as Landau damping is the same for both the inter-layer in-phase and out-of-phase modes, they tend to cancel out each other in the effective interaction, as we can see in Eq. (4.32). Therefore the gap should vanish in this limit too.

From the considerations of these two limiting cases, we conclude that the gap must reach

the maximum at some finite β value. In fact this β value depends on the specific value of the inter-layer distance d as we see in Fig. 4.7.

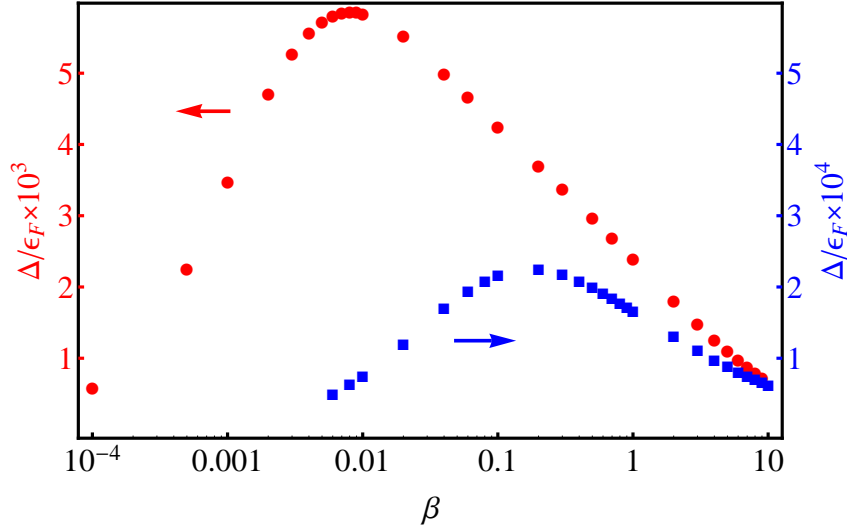


Figure 4.7: The bilayer pairing gap Δ as a function of the parameter β . The circles denote the data for $d = 10\ell_B$; while the squares denote the data for $d = 50\ell_B$. Notice that the two plots are using two different vertical axis scales, as indicated by the two arrows.

4.5 Conclusion

To summarize, we have shown that the full frequency dependence of the effective interaction is important and alters the conclusion obtained by Bonesteel[120], which is based on a small frequency analysis. For both short-ranged contact interaction and long-ranged Coulomb interaction, there can be a *continuous* transitions (instead of a discontinuous one) from the HLR state to a chiral pairing state in an odd angular momentum channel, as we tune the two coupling constants which characterize the density-current and current-current interactions. In practice, this tuning can be achieved by changing the width of the quantum well or of the semiconductor inversion layer, although the precise control of them can be difficult. This possible transition by changing the width of the electron layer has been also discussed in previous variational Monte Carlo studies[99, 196]. In fact, recent experiments have observed 1/2 and 1/4 fractional quantum Hall effects in asymmetric wide quantum wells [197, 198, 86, 199], although they are absent in the o-

original experiments performed in narrow quantum wells. These states can be interpreted as chiral odd wave pairing state of composite fermions [22]. And correspondingly, the change from a gapless state in narrow quantum wells to a fractional quantum Hall state in wide wells is suggestive of a transition from the HLR state to a chiral odd wave pairing state of composite fermions.

We have also constructed the phase diagrams for different angular momentum channels and found that the phase diagram for $\ell = 1$ channel pairing can be quite different from that for higher angular momentum channels $\ell \geq 3$. For $\ell = 1$ we always need large enough density-current interaction to stabilize the chiral pairing state. But for $\ell \geq 3$, even small density-current and large current-current interactions can result in a chiral pairing state, because of the attractive nature of the current-current interaction at high frequencies.

Although in all our above analysis we treat the composite fermions as point particles, the finite size effect as well as the short-range part of the electron-electron interaction might be important, [200, 201] to explain why the fractional quantum Hall state is stable at $\nu = 5/2$ while they are absent at other Landau level half fillings $\nu = 1/2, 3/2, 7/2, \dots$. Also the screening of the Coulomb interaction due to the filled Landau levels [202] may play an important role in distinguishing $\nu = 5/2$ from other half-filled Landau levels. Another assumption we made in our current analysis is that the single layer lowest Landau level composite fermion system is spin-polarized. Therefore the resulting pairing is in chiral odd-wave channel. But a recent numerical study showed that this incompressible state could either be a Moore-Read spin polarized Pfaffian state or a Halperin spin unpolarized 331 state[203]. Currently we do not have a definite answer to this. These could be subjects of future studies.

There is also a recent experiment revealing some new features of the $\nu = 1/2$ state which is difficult to understand according to the existing theories[204].

We also applied the full frequency dependent analysis to the double layer half-filled problem considered previously by Bonesteel *et al.* [194] It turns out that the full frequency dependence of the effective interaction does not change their qualitative conclusion. This is because the two contributions to the effective interaction coming from the in-phase and out-of-phase mode fluctuations of the CS gauge field cancel each other out at high

frequencies. Thus the net effective interaction is non-zero only in a very small frequency range near $\omega = 0$. So the small frequency analysis is a good approximation. [194]

After our work was completed we noticed that similar conclusions were recently reached by M. A. Metlitski *et al.* [114] from a renormalization group analysis. We also note two interesting related papers. [205, 206] It is clear that a more complex treatment of the coupled Eliashberg equations and fluctuation effects must be considered in the future work.

CHAPTER 5

Pairing of particle-hole symmetric composite fermions in half-filled Landau level

5.1 Introduction

The nature of the compressible state at $\nu = 1/2$ filling fraction in the fractional quantum Hall regime has been a fascinating topic since the pioneering work by Halperin, Lee, and Read (HLR) [23]. In the HLR picture this state is interpreted as a liquid of non-relativistic composite fermions (CFs) coupled to a fluctuating Chern-Simons (CS) gauge field. It provides a nice explanation for the acoustic wave propagation experimental observations [15].

However, the HLR theory has a long-standing issue in that it is incompatible with the particle-hole symmetry defined for a single Landau level [94, 95] in the zero Landau level mixing limit, as already discussed in Section 1.2.3 of Chapter 1. To resolve this issue recently Dam Thanh Son [2] has proposed a particle-hole symmetric theory in which the underlying composite fermions are taken to be Dirac particles. As in the HLR picture, these Dirac CFs are electrical neutral and coupled to an emergent gauge field. However, in this new picture the emergent gauge field does not have a Chern-Simons term. This proposal has generated a great deal of interest [139, 140, 126, 136, 128, 125, 135, 137, 127, 141, 142] because it can not only resolve the old particle-hole symmetry issue but also provide another avenue to study some seemingly completely unrelated topics such as strongly-correlated topological insulator surface states [125].

Cooper pairing of the CFs can give rise to incompressible gapped states which possess nonabelian braiding statistics [17, 22] and are potentially useful for topological quantum computation [19], as discussed in Chapter 1. In the traditional HLR picture, pairing CFs can lead to the Moore-Read Pfaffian state. However, because of lacking the particle-hole

symmetry, the anti-Pfaffian state [100, 101] —the particle-hole conjugate of the Moore-Read Pfaffian state —is impossible. In contrast, in Son’s new Dirac CF theory both the Moore-Read Pfaffian and anti-Pfaffian states are put on equal footing. Furthermore, a new putative particle-hole symmetric pairing state has also been proposed. However, the possible underlying pairing mechanism for realizing these states is not clear at all. In fact, in a recent work [136] the authors there considered an effective interaction, derived from the original electron-electron Coulomb interaction, in the BCS pairing channel and found that there is no pairing instability in any angular momentum channel ℓ .

Here we apply the new pairing mechanism from a repulsive force discussed in Section 1.2.2 to the particle hole symmetric Dirac composite fermion theory. We show that there can be nonzero pairing of Dirac CFs in angular momentum channels $|\ell| \geq 1$, including the Moore-Read Pfaffian and anti-Pfaffian states, which correspond to the $\ell = \mp 2$ channels. There is a quantum phase transition from the Dirac CF liquid state to the $|\ell| \geq 1$ pairing states as we tune the effective coupling constant. However, the $\ell = 0$ channel pairing, which is particle-hole symmetric and corresponds to the putative particle-hole symmetric Pfaffian state proposed in Ref. [2] previously, turns out to be impossible in our current treatment.

5.2 Model

The low energy effective(Euclidean) action of the Dirac CF field ψ in $2 + 1d$ is [2]

$$S_{\text{CF}} = \int d\tau d^2x \{ \bar{\psi} \gamma_\mu (\partial_\mu + i a_\mu) \psi - i \frac{B}{4\pi} a_0 \}, \quad (5.1)$$

where $\bar{\psi} = \psi^\dagger \gamma_0$ and the ψ field carries a 2-component pseudo-spin degrees of freedom. The three gamma matrices are chosen to be $\{\gamma_0, \gamma_1, \gamma_2\} = \{\sigma_3, \sigma_1, \sigma_2\}$ with $\sigma_1, \sigma_2, \sigma_3$ the three Pauli matrices. We have also set $\hbar = e = c = 1$ and the Fermi velocity $v_F = 1$. a_μ is the emergent gauge field that the Dirac CFs couple to. $\mu = 0, 1, 2$ represent the imaginary time τ and spatial x, y directions respectively. Throughout this whole Chapter 5 we will use Greek letter subscripts to denote the time-spatial 3-vector components and Latin letter subscripts for the spatial vectors. In the 2nd term of Eq. (5.1), B is the external physical magnetic field. As mentioned before, the key differences of S_{CF} from the HLR theory are: there is no Chern-Simons term for the gauge field a_μ and the new CFs are

relativistic particles. Differentiating S_{CF} with respect to a_0 gives $\bar{\psi}\gamma^0\psi = \frac{B}{4\pi}$, which shows that the Dirac CFs density is equal to twice of the B flux density. Therefore to electrons, the Dirac CFs are double vortex objects. Furthermore the emergent magnetic field strength is given by $b(\mathbf{x}) = \nabla \times \mathbf{a} = 4\pi\rho'_e(\mathbf{x})$. Here $\rho'_e = \rho_e - \rho_{\nu=1/2}$ is the deviation of the original electric charge density ρ_e from its half filled Landau level value $\rho_{\nu=1/2}$. A prime superscript is added to ρ'_e to distinguish it from ρ_e . We see that the original electric field and magnetic flux density interchange their roles in the new Dirac CF theory. In this sense the new theory is electro-magnetic dual [136] to the original electron problem.

At mean field level $\langle b(\mathbf{x}) \rangle = \rho'_e = 0$ because the electron Landau level is exactly at half filling. Therefore the Dirac CFs are described by a free Dirac Hamiltonian

$$H = v_F \mathbf{p} \cdot (\hat{z} \times \boldsymbol{\sigma}) \quad (5.2)$$

at zero field $b = 0$. The dispersion is simply a Dirac cone with two branches $\epsilon_{\mathbf{k}}^{\pm} = s \hbar v_F |\mathbf{k}|$ where $s = \pm$. Because the Dirac CF has a finite density $B/4\pi$, the Fermi energy $\epsilon_F = v_F k_F$ is finite with the Fermi wavevector given by $k_F = \sqrt{B}$, same as that in the HLR picture.

Beyond the mean field level there will be gauge fields a_{μ} fluctuations. In general these fluctuations can mediate some effective interaction and may provide the necessary pairing glue between the Dirac CFs. To find out that answer we need one more ingredient: the dynamics of the gauge fields. This could be given by an emergent Maxwell term in the action: $S_{\text{Max}} \propto -\frac{1}{4g^2} \int d^3x f_{\mu\nu}^2$, where $f_{\mu\nu} = \partial_{\mu}a_{\nu} - \partial_{\nu}a_{\mu}$ is the field strength and g is some coupling constant. The other choice is to use the original Coulomb interaction between electrons: $\frac{e^2}{\epsilon_r |\mathbf{x}-\mathbf{x}'|} \rho'_e(\mathbf{x})\rho'_e(\mathbf{x}')$, where ϵ_r is the background dielectric constant, and translate it into an interaction between the emergent gauge fields a_{μ} by using $b(\mathbf{x}) = 4\pi\rho'_e(\mathbf{x})$. Written in the momentum space, the action of this term reads [136]

$$S_{\text{Coulomb}} = \frac{1}{2} \int \frac{d\Omega d^2\mathbf{q}}{(2\pi)^3} a_T(\Omega, \mathbf{q}) \frac{2\pi e^2}{\epsilon_r |\mathbf{q}|} \frac{|\mathbf{q}|^2}{16\pi^2} a_T(-\Omega, -\mathbf{q}). \quad (5.3)$$

The frequency Ω here and all frequencies defined throughout the rest of the paper should be understood as Matsubara frequencies. The temperature has been already set to $T = 0$ so that all Matsubara frequencies are continuous. In the action S_{Coulomb} only the spatial transverse component of gauge fields is involved, as indicated by the subscript ‘‘T’’ on

$a_T(\Omega, \mathbf{q}) = \epsilon_{ij} \hat{q}_i a_j(\Omega, \mathbf{q})$, where ϵ_{ij} is the antisymmetric tensor and the summation convention is assumed. In Eq. (5.3) the $2\pi e^2/\epsilon_r |\mathbf{q}|$ factor comes from the 2D Fourier transform of the electron-electron Coulomb interaction. $\frac{|\mathbf{q}|^2}{16\pi^2}$ factor comes from the conversion from ρ'_e to a_T . Now we see that the Lagrangian density of S_{Coulomb} is $\propto |\mathbf{q}|$ while that of the Maxwell term S_{Max} is $\propto f_{\mu\nu}^2 \propto |\mathbf{q}|^2$. Therefore in the long wavelength limit, the Coulomb term dominates and the Maxwell term [136] can be dropped. Taking S_{Coulomb} as our bare gauge field action we can readily read off the bare gauge field propagator inverse, which has only a transverse component

$$[\mathcal{D}_T^{(0)}]^{-1}(\Omega, \mathbf{q}) = \frac{e^2}{8\pi\epsilon_r} |\mathbf{q}|. \quad (5.4)$$

We add a superscript “(0)” in $\mathcal{D}_T^{(0)}$ to indicate that it is a bare gauge field propagator without including the screening effects from the finite density Dirac CFs.

Integrating out the gauge fields a_T gives a current-current interaction between Dirac CFs described by the following action

$$S_{\text{int}} = \frac{1}{2} \int \frac{d\Omega d^2\mathbf{q}}{(2\pi)^3} J_T(\Omega, \mathbf{q}) \mathcal{D}_T^{(0)}(\Omega, \mathbf{q}) J_T(-\Omega, -\mathbf{q}), \quad (5.5)$$

where $J_T(\Omega, \mathbf{q}) = \epsilon_{ij} \hat{q}_i J_j(\Omega, \mathbf{q})$ is the transverse component of CF current operator. For Dirac CFs the current density $J_i(\Omega, \mathbf{q}) = v_F \int d\omega d^2\mathbf{k}/(2\pi)^3 \psi^\dagger(\omega + \Omega, \mathbf{k} + \mathbf{q}) i\gamma_0 \gamma_i \psi(\omega, \mathbf{k})$ is equivalent to the transverse pseudo-spin density. Therefore the transverse current can be written as follows

$$J_T(q) = v_F \int \frac{d^3k_1}{(2\pi)^3} \frac{d^3k_2}{(2\pi)^3} (2\pi)^3 \delta^{(3)}(k_2 - k_1 - q) \psi^\dagger(k_2) [\epsilon_{ij} \hat{q}_i i\gamma_0 \gamma_j] \psi(k_1), \quad (5.6)$$

where we have used the relativistic notation $k_i = (\omega_i, \mathbf{k}_i)$, $q \equiv (\Omega, \mathbf{q})$ for brevity. The magnitude of the vector \mathbf{k}_i will be denoted by $|\mathbf{k}_i|$ so that no confusion will be caused. Because the gamma matrix $\gamma_0 \gamma_j$ in Equation (5.6) does not commute with the Dirac Hamiltonian in Equation (5.2), J_T mixes eigenstates of the two branches of the Dirac cone dispersion. In other words J_T mixes particles near the CF Fermi surface, belonging to the $\epsilon_{\mathbf{k}}^+$ branch, with their anti-particle conjugates buried deep in the Dirac sea, belonging to the $\epsilon_{\mathbf{k}}^-$ branch. However, our theory is trustworthy only as a low energy effective theory near the Fermi surface. Therefore we need to project out the interaction only between those low energy degrees of freedom near the Fermi surface. This can be done by replacing

$\psi(k_i)$ in Equation (5.6) with [136]

$$P_{\mathbf{k}_i}^{(+)}\psi(k_i) = \frac{1}{\sqrt{2}} \begin{pmatrix} ie^{-i\theta_{\mathbf{k}_i}} \\ 1 \end{pmatrix} \chi(k_i). \quad (5.7)$$

Here $P_{\mathbf{k}_i}^{(+)} \equiv \frac{1}{2}[1 + i\gamma_0\boldsymbol{\gamma} \cdot \hat{\mathbf{k}}_i]$ is the projection operator for the energy branch $\epsilon_{\mathbf{k}_i}^+$. $\theta_{\mathbf{k}_i}$ is the azimuthal angle of the momentum vector \mathbf{k}_i in the xy plane. $\chi(k_i)$ is now a scalar field representing quasiparticles near the Fermi surface.

Replacing $\psi(k_i)$ with $P_{\mathbf{k}_i}^{(+)}\psi(k_i)$ in the integrand in Equation (5.6) leads to

$$\begin{aligned} & \psi^\dagger(k_2)P_{\mathbf{k}_2}^{(+)}[\epsilon_{ij}\hat{q}_i i\gamma_0\gamma_j]P_{\mathbf{k}_1}^{(+)}\psi(k_1) \\ &= \chi^\dagger(k_2)\frac{1}{\sqrt{2}} \begin{pmatrix} -ie^{i\theta_{\mathbf{k}_2}} & 1 \end{pmatrix} \begin{bmatrix} 0 & e^{-i\theta_{\mathbf{q}}} \\ e^{i\theta_{\mathbf{q}}} & 0 \end{bmatrix} \frac{1}{\sqrt{2}} \begin{pmatrix} ie^{-i\theta_{\mathbf{k}_1}} & 1 \end{pmatrix} \chi(k_1) \end{aligned} \quad (5.8)$$

$$= \chi^\dagger(k_2)\frac{i}{2}[e^{i(\theta_{\mathbf{q}}-\theta_{\mathbf{k}_1})} - e^{i(\theta_{\mathbf{k}_2}-\theta_{\mathbf{q}})}]\chi(k_1). \quad (5.9)$$

Then we make the Fermi surface approximation: $|\mathbf{k}_2| = |\mathbf{k}_1| = k_F$ so that for $\mathbf{q} = \mathbf{k}_2 - \mathbf{k}_1$ we have [136]

$$\theta_{\mathbf{q}} = \frac{\pi}{2} + \frac{\theta_{\mathbf{k}_1} + \theta_{\mathbf{k}_2}}{2}. \quad (5.10)$$

Substituting this result into Eq. (5.9) gives

$$\psi^\dagger(k_2)P_{\mathbf{k}_2}^{(+)}[\epsilon_{ij}\hat{q}_i i\gamma_0\gamma_j]P_{\mathbf{k}_1}^{(+)}\psi(k_1) = -\chi^\dagger(k_2)e^{i\frac{\theta_{\mathbf{k}_2}-\theta_{\mathbf{k}_1}}{2}}\chi(k_1). \quad (5.11)$$

Therefore the transverse component current is [136]

$$J_T(q) = -v_F \int \frac{d^3k_1}{(2\pi)^3} \frac{d^3k_2}{(2\pi)^3} (2\pi)^3 \delta^{(3)}(k_2 - k_1 - q) e^{i\frac{\theta_{\mathbf{k}_2}-\theta_{\mathbf{k}_1}}{2}} \chi^\dagger(k_2)\chi(k_1). \quad (5.12)$$

In this expression the $e^{i\frac{\theta_{\mathbf{k}_2}-\theta_{\mathbf{k}_1}}{2}}$ factor reflects the fact that for our Dirac CF described by the Hamiltonian in Equation (5.2) the transverse pseudo-spin direction $\hat{z} \times \boldsymbol{\sigma}$ is locked to the momentum direction \mathbf{p} . So there is a nontrivial π Berry phase picked up by $J_T(\Omega, \mathbf{q})$, which is nothing but the transverse spin density, if the momentum \mathbf{k}_2 is traversed around \mathbf{k}_1 by 2π .

Substituting the expression of J_T from Equation (5.12) into Equation (5.5) leads to [136]

$$\begin{aligned} S_{\text{int}} &= \frac{1}{2} \int \prod_{i=1}^4 \frac{d^3k_i}{(2\pi)^3} (2\pi)^3 \delta^{(3)}(k_3 + k_4 - k_1 - k_2) \\ &\times \frac{8\pi\epsilon_r v_F^2}{e^2} \frac{\exp\{-\frac{i}{2}[\theta_{\mathbf{k}_1} + \theta_{\mathbf{k}_2} - \theta_{\mathbf{k}_3} - \theta_{\mathbf{k}_4}]\}}{|\mathbf{k}_1 - \mathbf{k}_3|} \chi^\dagger(k_4)\chi(k_2)\chi^\dagger(k_3)\chi(k_1). \end{aligned} \quad (5.13)$$

Then consider the interaction in the BCS channel: $k_1 = -k_2 = k \equiv (\omega, \mathbf{k})$, and $k_3 = -k_4 = k' \equiv (\omega', \mathbf{k}')$, and introduce the frequency and momentum transfer as: $\Omega = \omega' - \omega$ and $\mathbf{q} = \mathbf{k}' - \mathbf{k}$. We make Fermi surface approximations: $|\mathbf{k}| = |\mathbf{k}'| = k_F$. Then the interaction in the BCS channel can be readily read off from S_{int} as

$$V_{\text{BCS}}(\mathbf{q}) = \frac{8\pi v_F^2 \epsilon_r}{2k_F e^2} \frac{e^{-i\theta_{\mathbf{q}}}}{|\sin \frac{\theta_{\mathbf{q}}}{2}|}. \quad (5.14)$$

It can be easily shown that this interaction is repulsive in all angular momentum channels and therefore can not give any pairing [for details see Ref. [136]].

Now we incorporate the screening effects from the finite density Dirac CFs on the gauge field within the random phase approximation (RPA). In the limit $|\Omega| < v_F |\mathbf{q}| \ll \epsilon_F$, the transverse current-current response function \mathcal{R}_T of the Dirac CFs is given by $\mathcal{R}_T(\Omega, \mathbf{q}) = -\frac{\epsilon_F}{2\pi} \frac{|\Omega|}{v_F |\mathbf{q}|}$ (for details see the Appendix B.1.2) and the RPA renormalized gauge field propagator can be obtained from the Dyson equation

$$\mathcal{D}_T^{\text{RPA}}(\Omega, \mathbf{q}) = \frac{\mathcal{D}_T^{(0)}(\Omega, \mathbf{q})}{1 - \mathcal{R}_T(\Omega, \mathbf{q})\mathcal{D}_T^{(0)}(\Omega, \mathbf{q})}. \quad (5.15)$$

We can define a dynamic dielectric function as $\epsilon(\Omega, \mathbf{q}) = 1 - \mathcal{R}_T(\Omega, \mathbf{q})\mathcal{D}_T^{(0)}(\Omega, \mathbf{q})$ so that $\mathcal{D}_T^{\text{RPA}}(\Omega, \mathbf{q}) = \mathcal{D}_T^{(0)}(\Omega, \mathbf{q})/\epsilon(\Omega, \mathbf{q})$. Similar to $\mathcal{D}_T^{(0)}$, $\mathcal{D}_T^{\text{RPA}}$ will mediate a current-current interaction between Dirac CFs, which is now frequency dependent and given by $V_{\text{eff}}(\Omega, \mathbf{q}) = V_{\text{BCS}}(\mathbf{q})/\epsilon(\Omega, \mathbf{q})$. Consider a pairing order parameter $\langle \chi(-k)\chi(k) \rangle \sim e^{i\ell'\theta_{\mathbf{k}}}$ in the $\ell' = \ell + 1$ channel, which corresponds to pairing the original Dirac spinors $P_{\mathbf{k}}^{(+)}\psi$ in the ℓ channel. Note that in this Chapter 5 by angular momentum channels ℓ, ℓ' we mean the angular momentum component along the \hat{z} direction is ℓ, ℓ' . The difference between ℓ and ℓ' comes from the nontrivial Berry phase factor carried by the spinor $P_{\mathbf{k}}^{(+)}\psi(k)$ [see Eq. (5.7) and Section 5.4 for more details]. Integrating V_{eff} over the Fermi surface in the $\ell' = \ell + 1$ angular momentum channel gives a dimensionless quantity

$$\tilde{V}_{\ell}(\tilde{\Omega}) \equiv N_0 \int \frac{d\theta_{\mathbf{q}}}{2\pi} V_{\text{eff}}(\Omega, \mathbf{q}) e^{i\ell'\theta_{\mathbf{q}}} \quad (5.16)$$

$$= \alpha \int_{-\pi}^{\pi} \frac{d\theta}{2\pi} \frac{e^{i\ell\theta}}{|\sin \frac{\theta}{2}|} \frac{2}{1 + \alpha \frac{|\tilde{\Omega}|}{\sin^2 \frac{\theta}{2}}}, \quad (5.17)$$

where $|\tilde{\Omega}| = |\Omega|/\epsilon_F$. $N_0 = \epsilon_F/2\pi v_F^2$ is the density of states of the free Dirac CFs at the Fermi energy ϵ_F . In the above equation we have also introduced an effective coupling

constant $\alpha = N_0 4\pi v_F^2 \epsilon_r / 2k_F e^2 = 1/\alpha'$, with $\alpha' \equiv e^2/\epsilon_r v_F$ the fine structure constant of the Dirac CFs. That it is $1/\alpha'$, instead of α' , that serves as our coupling constant here reflects the electromagnetic duality [136] in our problem. Since we do not have a good estimation of the v_F for the composite fermions, in the following we treat α as a generic tuning parameter. Without any confusion we will continue calling \tilde{V}_ℓ an effective interaction. With \tilde{V}_ℓ we can solve the self-consistent equation of the pairing gap Δ_ℓ , which is given by [123]

$$\tilde{\Delta}_\ell(\tilde{\omega}) = - \int \frac{d\tilde{\omega}'}{2\pi} \tilde{V}_\ell(\tilde{\omega} - \tilde{\omega}') \frac{\tilde{\Delta}_\ell(\tilde{\omega}')}{\sqrt{(\tilde{\omega}')^2 + |\tilde{\Delta}_\ell(\tilde{\omega}')|^2}}, \quad (5.18)$$

where all quantities with tilde are dimensionless: frequencies $\tilde{\omega} = \omega/\epsilon_F, \tilde{\omega}' = \omega'/\epsilon_F$ and the pairing gap $\tilde{\Delta}_\ell = \Delta_\ell/\epsilon_F$. As emphasized in our previous work [123, 207], a complete solution to the pairing problem needs to take into account the fermion wavefunction renormalization factor $Z(\omega)$. This factor has an anomaly on the Fermi surface: $Z(\omega) \rightarrow 0$ as $\omega \rightarrow 0$ in the Dirac CF liquid phase, similar to the HLR picture. However, in a pairing phase this anomaly will be cutoff at frequencies of the order of the pairing gap if that gap is large enough. In other words, setting $Z(\omega) \approx 1$ should be qualitatively correct as long as the coupling constant α is not too close to its critical point value α_c . Near the critical point α_c , this vanishing of quasiparticle residue $Z(\omega) \rightarrow 0$ competes against the pairing instability and much more careful investigations are needed. We will leave that for future work and simply set $Z = 1$ in the following.

In the next section we first plot out $\tilde{V}_\ell(\tilde{\Omega})$ to show that \tilde{V}_ℓ has a sizable attraction at high frequencies for $|\ell| \geq 1$; while it is repulsive in the whole frequency range for $\ell = 0$. Then we present our numerical results to the above self-consistent gap equation for different channels ℓ .

5.3 Results

5.3.1 The effective interaction $\tilde{V}_\ell(\tilde{\Omega})$

We first notice that $\tilde{V}_\ell(\tilde{\Omega})$ is identical for angular momentum channels ℓ and $-\ell$. This reflects the fact that the interaction \tilde{V}_ℓ itself respects the particle-hole symmetry defined for the $\nu = 1/2$ Landau level problem, under which the ℓ channel pairing is transformed

into the $-\ell$ channel pairing [for details see Appendix B.2 and Ref. [2]. Therefore we only need to plot out $\tilde{V}_\ell(\tilde{\Omega})$ for channels $\ell \geq 0$. This is shown in Fig. 5.1. From this plot first

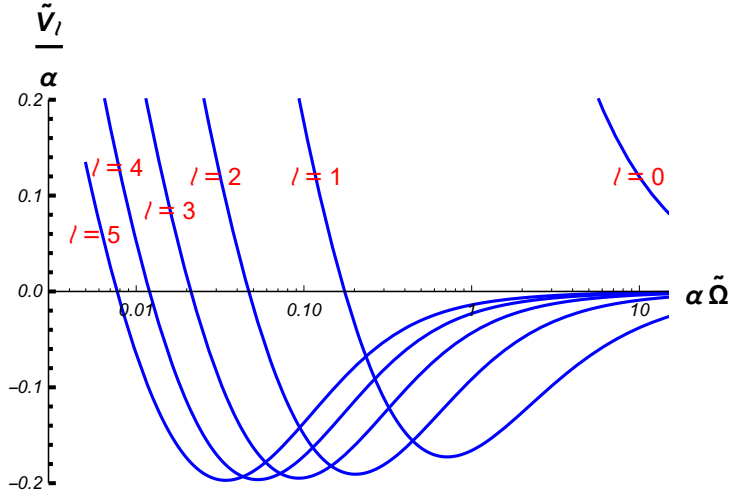


Figure 5.1: Loglinear plots of $\tilde{V}_\ell(\tilde{\Omega})/\alpha$ as a function of $\alpha\tilde{\Omega}$ for $\ell = 0, 1, 2, 3, 4, 5$. Notice that the horizontal axis is in a logarithmic scale.

we see that the $\ell = 0$ channel effective interaction is completely repulsive in the whole frequency range. Therefore there can not be any pairing in this channel. Since $\ell = 0$ channel pairing order parameter is invariant under the particle-hole symmetry transformation, this channel corresponds to the putative particle-hole symmetric Pfaffian state proposed in Ref. [2]. Therefore in our pairing mechanism, the particle-hole symmetric Pfaffian state does not exist.

For $|\ell| \geq 1$, although $\tilde{V}_\ell(\tilde{\Omega})$ is repulsive and diverges logarithmically as $\tilde{V}_\ell(\tilde{\Omega}) \sim -\frac{\alpha}{\pi} \log|\tilde{\Omega}|$ in the small frequency limit $\tilde{\Omega} \rightarrow 0$, it has considerable attractions at high frequencies. The balance between the repulsion and attraction is controlled by the coupling constant α . Depending on the magnitude of α , such a balance may be tipped over in favor of a pairing state. In the next subsection we show that this is indeed the case by solving the gap Equation (5.18) numerically.

5.3.2 Solution to the pairing gap equation

We first cut off the effective interaction $\tilde{V}_\ell(\tilde{\Omega})$ and the frequency integral at $|\tilde{\Omega}| \geq 1$ in the gap Eq. (5.18). We choose the frequency grid to be 5×10^4 and solve the gap equation by iteration until a desired convergence accuracy is achieved, following Ref. [123].

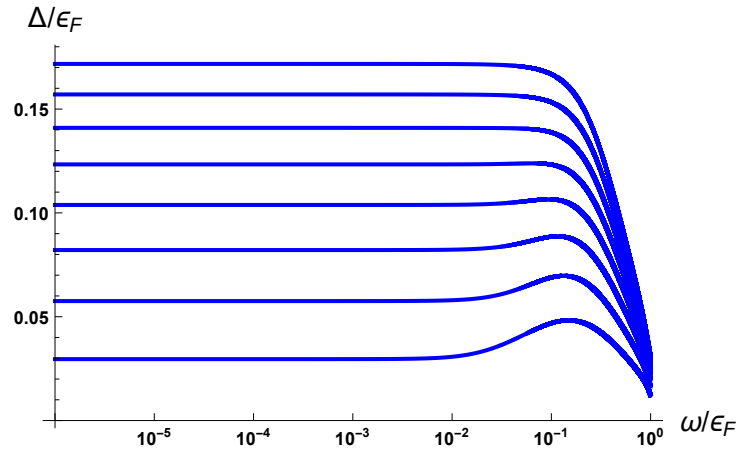


Figure 5.2: The plot of gap $\Delta_\ell(\omega)$ as a function of the frequency ω for angular momentum channel $\ell = 1$. From top to bottom: $\alpha = 24, 22, 20, 18, 16, 14, 12, 10$.

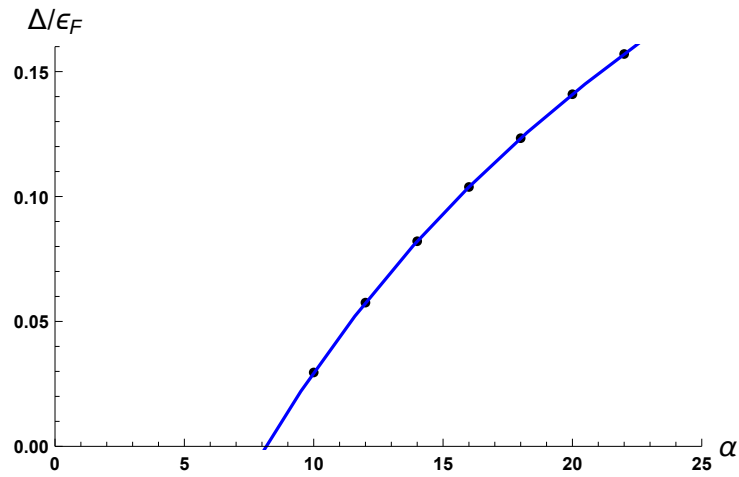


Figure 5.3: Plot of gap $\Delta_\ell = \Delta_\ell(\omega = 0)$ as a function of α for angular momentum channel $\ell = 1$. The critical value of α is estimated to be $\alpha_c \approx 8$.

Fig. 5.2 shows the results of $\Delta_\ell(\omega)$ for angular momentum channel $\ell = 1$. Different curves in this figure correspond to different values of the coupling constant α . From these curves we see that $\Delta_\ell(\omega)$ falls off rapidly as $\omega/\epsilon_F \rightarrow 1$. This is due to our sharp cutoff of \tilde{V}_ℓ at $\omega/\epsilon_F = 1$. As $\omega \rightarrow 0$, clearly $\Delta_\ell(\omega)$ reaches a finite constant $\Delta_\ell \equiv \Delta_\ell(\omega = 0)$. Remember that we are working in Matsubara frequency space. Therefore Δ_ℓ gives the $T = 0$ thermodynamic pairing gap. As we can see in Fig. 5.2 the size of Δ_ℓ decreases progressively as we decrease the coupling constant from $\alpha = 24$ to $\alpha = 10$. Naturally we would expect that Δ_ℓ eventually vanish at certain critical value of $\alpha = \alpha_c$, below which the Dirac CF liquid state is stabilized instead. This is explicitly shown for $\ell = 1$ in Fig. 5.3, where we plot out the Δ_ℓ values extracted from Fig. 5.2 for different α values considered there. An extrapolation to $\Delta_\ell = 0$ shows that the gap vanishes at $\alpha_c \approx 8$. Therefore indeed there is a quantum phase transition from the $\ell = 1$ pairing state to the Dirac CF liquid state as we decrease α across α_c towards zero.

We can do similar analysis for other higher angular momentum channels ℓ . The results for $\ell = 1, 2, 3$ are displayed in Fig. 5.4. From this plot we see that at the same coupling constant value the gap size Δ_ℓ decreases as ℓ increases. This is understandable given that the frequency range of sizable attraction in $\tilde{V}_\ell(\Omega)$ decreases with ℓ , as we can see from Fig. 5.1 (notice that the horizontal frequency axis is in a logarithmic scale). This feature is also similar to what have been found in the transverse gauge field problem in Ref. [123]. However, unlike there the critical value α_c for different channels are very close to each other in our problem. For $\ell \geq 2$, $\alpha_c \approx 7$ and we can not resolve the difference between α_c for different channels.

5.4 Discussion

As already mentioned before, the pairing angular momentum channel ℓ' for the order parameter $\langle \chi(-k)\chi(k) \rangle$ is different from that of the pairing order parameter in terms of pseudo-spinors $P_{\mathbf{k}}^{(+)}\psi(k)$ because of the spinor's Berry phase factor. Now we discuss the pairing order parameters $\hat{\Delta}$ in terms of the $P_{\mathbf{k}}^{(+)}\psi(k)$ field. A hat has been put onto $\hat{\Delta}$ to indicate that $\hat{\Delta}$ is a 2×2 matrix. In general we can parametrize this matrix as

$$\hat{\Delta}(k) = [\Delta_s(k) + \mathbf{d}(k) \cdot \boldsymbol{\sigma}]i\sigma_2, \quad (5.19)$$

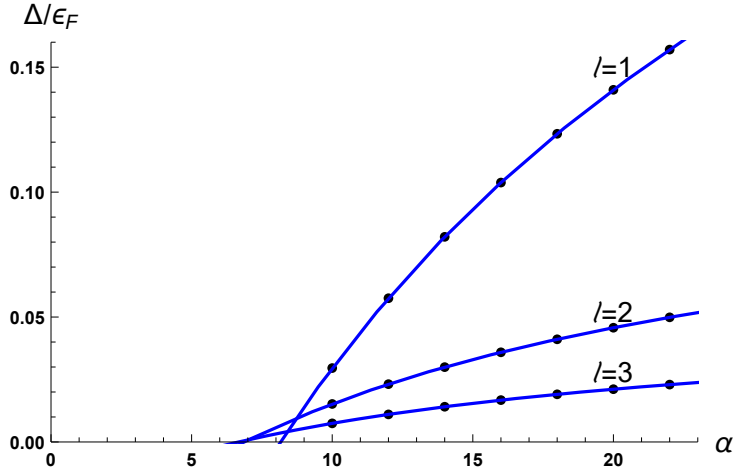


Figure 5.4: Plots of the gap $\Delta_\ell = \Delta_\ell(\omega = 0)$ as a function of the effective coupling constant α for angular momentum channel $\ell = 1, 2, 3$. The critical coupling constants for different channels are very close to each other. For $\ell = 1, \alpha_c \approx 8$; while for $\ell \geq 2, \alpha_c \approx 7$. We can not resolve the different between α_c for difference $\ell \geq 2$ channels.

where $\Delta_s(k)$ gives the pairing order parameter in the pseudo-spin singlet channel while the vector $\mathbf{d}(k)$ characterizes the triplet channel pairing. In the following discussion we assume the Cooper pairing in these two channels are decoupled. This assumption is not obvious given that the pseudo-spin is coupled to the orbital momentum and is therefore not a conserved quantity for our Dirac CFs. But we will assume such a decoupling can be approximately made when only the low energy degrees of freedom near the Fermi surface participate the pairing.

The pseudo-spin singlet channel order parameter

$$\hat{\Delta}(k) = \langle \psi^T(-k) P_{-\mathbf{k}}^{(+)} i\sigma_2 P_{\mathbf{k}}^{(+)} \psi(k) \rangle \quad (5.20)$$

is the one adopted in Ref. [2]. Substituting the definition of $P_{\mathbf{k}}^{(+)} \psi(k)$ from Eq. (5.7) into this order parameter leads to $\hat{\Delta}(k) \propto i\sigma_2 e^{-i\theta_{\mathbf{k}}} \langle \chi(k) \chi(-k) \rangle$. In other words $\Delta_s(k) \propto e^{-i\theta_{\mathbf{k}}} \langle \chi(k) \chi(-k) \rangle$. This shows explicitly that if $\Delta_s(k) \propto i\sigma_2 \Delta_\ell e^{i\ell\theta_{\mathbf{k}}}$ is in the ℓ channel, then $\langle \chi(-k) \chi(k) \rangle \propto e^{i(\ell+1)\theta_{\mathbf{k}}}$ is in a channel $\ell' = \ell + 1$, as mentioned before. Because Fermi statistics requires $\hat{\Delta}(k)$ to be antisymmetric and it is already antisymmetric in the pseudo-spin space, then $\Delta_s(k)$ needs to be *symmetric*; that is, only those *even* ℓ channels are possible. These include the Moore-Read Pfaffian state, corresponding to the pairing channel $\ell = -2$, and its particle-hole conjugate, the anti-Pfaffian state [100,

101], corresponding the $\ell = 2$ pairing channel(see Appendix B.3 and Ref. [2] for more details). Although the $\ell = 0$ channel pairing is also symmetry allowed, it is energetically unfavorable in our pairing mechanism as emphasized previously.

If the order parameter is chosen in the pseudo-spin triplet channel instead: $\hat{\Delta}(k) = \langle \psi^T(-k)P_{-\mathbf{k}}^{(+)} \mathbf{d} \cdot \boldsymbol{\sigma} i\sigma_2 P_{\mathbf{k}}^{(+)} \psi(k) \rangle$, then the order parameter needs to be *antisymmetric* functions of the momentum. In other words, only *odd* ℓ pairing channels are allowed. These include the $|\ell| = 1$ channels, which have the largest pairing gap among all channels in our numerical solutions when α is large and not too close to α_c , as seen in Fig. 5.4.

We consider that both the pseudo-spin singlet and triplet order parameters are allowed so that the spatial pairing channel ℓ can be either even or odd. This is in contrast to the Ref. [2], where only the pseudo-spin singlet order parameter was considered such that only even ℓ channels were possible. The competition between different ℓ channels requires much more careful analysis especially given that the α_c we have found for different channels are quite close to each other, although the largest pairing gap of $|\ell| = 1$ channel for typical coupling constants in Fig. 5.4 tends to suggest that $|\ell| = 1$ channels are most robust. If $|\ell| = 1$ channels, or other $|\ell| \neq 2$ channels, are indeed more favorable than $|\ell| = 2$ channels, then interesting questions to ask would be: what is the nature of these states? What do the corresponding lowest Landau level wavefunctions look like? Do they support excitations possessing non-abelian statistics? These questions need to be further investigated in the future.

5.5 Conclusion

To conclude we have constructed a specific pairing mechanism for the Dirac composite fermions proposed recently for the half filled Landau levels. By taking advantages of the attraction of a dynamically screened effective interaction at high Matsubara frequencies we show that there can be nonzero pairing in angular momentum channels $|\ell| \geq 1$ at certain coupling constant values. As the coupling constant is varied, there can be a quantum phase transition from the pairing state to the Dirac CF liquid state. Apart from the well known Moore-Read Pfaffian state($\ell = -2$) and its particle-hole conjugate($\ell = 2$): the anti-Pfaffian state, other Pfaffian states are also possible. However, in contrast to

the channels $|\ell| \geq 1$, the $\ell = 0$ particle-hole symmetric channel effective interaction is completely repulsive in the whole frequency range considered, which therefore renders the putative particle-hole symmetric Pfaffian state impossible in our pairing mechanism.

APPENDIX A

Appendices for Chapter 3

A.1 Recursive Green's function method

The recursive Green's function method studies a quasi-one-dimensional system, which is a square lattice with a very long axis of length La along the x -direction and a shorter axis of width Ma along the y -direction in our problem. The system can be built up recursively in the x -direction by connecting many one-dimensional stripes together. Each stripe has a direct coupling only to its nearest neighboring ones. This property is essential for the recursion. In our Hamiltonian \mathcal{H} the third nearest neighbor hopping t'' provides the farthest direct coupling along the x -direction. It connects two sites $2a$ apart. Therefore each stripe necessarily contains two columns of the square lattice sites so that the direct coupling exists only between two adjacent stripes. The blue dashed rectangle in Fig. A.1 shows one such stripe. We define each of such stripes as a principal layer, so each layer contains $2M$ sites.

Our goal is to compute the diagonal matrix elements of the exact Green's function G in order to get the DOS. For this purpose we first calculate $G_i \equiv \langle i|G|i \rangle$ for each layer i . The ket $|i \rangle$ represents a state where the Bogoliubov quasiparticles are found in the i th principal layer. It has $4M$ components, of which the first $2M$ ones give the electron part wavefunction, while the rest $2M$ ones define the hole part. Therefore $G_i = G_i(j, j')$ is a $4M \times 4M$ matrix with $j, j' = 1, 2, \dots, 4M$. For brevity we will suppress the matrix element indices hereafter, if there is no confusion.

The exact Green's function G_i can be computed by (for derivations see Ref.[191])

$$G_i = [G_i^{0-1} - \mathcal{H}_{i,i-1} G_{i-1}^L \mathcal{H}_{i-1,i} - \mathcal{H}_{i,i+1} G_{i+1}^R \mathcal{H}_{i+1,i}]^{-1}, \quad (\text{A.1})$$

as schematically shown in Fig. A.1. Here $G_i^0 \equiv [E - \langle i|\mathcal{H}|i \rangle]^{-1}$ is the bare Green's function of the isolated i th principal layer, with the superscript 0 indicating it is defined

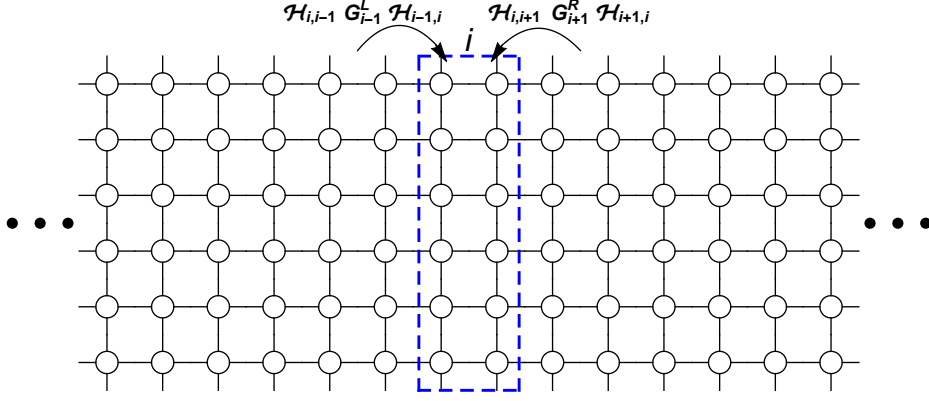


Figure A.1: Schematic diagram of the recursive Green's function calculation. The sites enclosed by the blue dashed rectangle define the i th principal layer. The exact Green's function G_i has two self-energy contributions from both the left semi-infinite stripe and the right one. The left stripe is characterized by its surface Green's function G_{i-1}^L with the $(i-1)$ th layer its surface; while the right one is characterized by another surface Green's function G_{i+1}^R with the $(i+1)$ th layer its surface.

as if all other layers are deleted. The matrix $\mathcal{H}_{i,i-1} \equiv \langle i | \mathcal{H} | i-1 \rangle$ contains all the Hamiltonian matrix elements connecting sites in the layer $i-1$ to the layer i . Similarly $G_{i-1}^L \equiv \langle i-1 | G^L | i-1 \rangle$ is a matrix defined on the $(i-1)$ th principal layer, where G^L is the exact Green's function of a subsystem of our original lattice with all layers to the right of the $(i-1)$ th layer deleted, as shown in Fig. A.2. The superscript "L" here means that this subsystem, including a left lead, is extended to the $x = -\infty$. Since the $(i-1)$ th layer is the surface of this subsystem, we will call G_{i-1}^L the left surface Green's function. Similarly $G_{i+1}^R \equiv \langle i+1 | G^R | i+1 \rangle$ is another surface Green's function of a subsystem of our original lattice with all the layers to the left of the $(i+1)$ th layer deleted. Once G_{i-1}^L, G_{i+1}^R are known, G_i can be computed immediately from Eq. A.1.

The central task is then to compute G_{i-1}^L and G_{i+1}^R . This can be done recursively. Take G_{i-1}^L as an example. We start with the leftmost layer $i = 1$. There our central system is connected to a semi-infinite lead, which contains infinite number of layers of the same width M , numbered by $i = \dots, -2, -1, 0$. We denote this left lead's surface Green's function as G_s^L , whose computation will be presented in the following Appendix A.1.1. Then we add the $i = 1$ st layer of our central system, but not other layers, to this lead so that we get a new semi-infinite stripe. This new stripe has a new surface Green's

function denoted as G_1^L , which can be computed from G_s^L by

$$G_1^L = [G_1^{0-1} - \mathcal{H}_{1,0} G_s^L \mathcal{H}_{0,1}]^{-1} \quad (\text{A.2})$$

where $\mathcal{H}_{1,0}$ connects sites in the surface layer $i = 0$ of the left lead to the $i = 1$ st layer of our central system. Similarly we can repeat this process by adding one more layer of our central system to the semi-infinite stripe each time, and build up the whole system. In general at an intermediate stage, we may have a semi-infinite stripe, whose surface is, say, the $(i - 2)$ th layer with a surface Green's function G_{i-2}^L . Then the $(i - 1)$ th layer is connected to that stripe to form a new semi-infinite system, which has a new surface Green's function G_{i-1}^L . And G_{i-1}^L can be calculated from G_{i-2}^L by the following recursive relation

$$G_{i-1}^L = [G_{i-1}^{0-1} - \mathcal{H}_{i-1,i-2} G_{i-2}^L \mathcal{H}_{i-2,i-1}]^{-1} \quad (\text{A.3})$$

This is schematically illustrated in Fig. A.2.

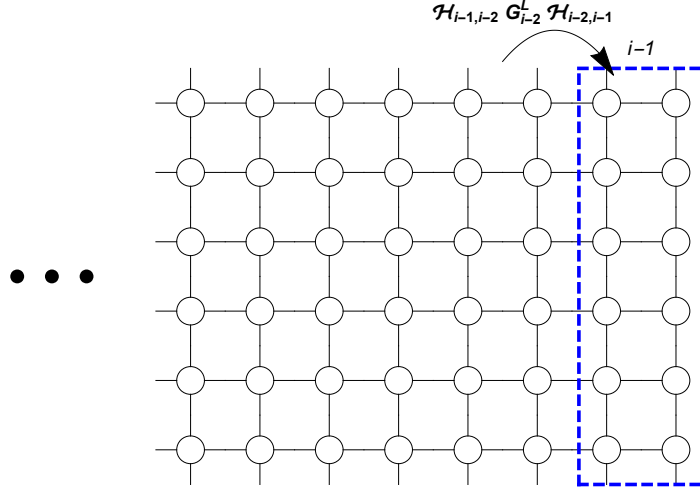


Figure A.2: Schematic diagram for the G_{i-1}^L computation. The sites enclosed by the blue dashed rectangle belong to the $(i - 1)$ th principal layer, which is also the surface layer of this semi-infinite stripe.

Similarly the right surface Green's function G_{i+1}^R can be computed from G_{i+2}^R via

$$G_{i+1}^R = [G_{i+1}^{0-1} - \mathcal{H}_{i+1,i+2} G_{i+2}^R \mathcal{H}_{i+2,i+1}]^{-1} \quad (\text{A.4})$$

This recursive relation starts with $G_{L/2}^R$ at the rightmost layer $i = L/2$ of our central system, where it is connected to another semi-infinite stripe lead extended to $x = \infty$.

Note that the central system has only $L/2$ principal layers because each layer contains two columns of the sites, and there are only L columns in total. The layers in this right lead are numbered by $i = L/2 + 1, L/2 + 2, \dots$. We denote the right lead's surface Green's function as G_s^R . Then $G_{L/2}^R$ can be computed from G_s^R by

$$G_{L/2}^R = [G_{L/2}^0{}^{-1} - \mathcal{H}_{L/2, L/2+1} G_s^R \mathcal{H}_{L/2+1, L/2}]^{-1} \quad (\text{A.5})$$

where $\mathcal{H}_{L/2, L/2+1}$ connects our central system to the right lead and contains t, t', t'' only.

A.1.1 Surface Green's function G_s^L, G_s^R of the leads

G_s^L, G_s^R can be computed by solving a self-consistent 2×2 matrix equation. We now give a detail discussion on how to compute G_s^L , but only briefly mention the final results for G_s^R at the end.

The left lead Hamiltonian contains only the hopping parameters t, t', t''

$$\begin{aligned} H_{\text{lead}} = & \sum_{i=-\infty}^0 \sum_{j=1}^M \{ -t [c_{i-1, j}^\dagger c_{i, j} + c_{i, j+1}^\dagger c_{i, j}] \\ & + t' [c_{i-1, j+1}^\dagger c_{i, j} + c_{i-1, j-1}^\dagger c_{i, j}] \\ & - t'' [c_{i-2, j}^\dagger c_{i, j} + c_{i, j+2}^\dagger c_{i, j}] + \text{h.c.} - \mu c_{i, j}^\dagger c_{i, j} \} \end{aligned} \quad (\text{A.6})$$

To be compatible with our central system Hamiltonian, which contains superconductivity, our lead Hamiltonian should have both an electron part and a hole part so that the full Hamiltonian $\mathcal{H}_{\text{lead}}$ is

$$\mathcal{H}_{\text{lead}} = \begin{pmatrix} H_{\text{lead}} & 0 \\ 0 & -H_{\text{lead}} \end{pmatrix}. \quad (\text{A.7})$$

Correspondingly the surface Green's function takes a block diagonal form

$$G_s(E^+) \begin{pmatrix} [E^+ - H_{\text{lead}}]^{-1} & 0 \\ 0 & [E^+ + H_{\text{lead}}]^{-1} \end{pmatrix} \quad (\text{A.8})$$

where for brevity we have introduced $E^+ = E + i\delta$. We will denote the two diagonal terms as $G_{ee} = [E^+ - H_{\text{lead}}]^{-1}$ and $G_{hh} = [E^+ + H_{\text{lead}}]^{-1}$. Apparently G_{hh} can be obtained from G_{ee} by simple substitutions: $\{t, t', t'', \mu\} \Rightarrow \{-t, -t', -t'', -\mu\}$. Therefore we only need to discuss how to compute G_{ee} .

Because of the periodic boundary condition along the y -direction, we can decompose $G_{ee}(E^+)$ into different momentum k_y channels

$$G_{ee}(E^+) = \sum_{k_y} |\chi_{k_y}\rangle \langle \chi_{k_y}| g(k_y, E^+) \quad (\text{A.9})$$

with $|\chi_{k_y}\rangle = \sum_{j=1}^M \frac{e^{ik_y j a}}{\sqrt{M}} |j\rangle$, and $k_y = \frac{2n\pi}{Ma}$ with $n = 1, 2, 3, \dots, M$. Each channel is described by a semi-infinite one dimensional chain effective Hamiltonian $H_{\text{eff}}(k_y) \equiv \langle \chi_{k_y} | H_{\text{lead}} | \chi_{k_y} \rangle$, given by

$$H_{\text{eff}}(k_y) = \sum_{i=-\infty}^0 \{ (-2t \cos k_y - 2t'' \cos 2k_y - \mu) c_i^\dagger c_i + [(-t + 2t' \cos k_y) c_i^\dagger c_{i-1} - t'' c_i^\dagger c_{i-2} + \text{h.c.}] \}. \quad (\text{A.10})$$

And $g(k_y, E^+)$ is the corresponding surface Green's function of this one dimensional chain.

To compute $g(k_y, E^+)$ we group every two adjacent sites $(c_{i-1}^\dagger, c_i^\dagger)$ of the one dimensional chain together into a cell, indexed by the cell number n , so that $H_{\text{eff}}(k_y)$ can be rewritten in a form such that direct couplings exist only between two nearest neighboring cells

$$H_{\text{eff}}(k_y) = \sum_{n=-\infty}^0 (c_{2n-1}^\dagger, c_{2n}^\dagger) \begin{bmatrix} -t'' & -t + 2t' \cos k_y \\ 0 & -t'' \end{bmatrix} \begin{pmatrix} c_{2n-3} \\ c_{2n-2} \end{pmatrix} + \text{h.c.} \\ + \sum_{n=-\infty}^0 (c_{2n-1}^\dagger, c_{2n}^\dagger) \begin{bmatrix} -2t \cos k_y - 2t'' \cos 2k_y - \mu & & \\ & -t + 2t' \cos k_y & \\ & & -t + 2t' \cos k_y \\ & & & -2t \cos k_y - 2t'' \cos 2k_y - \mu \end{bmatrix} \begin{pmatrix} c_{2n-1} \\ c_{2n} \end{pmatrix}. \quad (\text{A.11})$$

Since $g(k_y, E^+)$ is a surface Green's function, it should satisfy the same recursive relation given in Eq. (A.3), which is rewritten here as

$$g = [G_0^{0-1} - [H_{\text{eff}}]_{0,-1} G_{-1}^L [H_{\text{eff}}]_{-1,0}]^{-1} \quad (\text{A.12})$$

The only difference from there is now all the matrix elements are defined between different cells instead of layers. For clarity we have suppressed the k_y and E^+ dependence of all the quantities in this equation. G_0^0 is the bare Green's function of the isolated single cell

$n = 0$. Because each cell contains two sites, G_0^0 is a 2×2 matrix, given by

$$G_0^{0-1} \equiv E^+ - [H_{\text{eff}}]_{0,0} = E^+ - \begin{bmatrix} -2t \cos k_y - 2t'' \cos 2k_y - \mu & -t + 2t' \cos k_y \\ -t + 2t' \cos k_y & -2t \cos k_y - 2t'' \cos 2k_y - \mu \end{bmatrix}. \quad (\text{A.13})$$

Similarly the effective hopping matrices between the cell $n = 0$ and cell $n = -1$ can be read off directly from Eq. (A.11)

$$[H_{\text{eff}}]_{0,-1} = \begin{bmatrix} -t'' & -t + 2t' \cos k_y \\ 0 & -t'' \end{bmatrix}, \quad [H_{\text{eff}}]_{-1,0} = [H_{\text{eff}}]_{0,-1}^\dagger \quad (\text{A.14})$$

By definition G_{-1}^L in Eq. (A.12) is the surface Green's function of the same chain but with the cell $n = 0$ deleted. However, since the chain is semi-infinite, deleting the surface cell only gives another identical semi-infinite chain. Therefore G_{-1}^L should be the same as g . Then Eq. (A.12) becomes a self-consistent equation of g as

$$g^{-1} = \begin{bmatrix} E^+ + 2t \cos k_y + 2t'' \cos 2k_y + \mu & t - 2t' \cos k_y \\ t - 2t' \cos k_y & E^+ + 2t \cos k_y + 2t'' \cos 2k_y + \mu \end{bmatrix} - \begin{bmatrix} -t'' & -t + 2t' \cos k_y \\ 0 & -t'' \end{bmatrix} g \begin{bmatrix} -t'' & 0 \\ -t + 2t' \cos k_y & -t'' \end{bmatrix}. \quad (\text{A.15})$$

With this 2×2 matrix equation, for each k_y , we solve for g numerically by iterations until the results converge. Then the computed $g(k_y, E)$ is substituted back into Eq. (A.9) of $G_{\text{ee}}(E^+)$ to get G_{s}^L .

Similar derivations can be carried out for the right lead Green's function G_{s}^R . It turns out $G_{\text{s}}^R = (G_{\text{s}}^L)^T$, where T is the transpose operation. This result is a manifestation of the fact that the two semi-infinite leads can be connected to each other by a reflection symmetry operation along the x -direction.

A.2 Bond phase field θ_{ij} of Δ_{ij}

The phase field θ_{ij} is defined on the bond \overline{ij} , which connects two nearest neighboring sites i and j . Therefore it is natural to use the phase fields ϕ_i and ϕ_j , on the site i and

site j respectively, to define $\theta_{ij} = \frac{\phi_i + \phi_j}{2}$. However this definition does not guarantee that whenever a closed path encloses a vortex, θ_{ij} along that path will pick up a 2π phase as the vortex is wound once. Therefore this θ_{ij} can not give the correct vortices configuration. It is incorrect whenever a vortex branch cut is crossed. To see this clearly, we map the phase field ϕ_i along a closed path that encloses a vortex onto a unit circle since ϕ_i is defined only modulo 2π , as schematically shown in Fig. A.3. In this figure, the blue arc segment corresponds to the bond \overline{ij} on the closed path. Therefore an appropriate θ_{ij} should be equal to some value of the phase field on this segment. When the bond \overline{ij} does not cross any branch cut, $\theta_{ij} = \frac{\phi_i + \phi_j}{2}$ is indeed on the blue segment and can be a good definition of θ_{ij} , as illustrated in Fig. A.3a; however, if the bond \overline{ij} crosses a branch cut, we see that $\frac{\phi_i + \phi_j}{2}$, indicated by the red arrow in Fig. A.3b, is not on the blue segment and can not be an appropriate definition of θ_{ij} . In this latter case, $\theta_{ij} = \frac{\phi_i + \phi_j}{2} - \pi$ instead can be a good definition, since it falls onto the blue arc segment, as indicated by the blue arrow in Fig. A.3b.

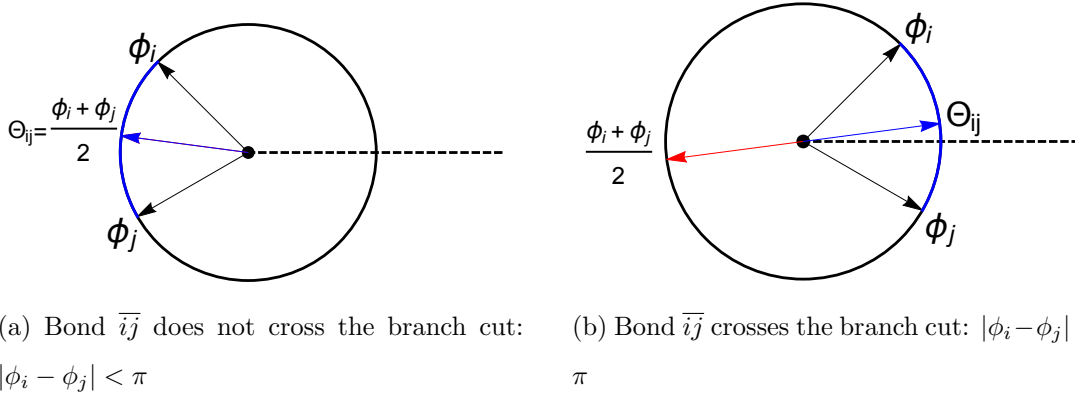


Figure A.3: The black dot in the center represents a vortex. The dashed line, extended to the infinity, is its branch cut. The blue arc segment corresponds to the bond \overline{ij} on a closed path. The phases ϕ_i, ϕ_j are measured counter-clock wisely from the upper side of the branch cut. In Fig. A.3a, the bond \overline{ij} does not cross the branch cut, and $(\phi_i + \phi_j)/2$ is a good definition for θ_{ij} ; however, if the bond \overline{ij} crosses a branch cut, as in Fig. A.3b, then $(\phi_i + \phi_j)/2$ can not be a correct definition of θ_{ij} . Instead $(\phi_i + \phi_j)/2 - \pi$ gives an appropriate definition of θ_{ij} .

Based on these two scenarios, a good definition of θ_{ij} will be

$$e^{i\theta_{ij}} = e^{i\frac{\phi_i + \phi_j}{2}} \operatorname{sgn}\left[\cos\frac{\phi_i - \phi_j}{2}\right] \quad (\text{A.16})$$

This definition of θ_{ij} guarantees that whenever the phase field ϕ_i along a closed path crosses a branch cut once, the defined θ_{ij} crosses the same branch cut once as well. When there are multiple vortices enclosed, we only need to linearly superpose the contributions from each vortex together to the field ϕ_i and θ_{ij} respectively. It is not difficult to see that the above definition of θ_{ij} is still good in these cases. For our numerical calculation convenience, we rewrite the above definition of θ_{ij} in a slightly different way

$$e^{i\theta_{ij}} = \frac{e^{i\phi_i} + e^{i\phi_j}}{|e^{i\phi_i} + e^{i\phi_j}|} \quad (\text{A.17})$$

A.3 The ansatz $\left(\frac{\xi}{r_{\text{eff}}}\right)^q = \sum_n \left(\frac{\xi}{r_n}\right)^q$

The pairing amplitude on the bond, that connects two nearest neighboring sites \mathbf{r}_i and \mathbf{r}_j , is calculated by the following ansatz:

$$|\Delta_{ij}| = \Delta \frac{r_{\text{eff}}}{\sqrt{\xi^2 + r_{\text{eff}}^2}} \quad (\text{A.18})$$

with r_{eff} given by

$$\left(\frac{\xi}{r_{\text{eff}}}\right)^q = \sum_{n=1}^{N_v} \left(\frac{\xi}{r_n}\right)^q \quad (\text{A.19})$$

where $r_n = \left|\frac{\mathbf{r}_i + \mathbf{r}_j}{2} - \mathbf{R}_n\right|$ is the distance from the bond center $\frac{\mathbf{r}_i + \mathbf{r}_j}{2}$ to the n th vortex center \mathbf{R}_n , q is some positive number, and N_v is the total number of vortices.

If we consider a special case that there is only one vortex, for instance the n th vortex, then Eq. (A.19) is reduced to $r_{\text{eff}} = r_n$, and

$$|\Delta_{ij}| = \Delta \frac{r_n}{\sqrt{r_n^2 + \xi^2}} \quad (\text{A.20})$$

In other words, we can define the pairing amplitude $|\Delta_n|$ for the case when only the n th vortex is present as follows

$$|\Delta_n| \equiv \Delta \frac{r_n}{\sqrt{r_n^2 + \xi^2}} \quad (\text{A.21})$$

so that $|\Delta_{ij}| = |\Delta_n|$.

When more than the n th vortex is present, $|\Delta_{ij}|$ should become smaller than $|\Delta_n|$. This requires $r_{\text{eff}} < r_n$ because $|\Delta_{ij}|$ is an increasing function of r_{eff} , as seen in Eq. (A.18). We sum the contributions from each vortex to $|\Delta_{ij}|$ simply by adding the q th inverse moment ($q > 0$) of all r_n together to define an effective distance r_{eff} as in Eq. (A.19). Using the q th inverse moment, instead of the q th moment guarantees that $r_{\text{eff}} < r_n$ when there is more than one vortex. Furthermore it ensures that the terms $(\frac{\xi}{r_n})^q$ with small r_n on the right hand side of Eq. (A.19) contribute more significantly than those with larger r_n . This is consistent with the physical intuition that vortices nearby are more important in determining r_{eff} , and therefore $|\Delta_{ij}|$, than those that are far away. Also when there are more vortices present, N_v becomes larger and the resultant $|\Delta_{ij}|$ from Eq. (A.19) becomes smaller. This again agrees with our expectation.

The $|\Delta_{ij}|$ defined above increases monotonically with the parameter q for a given vortices configuration. To see this we only need to show r_{eff} increases with q . For that purpose we can rewrite Eq. (A.19) as follows

$$\log \frac{r_{\min}}{r_{\text{eff}}} = \frac{1}{q} \log \left\{ 1 + \sum'_n \left(\frac{r_{\min}}{r_n} \right)^q \right\} \quad (\text{A.22})$$

where $r_{\min} = \min\{r_n\}$ is the distance between the closest vortex and the bond, and the prime sign in the summation means this closest vortex is excluded. The right hand side of Eq. (A.22) is a monotonic decreasing function of q because in the summation each $\frac{r_{\min}}{r_n} < 1$. Therefore r_{eff} increases monotonically with q , so does $|\Delta_{ij}|$.

An appropriate value of q can not be determined without solving the whole problem self-consistently, therefore we performed simulations for different q to see if our conclusions depend on q or not. One example data of the oscillation spectrum for the two-fold DDW order case is shown in Fig. A.4. From this figure, we observe that the oscillation amplitude decreases as q is increased from $q = 1$ to $q = 3$. This is consistent with the analyses that $|\Delta_{ij}|$ is a monotonic increasing function of q , since larger q gives larger $|\Delta_{ij}|$, which means stronger vortex scattering and therefore stronger suppression of the oscillation amplitudes.

Although the oscillation amplitudes can depend significantly on q , the oscillation frequencies remain unaffected by varying the q values, therefore the conclusion of Onsager's

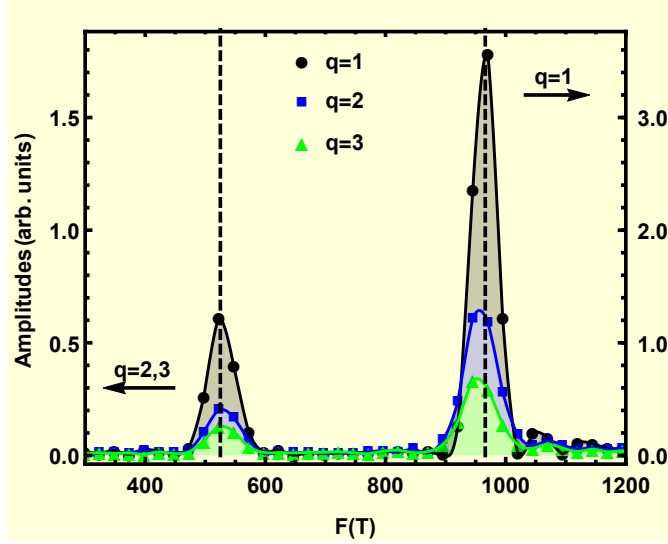


Figure A.4: Oscillation spectrum of the DOS for the two fold DDW order model with different q values but a fixed Δ . Note that the vertical axis scale for $q = 1$ is different from those for other q values. The two vertical dashed lines mark the two frequencies $F_e = 525T, F_h = 966T$.

relation being robust against the vortex scattering does not depend on the value of q .

A.4 Check of the results in Ref.[1]

We have checked the Fig.1 and Fig.3 of Ref.[1], using the same parameter sets, and find our conclusions remain the same. For both these two cases, the normal state, without magnetic field, can be described by the following Hamiltonian

$$\begin{aligned}
 H = & -t \sum_{\langle i,j \rangle} c_i^\dagger c_j + t' \sum_{\langle\langle i,j \rangle\rangle} c_i^\dagger c_j \\
 & + \sum_{\langle i,j \rangle} i (-1)^{x_i+y_i} \eta_{ij} \frac{W_0}{4} c_i^\dagger c_j - \mu \sum_i c_i^\dagger c_i.
 \end{aligned} \tag{A.23}$$

In this Hamiltonian the third term is a two-fold DDW order (or the staggered flux state order), and $\eta_{ij} = \pm 1$ is again the local d -wave symmetry factor.

1. First consider the Fig.1 of Ref.[1]. We use the same parameters $t = 1, t' = 0.3t, W_0 = 1.0t, \mu = -0.949t$. The normal state Fermi surface consists of four hole pockets with an area $\frac{A_F}{(2\pi/a)^2} \approx 2.5\%$ each. Fig. A.5 shows the computed DOS. We see there is no noticeable shift in the oscillation frequency when the vortex

scattering is present.

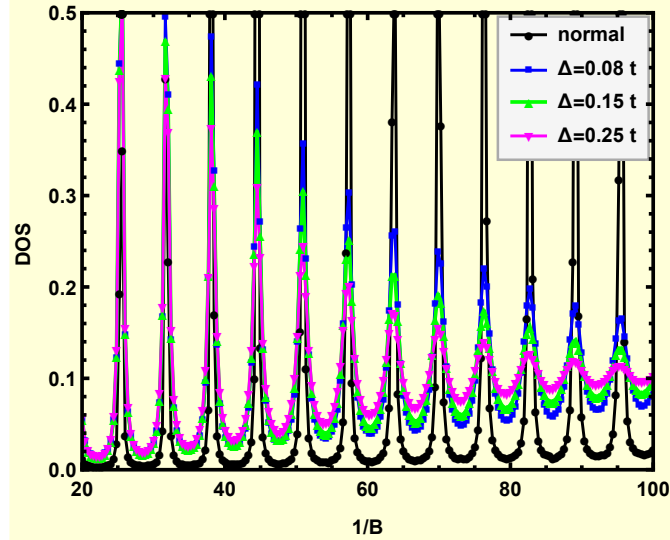


Figure A.5: DOS oscillation for $t = 1, t' = 0.3t, W_0 = 1.0t, \mu = -0.949t$. The unit for the field B is $\frac{\Phi_0}{2\pi a^2}$, with $\Phi_0 = hc/e$ the full flux quantum and a the lattice spacing. And the DOS unit is states/ t . In the legends the “normal” means $\Delta = 0$. The lattice size is $L = 2000, M = 80$, and in the Eq. (A.19) of $r_{\text{eff}}, q = 1$ rather than $q = 2$ has been chosen here.

2. Then consider the Fig.3 of Ref.[1]. In this case, the normal state does not have DDW, so $W_0 = 0$. For $t = 1, t' = 0.14t, \mu = -2.267t$, the obtained Fermi surface contains only a large hole pocket with an area $\frac{A_F}{(2\pi/a)^2} \approx 14\%$ at the Brillouin zone center. Fig. A.6 shows the corresponding DOS results. We see the oscillation amplitude gets heavily damped as Δ increases. Moreover, a small frequency shift $\delta F/F \approx 2\%$ becomes noticeable. However, this is different from a large 30% shift found in Ref.[1]. Also this 2% shift does not contradict our previous conclusion of no noticeable frequency shift. Because the shift here is obtained at magnetic fields that are larger than the experimentally applied fields ($\sim 50\text{T}$) by an order of magnitude. In Fig. A.6, $\frac{1}{B} = 10$ corresponds to $B = \frac{1}{10} \frac{\Phi_0}{2\pi a^2} \approx 450\text{T}$, since $\Phi_0/2\pi a^2 \approx 4500\text{T}$ if we take $a = 3.83\text{\AA}$ for YBCO.

Now we comment on some differences/equivalences between Ref.[1] and the Chapter 2 of this thesis on how to determine the superconductivity order parameter phase field ϕ_i .

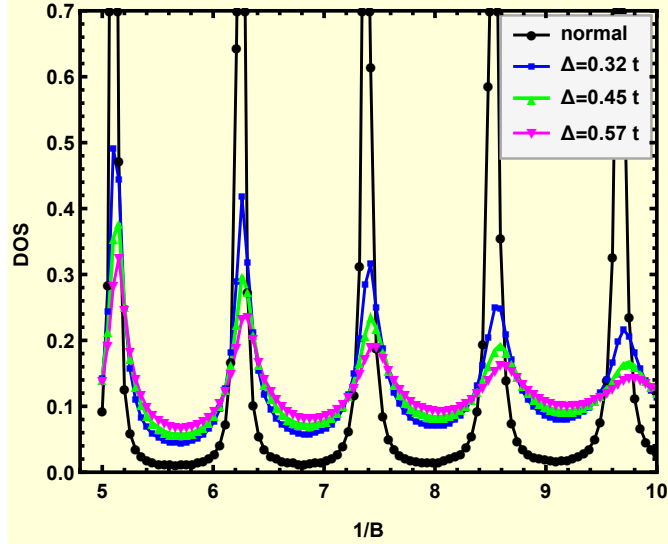


Figure A.6: DOS oscillation for $t = 1, t' = 0.14t, W_0 = 0, \mu = -2.267t$. In this simulation the system size is $L = 1000, M = 100$.

- Without vortices, the superfluid velocity $\mathbf{v}_s(\mathbf{r})$ can be obtained by minimizing the Ginzburg-Landau free energy, which in its continuum limit is

$$\mathcal{F} = \int d^2r \left\{ C \frac{1}{2} |\Delta(\mathbf{r})|^2 |\mathbf{v}_s(\mathbf{r})|^2 + \frac{\mathbf{h}^2}{8\pi} \right\}, \quad (\text{A.24})$$

where $\mathbf{v}_s(\mathbf{r}) = \frac{1}{m^*} [\hbar \nabla \phi(\mathbf{r}) - e^* \mathbf{A}/c]$ and $\mathbf{h} = \nabla \times \mathbf{A}$ is the magnetic field. The constant C is an \mathbf{r} independent constant, which is needed there to ensure that the first term in the curly braces has the correct dimension of a free energy density. In both Ref.[1] and our calculation the field \mathbf{h} is approximated by the external magnetic field \mathbf{B} . In Ref.[1] this is enforced by the constraint $\sum_{\text{plaquette}} A_{ij} = Ba^2$, where $A_{ij} = \int_{\mathbf{r}_i}^{\mathbf{r}_j} \mathbf{A} \cdot d\mathbf{l}$ and the summation is over all four bonds of a square plaquette. As a consequence of such an approximation, the second term of \mathcal{F} becomes a constant and can be dropped out. Then after the above integral being converted into a discrete sum for a lattice calculation, the free energy takes the following form

$$\mathcal{F} = \sum_{\bar{i}\bar{j}} C \frac{1}{2} |\Delta_{ij}|^2 |v_s(\mathbf{r}_{ij})|^2, \quad (\text{A.25})$$

where the summation is over all bonds $\bar{i}\bar{j}$, Δ_{ij} and $v_s(\mathbf{r}_{ij})$ are all defined on the bond $\bar{i}\bar{j}$, and $\mathbf{r}_{ij} = (\mathbf{r}_i + \mathbf{r}_j)/2$. This is the free energy used in Ref.[1]. However, the expression of $v_s(\mathbf{r}_{ij})$ needs some further clarifications. In its discretized form, (setting

$\hbar = e = c = m_e = a = 1$ for better comparison with Ref.[1]), $v_s(\mathbf{r}_{ij})$ is given by

$$v_s(\mathbf{r}_{ij}) = \int_{\mathbf{r}_j}^{\mathbf{r}_i} \mathbf{v}_s(\mathbf{r}) \cdot d\mathbf{l} = \frac{\phi_i - \phi_j}{2} - A_{ij}. \quad (\text{A.26})$$

Comparing this expression with the formula $v_s = (\phi_i - \phi_j) - A_{ij}$ used in Ref.[1], we see that there is a factor of 1/2 difference in the first term of v_s . The factor of 1/2 in the first term of v_s comes from the fact that the superconductivity momentum is carried by a Cooper pair which has a mass twice of that of an electron: $m^* = 2m_e$. There is no factor of 1/2 in front of A_{ij} because the Cooper pair also carries a charge which is twice of that of an electron: $e^* = 2(-e)$ so that $e^*\mathbf{A}/m^*c = (-e)\mathbf{A}/m_e c$. Therefore Eq. (A.26) should be the correct one for v_s .

In our case the superfluid velocity \mathbf{v}_s is obtained by solving the London equation instead, plus the Maxwell equations. However we know that minimizing the superconductor Ginzburg-Landau free energy will just give us the London equation. Therefore solving the London equation

$$\frac{4\pi\lambda^2}{c} \nabla \times \mathbf{J}_s + \mathbf{h} = 0 \quad (\text{A.27})$$

for the superfluid velocity $m\mathbf{v}_s(\mathbf{r})$ is equivalent to the free energy minimization in Ref.[1].

- When there are vortices, the free energy minimization in Ref.[1] is subjected to an additional constraint $\sum_{\text{loop}} \Delta\phi_i = 2\pi n$, where n is the number of vortices enclosed in the loop. While in our case, this constraint has been taken care of by augmenting the London equation with an additional vortex core term on the right hand side:

$$\frac{4\pi\lambda^2}{c} \nabla \times \mathbf{J}_s + \mathbf{h} = \hat{z} \Phi_s \sum_n \delta(\mathbf{r} - \mathbf{R}_n). \quad (\text{A.28})$$

Our expression of $m\mathbf{v}_s(\mathbf{r})$ in Eq. (3.11) is an explicit solution to this equation [73]. Therefore our calculation of $m\mathbf{v}_s$ is equivalent to the free energy minimization scheme in Ref.[1] even in the presence of vortices.

- In Ref.[1] the random vortex configurations are determined by a Monte Carlo annealing process which takes repulsion between vortices into account. We did not do such an annealing. Instead we simply take the vortex positions to be purely random, but we average our quantities over many different vortex realizations. However, we

do not think that this difference should alter our conclusions, given that the shift in the oscillation frequency we found for the physically reasonable parameter regime is negligibly small.

To summarize, using our $m\mathbf{v}_s(\mathbf{r})$ in Eq. (3.11) is equivalent to the free energy minimization scheme used in Ref.[1]. There is some difference between Ref.[1] and us on how the random vortex positions are simulated. However, we do not think this kind of difference can change our conclusions qualitatively.

APPENDIX B

Appendices for Chapter 5

B.1 The transverse current-current response function $\mathcal{R}_T(\Omega, \mathbf{q})$

B.1.1 The RPA equation

We define our gauge field propagator as

$$\mathcal{D}_{\mu\nu}^{(0)} = \langle T_\tau a_\mu a_\nu \rangle, \quad (\text{B.1})$$

where T_τ is the chronological time ordering operator and a_μ is the μ th component gauge field. $\mu = 0, 1, 2$ represents the imaginary time, and spatial x, y directions respectively. The average $\langle \dots \rangle$ is taken with respect to the bare gauge field action S_{Coulomb} defined in the main text. The superscript “(0)” on $\mathcal{D}^{(0)}$ shows that it is a bare gauge field propagator. From the action S_{CF} the current operator is

$$J_\mu = \frac{\delta S_{\text{CF}}}{\delta a_\mu} = v_F \bar{\psi} i \gamma_\mu \psi. \quad (\text{B.2})$$

Then the current-current response function can be defined as

$$\mathcal{R}_{\mu\nu} \equiv \langle T_\tau J_\mu J_\nu \rangle = -\langle T_\tau \bar{\psi} v_F \gamma_\mu \psi \bar{\psi} v_F \gamma_\nu \psi \rangle. \quad (\text{B.3})$$

Here the average is taken with respect to the mean field finite density Dirac Fermi sea. In defining $\mathcal{R}_{\mu\nu}$ we have only considered the paramagnetic contribution while ignored the diamagnetic contribution. However, this is justified. As shown in Ref. [208], for Dirac fermions the orbital diamagnetic susceptibility is identically zero if the Fermi energy is not at the Dirac point. Fourier transformed into the momentum space the response function can be rewritten as

$$\mathcal{R}_{\mu\nu}(q) = v_F^2 \int \frac{d\omega d^2\mathbf{k}}{(2\pi)^3} \text{Tr}[\gamma_\mu \mathcal{G}(k) \gamma_\nu \mathcal{G}(k+q)], \quad (\text{B.4})$$

where $k \equiv (\omega, \mathbf{k})$ and $q = (\Omega, \mathbf{q})$. Remember that we have already taken the $T = 0$ limit so that the Matsubara frequencies ω, Ω are continuous. The trace “Tr” is taken with respect to the pseudo-spin indices. $\mathcal{G}(k)$ is the free Dirac CF propagator given by

$$\mathcal{G}(k) \equiv \langle T_\tau \psi(k) \bar{\psi}(-k) \rangle = \gamma^0 \sum_{s=\pm} \frac{1}{i\omega - \epsilon_{\mathbf{k}}^s + \epsilon_F} P_{\mathbf{k}}^{(s)}, \quad (\text{B.5})$$

where $\epsilon_{\mathbf{k}}^s = sv_F |\mathbf{k}|$, with $s = \pm$, are the two branch energy dispersions of the noninteracting Dirac CFs. Correspondingly $P_{\mathbf{k}}^{(s)} = \frac{1}{2}[1 + s i\gamma_0 \boldsymbol{\gamma} \cdot \hat{\mathbf{k}}]$ are the two projection operators for those two branches.

With these definitions of gauge field propagator and response functions we can write down the RPA equation as

$$[\mathcal{D}^{\text{RPA}}]^{-1} = [\mathcal{D}^{(0)}]^{-1} - \mathcal{R}, \quad (\text{B.6})$$

which is a matrix equation. However, since $\mathcal{D}^{(0)}$ has only a spatial transverse component, we only need to consider the transverse current-current response function: $\mathcal{R}_T(\Omega, \mathbf{q}) = [\delta_{ij} - \hat{q}_i \hat{q}_j] \mathcal{R}_{ij}(\Omega, \mathbf{q})$. Its computation is given in the following subsection B.1.2.

B.1.2 The computation of $\mathcal{R}_T(\Omega, \mathbf{q})$

The computation of $\mathcal{R}_{\mu\nu}(\Omega, \mathbf{q})$ has been done before and can be found in, for example, Ref. [208, 209]. Here we recapitulate the derivation of \mathcal{R}_T using our own notations and conventions by following Ref. [209].

Substituting the definition of \mathcal{G} into \mathcal{R}_{ij} gives

$$\mathcal{R}_{ij}(\Omega, \mathbf{q}) = v_F^2 \sum_{s,s'=\pm} \int \frac{d\omega d^2\mathbf{k}}{(2\pi)^3} \frac{\text{Tr}[\gamma_i \gamma_0 P_{\mathbf{k}}^{(s)} \gamma_j \gamma_0 P_{\mathbf{k}+\mathbf{q}}^{(s')}]}{\{i\omega - \epsilon_{\mathbf{k}}^s + \epsilon_F\} \{i\omega + i\Omega - \epsilon_{\mathbf{k}+\mathbf{q}}^{s'} + \epsilon_F\}} \quad (\text{B.7})$$

$$= \mathcal{R}_{ij}^{++} + \mathcal{R}_{ij}^{+-} + \mathcal{R}_{ij}^{-+}. \quad (\text{B.8})$$

In the above we have introduced $\mathcal{R}_{ij}^{ss'}$ with $\{s, s'\} = ++, +-, -+, --$ to denote the four terms from the summation in the first line. The term \mathcal{R}_{ij}^{--} , describing the particle-hole processes within the $\epsilon_{\mathbf{k}}^- = -v_F |\mathbf{k}|$ energy band, is zero because that band is fully occupied.

We first compute \mathcal{R}_{ij}^{++} . In the limit $|\mathbf{q}| \ll |\mathbf{k}| \sim k_F$, $P_{\mathbf{k}+\mathbf{q}}^{(s')} \approx P_{\mathbf{k}}^{(s')}$ in the denominator. Then by using the following trace identity for the gamma matrices (which are simply Pauli

matrices in our case)

$$\text{Tr}[\gamma_\mu \gamma_\nu \gamma_\rho \gamma_\sigma] = 2[\delta_{\mu\nu} \delta_{\rho\sigma} - \delta_{\mu\rho} \delta_{\nu\sigma} + \delta_{\mu\sigma} \delta_{\nu\rho}], \quad (\text{B.9})$$

we can obtain: $\text{Tr}[\gamma_i \gamma_0 P_{\mathbf{k}}^{(+)} \gamma_j \gamma_0 P_{\mathbf{k}}^{(+)}] = -\hat{\mathbf{k}}_i \hat{\mathbf{k}}_j$. Therefore

$$\mathcal{R}_{ij}^{++} \approx v_F^2 \int \frac{d\omega d^2 \mathbf{k}}{(2\pi)^3} (-\hat{\mathbf{k}}_i \hat{\mathbf{k}}_j) \frac{1}{i\omega - \epsilon_{\mathbf{k}}^+ + \epsilon_F} \frac{1}{i\omega + i\Omega - \epsilon_{\mathbf{k}+\mathbf{q}}^+ + \epsilon_F}. \quad (\text{B.10})$$

The above integration over ω can be complete by using the residue theorem. Then multiplying the obtained result by $[\delta_{ij} - \hat{\mathbf{k}}_i \hat{\mathbf{k}}_j]$ projects out the transverse component \mathcal{R}_T^{++} , which is given by

$$\begin{aligned} \mathcal{R}_T^{++} \approx & -v_F^2 \int \frac{d^2 \mathbf{k}}{(2\pi)^2} [1 - (\hat{\mathbf{k}} \cdot \hat{\mathbf{q}})^2] \left\{ \frac{\theta(\epsilon_F - v_F |\mathbf{k}|) \theta(v_F |\mathbf{k} + \mathbf{q}| - \epsilon_F)}{i\Omega - v_F |\mathbf{k} + \mathbf{q}| + v_F |\mathbf{k}|} \right. \\ & \left. - \frac{\theta(v_F |\mathbf{k}| - \epsilon_F) \theta(\epsilon_F - v_F |\mathbf{k} + \mathbf{q}|)}{i\Omega - v_F |\mathbf{k} + \mathbf{q}| + v_F |\mathbf{k}|} \right\}, \end{aligned} \quad (\text{B.11})$$

where $\theta(x)$ is the Heaviside step function. By making use of the approximation that $|\mathbf{k} + \mathbf{q}| \approx |\mathbf{k}| + \hat{\mathbf{k}} \cdot \mathbf{q}$ and working out the restrictions on $|\mathbf{k}|$ from the product of Heaviside functions we can perform the integration over $|\mathbf{k}|$ easily. The final result is

$$\mathcal{R}_T^{++} \approx -\frac{\epsilon_F}{2\pi} \int_{-\pi/2}^{\pi/2} \frac{d\phi}{2\pi} \sin^2 \phi \left\{ \frac{v_F |\mathbf{q}| \cos \phi}{i\Omega - v_F |\mathbf{q}| \cos \phi} - \frac{v_F |\mathbf{q}| \cos \phi}{i\Omega + v_F |\mathbf{q}| \cos \phi} \right\} \quad (\text{B.12})$$

$$= \frac{\epsilon_F}{4\pi} \int_{-\pi/2}^{\pi/2} \frac{d\phi}{\pi} \frac{2 \cos^2 \phi \sin^2 \phi}{\Omega^2 / (v_F |\mathbf{q}|)^2 + \cos^2 \phi}. \quad (\text{B.13})$$

To complete the rest angular integration we first change the integration variable from ϕ to $\phi' = 2\phi$ and then rewrite the integral as a contour integral over the complex variable $z = \exp(i\phi')$ along the contour $|z| = 1$. Then the integral can be done again by using the residue theorem. The result is

$$\int_{-\pi/2}^{\pi/2} \frac{d\phi}{\pi} \frac{2 \cos^2 \phi \sin^2 \phi}{\Omega^2 / (v_F |\mathbf{q}|)^2 + \cos^2 \phi} = \frac{1}{2\pi i} \oint_{|z|=1} \frac{dz}{z} \frac{(z - z^{-1})^2}{\beta + \frac{z + z^{-1}}{2}} = -\beta + \sqrt{\beta^2 - 1}, \quad (\text{B.14})$$

where we have introduced $\beta = 2\Omega^2 / (v_F |\mathbf{q}|)^2 + 1$ for clarity. Substituting this result back into \mathcal{R}_T^{++} we have

$$\mathcal{R}_T^{++}(\Omega, \mathbf{q}) = \frac{\epsilon_F}{2\pi} \left[-\frac{1}{2} - \frac{\Omega^2}{v_F^2 |\mathbf{q}|^2} + \sqrt{1 + \frac{\Omega^2}{v_F^2 |\mathbf{q}|^2} \frac{|\Omega|}{v_F |\mathbf{q}|}} \right]. \quad (\text{B.15})$$

The other two terms \mathcal{R}_{ij}^{+-} and \mathcal{R}_{ij}^{-+} can be computed similarly. We first work out the two traces

$$\text{Tr}[\gamma_i \gamma_0 P_{\mathbf{k}}^{(+)} \gamma_j \gamma_0 P_{\mathbf{k}}^{(-)}] = \text{Tr}[\gamma_i \gamma_0 P_{\mathbf{k}}^{(-)} \gamma_j \gamma_0 P_{\mathbf{k}}^{(+)}] = \hat{\mathbf{k}}_i \hat{\mathbf{k}}_j - \delta_{ij}. \quad (\text{B.16})$$

Next we perform the Matsubara frequency integration and then project out the transverse components. The results are as follows

$$\mathcal{R}_T^{+-} + \mathcal{R}_T^{-+} \approx -v_F^2 \int \frac{d^2\mathbf{k}}{(2\pi)^2} (\hat{\mathbf{k}} \cdot \hat{\mathbf{q}})^2 \left\{ \frac{\theta(v_F|\mathbf{k}| - \epsilon_F)}{i\Omega + v_F|\mathbf{k}| + v_F|\mathbf{k} + \mathbf{q}|} + \frac{\theta(v_F|\mathbf{k} + \mathbf{q}| - \epsilon_F)}{-i\Omega + v_F|\mathbf{k}| + v_F|\mathbf{k} + \mathbf{q}|} \right\} \quad (\text{B.17})$$

$$\approx -v_F^2 \int \frac{d^2\mathbf{k}}{(2\pi)^2} (\hat{\mathbf{k}} \cdot \hat{\mathbf{q}})^2 \frac{\theta(v_F|\mathbf{k}| - \epsilon_F)}{v_F|\mathbf{k}|} \quad (\text{B.18})$$

$$= - \int_{\epsilon_F}^{\infty} \frac{d(v_F|\mathbf{k}|)}{2\pi} \int_0^{2\pi} \frac{d\phi}{2\pi} \cos^2 \phi \quad (\text{B.19})$$

$$= \frac{\epsilon_F}{4\pi}. \quad (\text{B.20})$$

In the above from the first line to the second line we have used the approximation $|\Omega|, v_F|\mathbf{q}| \ll v_F|\mathbf{k}| \sim \epsilon_F$. From the 2nd line to the last line we have dropped a linear ultraviolet divergent term, which originates from the Dirac sea being infinitely deep and will disappear if the ultraviolet behavior is properly regularized, as discussed in Ref. [208] and mentioned in Ref. [209].

Combining the above results of $\mathcal{R}_T^{++}, \mathcal{R}_T^{+-}$ and \mathcal{R}_T^{-+} , we have, in the limit $|\Omega| < v_F|\mathbf{q}| \ll \epsilon_F$,

$$\mathcal{R}_T(\Omega, \mathbf{q}) = \frac{\epsilon_F}{2\pi} \left[-\frac{\Omega^2}{v_F^2|\mathbf{q}|^2} + \sqrt{1 + \frac{\Omega^2}{v_F^2|\mathbf{q}|^2} \frac{|\Omega|}{v_F|\mathbf{q}|}} \right] \approx \frac{\epsilon_F}{2\pi} \frac{|\Omega|}{v_F|\mathbf{q}|}. \quad (\text{B.21})$$

B.2 Particle-hole symmetry transformation of the order parameter $\hat{\Delta}$

How the Dirac CF fields ψ transform under the three symmetry operations: the physical charge conjugation \mathcal{C} , the time reversal \mathcal{T} , and a $2d$ parity symmetry operation \mathcal{P} , has been discussed in detail in Ref. [2]. For a half-filled Landau level the particle-hole transformation not only flips the sign of physical charges but also inverse the external magnetic field direction. Therefore it is a combination of \mathcal{C} and \mathcal{T} : \mathcal{CT} . Under this transformation [2],

$$\mathcal{CT}\psi(t, \mathbf{x})(\mathcal{CT})^{-1} = -i\sigma_2\psi(-t, \mathbf{x}). \quad (\text{B.22})$$

In other words the Dirac CF fields $\psi(t, \mathbf{x})$ behaves like Kramers doublets under \mathcal{CT} . From this we can deduce how the pairing order parameter transforms. Since there can

be different types of pairing order parameter, we discuss how each of them transforms under \mathcal{CT} .

1. Pseudo-spin singlet channel: $\hat{\Delta}(t_1, \mathbf{x}_1; t_2, \mathbf{x}_2) = \langle \psi^T(t_1, \mathbf{x}_1) i\sigma_2 \psi(t_2, \mathbf{x}_2) \rangle$. For clarity we have simply abbreviated the projected pseudo-spinor field $P_{\mathbf{k}}^+ \psi$ as ψ here. Under the \mathcal{CT} ,

$$\mathcal{CT} \hat{\Delta}(\mathbf{x}_1; \mathbf{x}_2) (\mathcal{CT})^{-1} = \langle \psi^T(\mathbf{x}_1) (i\sigma_2) i\sigma_2 (-i\sigma_2) \psi(\mathbf{x}_2) \rangle^* = \hat{\Delta}^*(\mathbf{x}_1; \mathbf{x}_2), \quad (\text{B.23})$$

where the complex conjugation comes from the fact that \mathcal{CT} is an anti-unitary operation. Since we are only interested in how the spatial part of the pairing gap transforms under \mathcal{CT} , we have ignored the time dependence in this equation. We see that as far as the spatial part of $\Delta(\mathbf{x}_1; \mathbf{x}_2)$ is concerned, the particle-hole transformation is equivalent to a complex conjugation. Therefore the ℓ -wave channel pairing order parameter $\hat{\Delta}(\mathbf{k}) \propto e^{i\ell\theta_{\mathbf{k}}}$ will be transformed into the $-\ell$ channel by the \mathcal{CT} operation. Hence the $\ell = 0$ channel is particle-hole symmetric; also the Moore-Read Pfaffian state, corresponding to $\ell = -2$ channel, and the anti-Pfaffian state proposed in Ref. [100, 101], corresponding to $\ell = +2$ pairing, are particle hole conjugates of each other.

2. Pseudo-spin triplet channel: $\hat{\Delta} = \langle \psi^T \mathbf{d} \cdot \boldsymbol{\sigma} i\sigma_2 \psi \rangle$, where \mathbf{d} is some vector which might be position dependent. From the above singlet discussions we see that if we only care about how the spatial part of the order parameter $\hat{\Delta}$ transforms under \mathcal{CT} , there is no difference between the singlet and triplet case. It is simply a complex conjugation.

To summarize, under \mathcal{CT} , the ℓ wave angular momentum channel pairing will be transformed into the $-\ell$ channel pairing, regardless of the form of the order parameter $\hat{\Delta}$.

B.3 Pairing channels ℓ of particle hole symmetric CFs for the Moore-Read Pfaffian and anti-Pfaffian wavefunctions

The strategy to identify which pairing channel ℓ of the Dirac composite fermions corresponds to the Moore-Read Pfaffian wavefunction and its particle-hole conjugate, the

anti-Pfaffian wavefunctions [100, 101], is to consider the response of each of them to some perturbations. This response can not be electronic because the Dirac CFs are neutral. A natural choice will be the spatial curvature because topologically distinct states couple to the curvature differently. In the current case, the pairing condensate of Dirac CFs is chiral and different pairing channels ℓ are topologically distinct. Therefore we can consider how a chiral ℓ -wave pairing state of the Dirac CFs and the Moore-Read Pfaffian/anti-Pfaffian wavefunction respond to the curvature. If they were to describe the same state, their response to the curvature should be the same. This can be done by considering the so-called shift [210, 211, 2], which is a topological number that characterizes how a state responds to the nontrivial curvature on a sphere. Originally this concept of shift is introduced for quantum Hall states but has been recently generalized to chiral superfluid condensates as well. Another approach could be comparing the chiral central charge [140] of the boundary theory of the chiral ℓ -wave Dirac CFs pairing state with that of the Moore-Read Pfaffian/anti-Pfaffian wavefunction. In the following we follow the first approach and compute the shift. The following discussions closely follow those of Ref. [2] but are expanded in more detail.

To establish the connection between Dirac CF pairing states and the Moore-Read Pfaffian/anti-Pfaffian wavefunctions we first recapitulate what D. T. Son has done in constructing the particle-hole symmetric CF theory in Ref. [2]. This is schematically shown in the Fig. B.1. Corresponding to those three steps we are going to do the following three steps to complete our identification:

- (1) Compute the shift \mathcal{S} of the Moore-Read Pfaffian and anti-Pfaffian wavefunctions, which are written in terms of the non-relativistic electron coordinates.
- (2) Map the shift \mathcal{S} to the so-called relativistic shift κ defined for the Dirac fermions in its zero-th Landau level, as shown in the second box of Fig. B.1. Precise definition of κ will come later.
- (3) Compute the same quantity shift κ for the Dirac CF pairing condensates in different ℓ channels and compare it with the shift value obtained in the step (2).

In this way we can identify which channel corresponds to Moore-Read Pfaffian/anti-Pfaffian wavefunction.

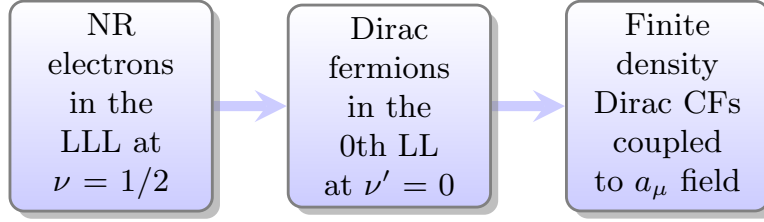


Figure B.1: The three steps construction of the Dirac CF theory in Ref. [2]. In the 1st box “NR” stands for non-relativistic and “LLL” is the abbreviation of lowest Landau level. In the 2nd box ‘LL’ means Landau level. Notice that the Dirac fermions in the 2nd box still carry electric charge and are different from the Dirac CFs in the 3rd box. In box 3, “zero field” means zero emergent magnetic field. Notice that the filling fraction ν, ν' are related to each other by $\nu' = \nu - 1/2$.

B.3.1 The shift \mathcal{S} of the Moore-Read Pfaffian and anti-Pfaffian wavefunctions

B.3.1.1 The Moore-Read Pfaffian wavefunction

The Moore-Read Pfaffian wavefunction is given by

$$\Psi_{\text{MR}}(z_1, \dots, z_{N_e}) = \text{Pf} \left(\frac{1}{z_i - z_j} \right) \prod_{i < j} (z_i - z_j)^2 e^{-\sum |z_i|^2 / 4\ell_B^2}, \quad (\text{B.24})$$

where ℓ_B is the magnetic length, $z_i = x_i + iy_i$ is the i th electron coordinate and N_e gives the total number of electrons. And the Pfaffian in the above is defined as

$$\text{Pf} \left(\frac{1}{z_i - z_j} \right) \equiv \mathcal{A} \left\{ \frac{1}{z_1 - z_2} \frac{1}{z_3 - z_4} \dots \frac{1}{z_{N_e-1} - z_{N_e}} \right\}, \quad (\text{B.25})$$

where the anti-symmetrizing sign \mathcal{A} means summing over all permutations of $\{1, 2, \dots, N_e\}$, which produce distinct pairs of $\frac{1}{z_i - z_j}$ in the product, and multiplying the product by the corresponding permutation sign.

The shift \mathcal{S} of a lowest Landau level wavefunction on certain manifold is defined as the mismatch between N_ϕ , the total number of magnetic flux quanta applied, and the total number of electrons N_e divided by the filling fraction ν , as follows

$$N_\phi = \frac{1}{\nu} N_e - \mathcal{S}. \quad (\text{B.26})$$

\mathcal{S} results from a nontrivial coupling of the wavefunction to the curvature of the manifold and therefore depends on both the topological nature of the wavefunction and the

topology of the manifold. Since a flat plane has zero Gauss curvature everywhere, it is topologically trivial and $\mathcal{S} = 0$ as expected. However, a sphere has a nonzero net Gauss curvature. Therefore if the wavefunction is topologically nontrivial, then the shift \mathcal{S} can be nonzero. Put onto the sphere, the above Pfaffian wavefunction Ψ_{MR} can be written in terms of spinor coordinates $(u, v) = (\cos \theta e^{i\phi/2}, \sin \theta e^{-i\phi/2})$ as

$$\Psi_{\text{MR}} = \text{Pf} \left(\frac{1}{u_i v_j - v_i u_j} \right) \prod_{1 \leq i < j \leq N_e} (u_i v_j - v_i u_j)^2.$$

Here θ and ϕ are the spherical polar and azimuthal angles respectively. As a lowest Landau level wavefunction on the sphere, Ψ_{MR} needs to be homogeneous of degree N_ϕ in the spinor variables (u_i, v_i) [12]. This leads to

$$N_\phi = -1 + 2(N_e - 1) = 2N_e - 3. \quad (\text{B.27})$$

Comparing it with the Equation (B.26), we can immediately read off the filling fraction $\nu = 1/2$, as expected, and the shift value $\mathcal{S} = 3$ [20].

B.3.1.2 The Anti-Pfaffian wavefunction

The anti-Pfaffian wavefunction was first introduced in Ref. [101, 100]. It is constructed by the particle-hole transformation from the Moore-Read wavefunction Ψ_{MR} . This transformation has been implemented explicitly for a lowest Landau level wavefunction by S. M. Girvin in Ref. [124]. Applying the transformation procedure to the Moore-Read wavefunction leads to [100]

$$\begin{aligned} \Psi_{\overline{\text{Pf}}}(z_i) = & \int \prod_{\alpha=1}^{N_h} d\eta_\alpha d\bar{\eta}_\alpha \Psi_{\text{MR}}(\bar{\eta}_\alpha) \prod_{\beta < \gamma}^{N_h} (\eta_\beta - \eta_\gamma) \prod_{i=1}^{N_e} \prod_{\alpha=1}^{N_h} (\eta_\alpha - z_i) \\ & \times \prod_{i < j}^{N_e} (z_i - z_j) e^{-\sum_{\alpha}^{N_h} |\eta_\alpha|^2 / 4\ell_B^2 - \sum_i^{N_e} |z_i|^2 / 4\ell_B^2}, \end{aligned} \quad (\text{B.28})$$

where the subscript $\overline{\text{Pf}}$ is used to denote the anti-Pfaffian wavefunction. The physical meaning of this wavefunction can be understood as follows:

1. First, fill up the lowest Landau level with N_e electrons. This is represented by the factor $\prod_{i < j}^{N_e} (z_i - z_j)$ (ignoring the Gaussian factor).
2. Then create N_h holes at arbitrary positions η_α in the filled Landau level by the factor $\prod_{i=1}^{N_e} \prod_{\alpha=1}^{N_h} (\eta_\alpha - z_i)$.

3. Next insert the factor $\prod_{\beta < \gamma}^{N_h} (\eta_\beta - \eta_\gamma)$ to ensure the Fermi statistics between those created N_h holes.
4. Then build in the Pfaffian correlations for the N_h holes and pair them up into the “Moore-Read” state $\Psi_{\text{MR}}(\bar{\eta}_\alpha)$. We put a quotation mark here because the argument $\bar{\eta}_\alpha$ in this function is anti-analytical instead of analytical. Therefore it is different from the Moore-Read wavefunction defined in the previous section by a sign flip of the pairing angular momentum channel ℓ .
5. At last, as an electron wavefunction, the hole variables $\eta_\alpha, \bar{\eta}_\alpha$ need to be integrated out.

To summarize, there are two key differences in the $\Psi_{\overline{\text{PF}}}$ wavefunction from the Ψ_{MR} wavefunction: (1) $\Psi_{\overline{\text{PF}}}$ can be interpreted as pairing of (composite)holes instead of electrons; (2) the pairing channel that $\Psi_{\overline{\text{PF}}}$ corresponds to is opposite to that of the Ψ_{MR} . These two features are consistent with the fact that the particle-hole transformation defined for the lowest Landau level not only flip the sign of electric charges but also inverse the direction of the external field which flips the sign of pairing channel.

In the wavefunction $\Psi_{\overline{\text{PF}}}$, N_h and N_e need to satisfy certain constraint [212]: the degree of each hole coordinate η_α needs to match with that of its complex-conjugate $\bar{\eta}_\alpha$ so that the integral over η_α and $\bar{\eta}_\alpha$ is non-vanishing. This gives

$$N_h - 1 + N_e = \frac{1}{\nu} N_h - \mathcal{S}_{\text{MR}}. \quad (\text{B.29})$$

In this formula the right hand side counts the degree of $\bar{\eta}_\alpha$ in the wavefunction $\Psi_{\text{MR}}(\bar{\eta}_\alpha)$ appeared in the above integrand in Equation (B.28). As have been already computed in the previous section, for the Moore-Read wavefunction, the shift is $\mathcal{S}_{\text{MR}} = 3$ and the filling fraction factor is $\nu = 1/2$. As in the Moore-Read wavefunction Ψ_{MR} case, we can put $\Psi_{\overline{\text{PF}}}$ onto a sphere. Then $\Psi_{\overline{\text{PF}}}(z_i)$ will be a homogeneous polynomial in each spinor variable. The degree of this polynomial is equal to the degree of the polynomial of z_i variable in the Equation (B.28): $N_e - 1 + N_h$. Again as a legitimate lowest Landau level wavefunction this degree needs to be equal to the number of magnetic flux quanta N_ϕ pierced through the sphere. In other words

$$N_\phi = N_e - 1 + N_h. \quad (\text{B.30})$$

Combing Eq. (B.29) and Eq. (B.30) and eliminating N_h we obtain

$$N_\phi = 2N_e + \mathcal{S}_{\text{MR}} - 2 \equiv \nu^{-1}N_e - \mathcal{S}_{\overline{\text{PF}}}. \quad (\text{B.31})$$

Therefore for an anti-Pfaffian state, the filling fraction is $\nu = 1/2$, as expected, and the shift is $\mathcal{S}_{\overline{\text{PF}}} = 2 - \mathcal{S}_{\text{MR}} = -1$. Since $\mathcal{S}_{\overline{\text{PF}}} \neq \mathcal{S}_{\text{MR}}$, the Moore-Read and anti-Pfaffian wavefunctions must be topologically distinct from each other.

B.3.2 The relativistic shift κ of the Dirac fermions in the 0th Landau level

The relativistic shift κ [213] of the Dirac fermions is defined as the mismatch between the total number of electric charge N'_e and the magnetic flux quanta N'_ϕ multiplied by the filling fraction ν' on a sphere as

$$N'_e = \nu'N'_\phi + \kappa. \quad (\text{B.32})$$

We have added a prime superscript on ν', N'_e, N'_ϕ to distinguish the quantities defined for the Dirac fermions in the 0th Landau level from those ν, N_e, N_ϕ , that are defined for the non-relativistic electrons in the LLL. For Dirac fermions ν' can be negative and zero. When the filling fraction is $\nu' = 0$, the definition of \mathcal{S} in Eq. (B.26) is impossible. That is why a new definition of the shift κ is necessary.

The relation between ν', N'_e, N'_ϕ and ν, N_e, N_ϕ are outlined as follows

1. $N_e = N'_e + \frac{1}{2}N'_\phi$. The 2nd term on the right hand side comes from the Dirac sea contribution which is finite.
2. $\nu = \nu' + 1/2$. The 1/2 term comes from the fact that in D. T. Son's construction, a half-filled electron Landau level corresponds to the Dirac fermions at neutrality point $\nu' = 0$.
3. The relation between N_ϕ and N'_ϕ depends on the curvature of the space.
 - On a flat plane, $N_\phi = N'_\phi$. This is because the zeroth Dirac Landau orbitals described by

$$\Psi_m(z) = \begin{pmatrix} z^m e^{-|z|^2/4\ell_B^2} \\ 0 \end{pmatrix} \quad (\text{B.33})$$

are the same as the LLL orbitals of non-relativistic fermions [2], if the second component “0” is ignored in the above. Therefore to describe the same state $N_\phi = N'_\phi$ is necessary.

- However, *on a sphere*, $N_\phi = N'_\phi - 1$ [2, 214], because on a sphere the lowest Landau level of the Dirac fermion with N'_ϕ magnetic flux quanta, is identical to the Landau levels of a non-relativistic electrons with $N_\phi = N'_\phi - 1$ magnetic flux quanta. To describe the same state, we demand $N_\phi = N'_\phi - 1$. This additional -1 shift comes from the fact that the Dirac fermions carry a pseudo-spin degree of freedom which can directly couple to the curvature of the sphere.

Substituting the above three relations $N_e = N'_e + \frac{1}{2}N'_\phi$, $\nu = \nu' + 1/2$, and $N_\phi = N'_\phi - 1$ into the definition of \mathcal{S} : $N_\phi = \frac{1}{\nu}N_e - \mathcal{S}$, we obtain the following relation

$$N'_e = \nu'N'_\phi + \nu(\mathcal{S} - 1). \quad (\text{B.34})$$

Comparing it with the definition of κ we conclude that

$$\kappa = \nu(\mathcal{S} - 1).$$

Therefore the relativistic shift κ for the Moore-Read Pfaffian and anti-Pfaffian wavefunctions are

$$\Psi_{\text{MR}} \quad \rightarrow \quad \mathcal{S} = 3 \quad \rightarrow \quad \kappa = +1, \quad (\text{B.35})$$

$$\Psi_{\overline{\text{PF}}} \quad \rightarrow \quad \mathcal{S} = -1 \quad \rightarrow \quad \kappa = -1. \quad (\text{B.36})$$

Notice that because for both Ψ_{MR} and $\Psi_{\overline{\text{PF}}}$ states $\nu' = 0$, we have

$$N'_e = \kappa = \pm 1 \quad (\text{B.37})$$

on a sphere, in contrast to the $N'_e = \kappa = 0$ on a plane. In other words, on a sphere, we need to add an additional net charge $N'_e = \kappa = \pm 1$ to maintain the Ψ_{MR} or $\Psi_{\overline{\text{PF}}}$ ground state wavefunction without inducing any fractional quasiparticle excitations.

B.3.3 The shift κ of chiral Dirac CF pairing condensates

The above concept of shift κ can be also generalized to chiral pairing condensates [213]. In the following we obtain the κ value for our chiral Dirac CF pairing condensates by some physical arguments [2].

Because the wavefunction $\Psi_{\text{MR}}/\Psi_{\overline{\text{Pf}}}$ is smooth in space, it should correspond to a chiral pairing state of Dirac CFs with a smooth order parameter texture, i. e. without any topological defects. However, if we try to put a chiral ℓ wave pairing condensate onto a sphere without applying any magnetic field (for the CFs it is the emergent magnetic field), the ground state pairing order parameter can not be smooth [17, 215] due to the nonzero net curvature of the sphere. Mathematically this conclusion comes from the Poincare-Hopf theorem [215]. If we want to maintain a smooth texture of the pairing order parameter, a magnetic monopole with a strength $-\ell/2$ at the origin of the sphere needs to be added to compensate for the curvature effect. That the monopole strength needed is $-\ell/2$ instead of $\ell/2$ is because the direction of the applied magnetic field needs to be opposite to the Gauss curvature of the sphere so that their effects cancel out each other. A monopole of strength $-\ell/2$ would correspond to $-\ell$ flux quanta of the emergent magnetic field b . Piercing $-\ell$ flux quanta of b through the sphere is equivalent to inducing additional physical charges of the amount $N'_e = -\ell \times \frac{1}{2} = -\ell/2$, because $b/4\pi = \rho'_e$ gives the physical charge density, as emphasized at the beginning of the main text.

Therefore if the ℓ wave chiral pairing condensate of Dirac CFs were to describe the same state as the wavefunction Ψ_{MR} or $\Psi_{\overline{\text{Pf}}}$, the induced physical charge amount $N'_e = -\ell/2$ needs to be identical to the N'_e found in Eq. (B.37). In other words, the following relation

$$N'_e = \kappa = -\ell/2 \tag{B.38}$$

needs to be satisfied. Therefore the Ψ_{MR} wavefunction corresponds to $\ell = -2\kappa = -2$ channel; while the $\Psi_{\overline{\text{Pf}}}$ wavefunction corresponds to $\ell = -2\kappa = +2$ channel. These results are summarized in Table B.1.

	\mathcal{S}	κ	ℓ
Ψ_{MR}	3	+1	-2
$\Psi_{\overline{\text{Pf}}}$	-1	-1	+2

Table B.1: Summary of the shift values and the corresponding pairing channels ℓ for the Moore-Read Pfaffian wavefunction Ψ_{MR} and the anti-Pfaffian wavefunction $\Psi_{\overline{\text{Pf}}}$.

REFERENCES

- [1] Kuang-Ting Chen and Patrick A. Lee. *Violation of the Onsager relation for quantum oscillations in superconductors*. Phys. Rev. B **79** (2009), 180510.
- [2] Dam Thanh Son. *Is the Composite Fermion a Dirac Particle?* Phys. Rev. X **5** (2015), 031027.
- [3] J. G. Bednorz and K. A. Müller. *Possible high- T_c superconductivity in the Ba-La-Cu-O system*. Zeitschrift für Physik B Condensed Matter **64** (1986), 189.
- [4] D. C. Tsui, H. L. Stormer, and A. C. Gossard. *Two-Dimensional Magnetotransport in the Extreme Quantum Limit*. Phys. Rev. Lett. **48** (1982), 1559.
- [5] M. R. Norman, D. Pines, and C. Kallin. *The pseudogap: friend or foe of high T_c ?* Advances in Physics **54** (2005), 715.
- [6] Sudip Chakravarty. *Quantum oscillations and key theoretical issues in high temperature superconductors from the perspective of density waves*. Reports on Progress in Physics **74** (2011), 022501.
- [7] Nicolas Doiron-Leyraud, Cyril Proust, David LeBoeuf, Julien Levallois, Jean-Baptiste Bonnemaïson, Ruixing Liang, DA Bonn, WN Hardy, and Louis Taillefer. *Quantum oscillations and the Fermi surface in an underdoped high- T_c superconductor*. Nature **447** (2007), 565.
- [8] E. M. Lifshitz and L. P. Pitaevskii. *Statistical Physics Part 2: Condensed Matter Theory (Course of the Theoretic Physics Vol. 9)*. Higher Education Press (2008).
- [9] Chetan Nayak. *Density-wave states of nonzero angular momentum*. Phys. Rev. B **62** (2000), 4880.
- [10] Sudip Chakravarty, R. B. Laughlin, Dirk K. Morr, and Chetan Nayak. *Hidden order in the cuprates*. Phys. Rev. B **63** (2001), 094503.
- [11] R. B. Laughlin. *Anomalous Quantum Hall Effect: An Incompressible Quantum Fluid with Fractionally Charged Excitations*. Phys. Rev. Lett. **50** (1983), 1395.
- [12] F. D. M. Haldane. *Fractional Quantization of the Hall Effect: A Hierarchy of Incompressible Quantum Fluid States*. Phys. Rev. Lett. **51** (1983), 605.
- [13] J. K. Jain. *Composite Fermions*. Cambridge University Press, New York (2007).
- [14] H. W. Jiang, H. L. Stormer, D. C. Isui, L. N. Pfeiffer, and K. W. West. *Transport anomalies in the lowest Landau level of two-dimensional electrons at half-filling*. Phys. Rev. B **40** (1989), 12013.
- [15] R. L. Willett, M. A. Paalanen, R. R. Ruel, K. W. West, L. N. Pfeiffer, and D. J. Bishop. *Anomalous sound propagation at $\nu = 1/2$ in a 2D electron gas: Observation of a spontaneously broken translational symmetry?* Phys. Rev. Lett. **65** (1990), 112.

- [16] R. Willett, J. P. Eisenstein, H. L. Störmer, D. C. Tsui, A. C. Gossard, and J. H. English. *Observation of an even-denominator quantum number in the fractional quantum Hall effect*. Phys. Rev. Lett. **59** (1987), 1776.
- [17] Gregory Moore and Nicholas Read. *Nonabelions in the fractional quantum hall effect*. Nuclear Physics B **360** (1991), 362 .
- [18] N. Read and G. Moore. *Fractional Quantum Hall Effect and Nonabelian Statistics*. Progress of Theoretical Physics Supplement **107** (1992), 157.
- [19] Chetan Nayak, Steven H. Simon, Ady Stern, Michael Freedman, and Sankar Das Sarma. *Non-Abelian anyons and topological quantum computation*. Rev. Mod. Phys. **80** (2008), 1083.
- [20] Martin Greiter, Xiao-Gang Wen, and Frank Wilczek. *Paired Hall state at half filling*. Phys. Rev. Lett. **66** (1991), 3205.
- [21] Martin Greiter, X.G. Wen, and Frank Wilczek. *Paired Hall states*. Nuclear Physics B **374** (1992), 567 .
- [22] N. Read and Dmitry Green. *Paired states of fermions in two dimensions with breaking of parity and time-reversal symmetries and the fractional quantum Hall effect*. Phys. Rev. B **61** (2000), 10267.
- [23] B. I. Halperin, Patrick A. Lee, and Nicholas Read. *Theory of the half-filled Landau level*. Phys. Rev. B **47** (1993), 7312.
- [24] Yoichi Kamihara, Takumi Watanabe, Masahiro Hirano, and Hideo Hosono. *Iron-Based Layered Superconductor $La[O_{1-x}F_x]FeAs$ ($x = 0.05 - 0.12$) with $T_c = 26K$* . Journal of the American Chemical Society **130** (2008), 3296.
- [25] X. H. Chen, T. Wu, G. Wu, R. H. Liu, H. Chen, and D. F. Fang. *Superconductivity at 43 K in $SmFeAsO_{1-x}F_x$* . Nature **453** (2008), 761.
- [26] Ren Zhi-An, Lu Wei, Yang Jie, Yi Wei, Shen Xiao-Li Xiao-Li, Zheng-Cai, Che Guang-Can, Dong Xiao-Li, Sun Li-Ling, Zhou Fang, and Zhao Zhong-Xian. *Superconductivity at 55K in Iron-Based F-Doped Layered Quaternary Compound $Sm[O_{1-x}F_x]FeAs$* . Chinese Physics Letters **25** (2008), 2215.
- [27] J. Bardeen, L. N. Cooper, and J. R. Schrieffer. *Theory of Superconductivity*. Phys. Rev. **108** (1957), 1175.
- [28] Jan Zaanen, Sudip Chakravarty, T Senthil, Philip Anderson, Patrick Lee, Jörg Schmalian, Masatoshi Imada, David Pines, Mohit Randeria, Chandra Varma *et al*. *Towards a complete theory of high T_c* . Nature Physics **2** (2006), 138.
- [29] C. C. Tsuei, J. R. Kirtley, C. C. Chi, Lock See Yu-Jahnes, A. Gupta, T. Shaw, J. Z. Sun, and M. B. Ketchen. *Pairing Symmetry and Flux Quantization in a Tricrystal Superconducting Ring of $YBa_2Cu_3O_{7-\delta}$* . Phys. Rev. Lett. **73** (1994), 593.
- [30] D. A. Wollman, D. J. Van Harlingen, W. C. Lee, D. M. Ginsberg, and A. J. Leggett. *Experimental determination of the superconducting pairing state in YBCO from the phase coherence of YBCO-Pb dc SQUIDS*. Phys. Rev. Lett. **71** (1993), 2134.

- [31] Tom Timusk and Bryan Statt. *The pseudogap in high-temperature superconductors: an experimental survey*. Reports on Progress in Physics **62** (1999), 61.
- [32] C. M. Varma, P. B. Littlewood, S. Schmitt-Rink, E. Abrahams, and A. E. Ruckenstein. *Phenomenology of the normal state of Cu-O high-temperature superconductors*. Phys. Rev. Lett. **63** (1989), 1996.
- [33] D. S. Marshall, D. S. Dessau, A. G. Loeser, C-H. Park, A. Y. Matsuura, J. N. Eckstein, I. Bozovic, P. Fournier, A. Kapitulnik, W. E. Spicer, and Z.-X. Shen. *Unconventional Electronic Structure Evolution with Hole Doping in $\text{Bi}_2\text{Sr}_2\text{CaCu}_2\text{O}_{8+\delta}$: Angle-Resolved Photoemission Results*. Phys. Rev. Lett. **76** (1996), 4841.
- [34] H. Ding, T. Yokoya, J. C. Campuzano, Takahashi T., M. Randeria, M. R. Norman, T. Mochiku, K. Kadowaki, and J. Giapintzakis. *Spectroscopic evidence for a pseudogap in the norm state of underdoped high- T_c superconductors*. Nature **382** (1996), 51.
- [35] M. R. Norman, H. Ding, M. Randeria, J. C. Campuzano, T. Yokoya, T. Takeuchi, T. Takahashi, T. Mochiku, K. Kadowaki, P. Guptasarma *et al.* *Destruction of the Fermi surface in underdoped high- T_c superconductors*. Nature **392** (1998), 157.
- [36] M. Gurvitch and A. T. Fiory. *Resistivity of $\text{La}_{1.825}\text{Sr}_{0.175}\text{CuO}_4$ and $\text{YBa}_2\text{Cu}_3\text{O}_7$ to 1100 K: Absence of saturation and its implications*. Phys. Rev. Lett. **59** (1987), 1337.
- [37] Neven Barisic, Mun K. Chan, Yuan Li, Guichuan Yu, Xudong Zhao, Martin Dressel, Ana Smontara, and Martin Greven. *Universal sheet resistance and revised phase diagram of the cuprate high-temperature superconductors*. Proceedings of the National Academy of Sciences **110** (2013), 12235.
- [38] C. M. Varma. *Non-Fermi-liquid states and pairing instability of a general model of copper oxide metals*. Phys. Rev. B **55** (1997), 14554.
- [39] Philip Phillips. *Mottness collapse and T -linear resistivity in cuprate superconductors*. Philosophical Transactions of the Royal Society of London A: Mathematical, Physical and Engineering Sciences **369** (2011), 1574.
- [40] G. Shirane, Y. Endoh, R. J. Birgeneau, M. A. Kastner, Y. Hidaka, M. Oda, M. Suzuki, and T. Murakami. *Two-dimensional antiferromagnetic quantum spin-fluid state in La_2CuO_4* . Phys. Rev. Lett. **59** (1987), 1613.
- [41] John M. Tranquada. *Antiferromagnetism in $\text{YBa}_2\text{Cu}_3\text{O}_{6+x}$ (invited)*. Journal of Applied Physics **64** (1988), 6071.
- [42] Sudip Chakravarty, Bertrand I. Halperin, and David R. Nelson. *Two-dimensional quantum Heisenberg antiferromagnet at low temperatures*. Phys. Rev. B **39** (1989), 2344.
- [43] H. Takagi, T. Ido, S. Ishibashi, M. Uota, S. Uchida, and Y. Tokura. *Superconductor-to-nonsuperconductor transition in $(\text{La}_{1-x}\text{Sr}_x)_2\text{CuO}_4$ as investigated by transport and magnetic measurements*. Phys. Rev. B **40** (1989), 2254.

- [44] Ruixing Liang, D. A. Bonn, and W. N. Hardy. *Evaluation of CuO₂ plane hole doping in YBa₂Cu₃O_{6+x} single crystals*. Phys. Rev. B **73** (2006), 180505.
- [45] Tao Wu, Hadrien Mayaffre, Steffen Krämer, Mladen Horvatić, Claude Berthier, WN Hardy, Ruixing Liang, DA Bonn, and Marc-Henri Julien. *Magnetic-field-induced charge-stripe order in the high-temperature superconductor YBa₂Cu₃O_y*. Nature **477** (2011), 191.
- [46] Tao Wu, Hadrien Mayaffre, Steffen Krämer, Mladen Horvatić, Claude Berthier, Philip L Kuhns, Arneil P Reyes, Ruixing Liang, WN Hardy, DA Bonn *et al.* *Emergence of charge order from the vortex state of a high-temperature superconductor*. Nature Communications **4** (2013), 2113.
- [47] G. Ghiringhelli, M. Le Tacon, M. Minola, S. Blanco-Canosa, C. Mazzoli, N. B. Brookes, G. M. De Luca, A. Frano, D. G. Hawthorn, F. He *et al.* *Long-range incommensurate charge fluctuations in (Y, Nd)Ba₂Cu₃O_{6+x}*. Science **337** (2012), 821.
- [48] J. Chang, E. Blackburn, A. T. Holmes, N. B. Christensen, Jacob Larsen, J Mesot, Ruixing Liang, DA Bonn, W. N. Hardy, A. Watenphul *et al.* *Direct observation of competition between superconductivity and charge density wave order in YBa₂Cu₃O_{6.67}*. Nature Physics **8** (2012), 871.
- [49] E. Blackburn, J. Chang, M. Hücker, A. T. Holmes, N. B. Christensen, Ruixing Liang, D. A. Bonn, W. N. Hardy, U. Rütt, O. Gutowski, M. v. Zimmermann, E. M. Forgan, and S. M. Hayden. *X-Ray Diffraction Observations of a Charge-Density-Wave Order in Superconducting Ortho-II YBa₂Cu₃O_{6.54} Single Crystals in Zero Magnetic Field*. Phys. Rev. Lett. **110** (2013), 137004.
- [50] N. E. Hussey, M. Abdel-Jawad, A. Carrington, A. P. Mackenzie, and L. Balicas. *A coherent three-dimensional Fermi surface in a high-transition-temperature superconductor*. Nature **425** (2003), 814.
- [51] N. E. Hussey. *Phenomenology of the normal state in-plane transport properties of high-T_c cuprates*. Journal of Physics: Condensed Matter **20** (2008), 123201.
- [52] Suchitra E Sebastian, Neil Harrison, and Gilbert G Lonzarich. *Towards resolution of the Fermi surface in underdoped high-T_c superconductors*. Reports on Progress in Physics **75** (2012), 102501.
- [53] Sudip Chakravarty. *From Complexity to Simplicity*. Science **319** (2008), 735.
- [54] N. David Mermin Neil W. Ashcroft. *Solid State Physics*. Thomson Learning, Inc. (1976).
- [55] D. Shoenberg. *Magnetic oscillation in metals*. Cambridge University Press (1984).
- [56] L. Onsager. *Interpretation of the de Haas-van Alphen effect*. The London, Edinburgh, and Dublin Philosophical Magazine and Journal of Science **43** (1952), 1006.
- [57] Michael R Norman and Cyril Proust. *Focus on fermiology of the cuprates*. New Journal of Physics **16** (2014), 045004.

- [58] E. M. Lifshitz and A. M. Kosevich. *Theory of Magnetic Susceptibility in Metals at Low Temperature*. J. Exper. Theoret. Phys. USSR **29** (1955), 730.
- [59] Brad Ramshaw. *Shubnikov-de Haas measurements and the spin magnetic moment of $YBa_2Cu_3O_{6.59}$* . Ph.D. thesis, The University of British Columbia (2012).
- [60] Pallab Goswami, Xun Jia, and Sudip Chakravarty. *Quantum oscillations in graphene in the presence of disorder and interactions*. Phys. Rev. B **78** (2008), 245406.
- [61] J. M. Luttinger. *Theory of the de Haas-van Alphen Effect for a System of Interacting Fermions*. Phys. Rev. **121** (1961), 1251.
- [62] J. M. Luttinger. *Fermi Surface and Some Simple Equilibrium Properties of a System of Interacting Fermions*. Phys. Rev. **119** (1960), 1153.
- [63] Sudip Chakravarty and Hae-Young Kee. *Fermi pockets and quantum oscillations of the Hall coefficient in high-temperature superconductors*. Proceedings of the National Academy of Sciences **105** (2008), 8835.
- [64] Andrea Allais, Debanjan Chowdhury, and Subir Sachdev. *Connecting high-field quantum oscillations to zero-field electron spectral functions in the underdoped cuprates*. Nature communications **5** (2014), 5771.
- [65] Andrew J. Millis and M. R. Norman. *Antiphase stripe order as the origin of electron pockets observed in 1/8-hole-doped cuprates*. Phys. Rev. B **76** (2007), 220503.
- [66] Hong Yao, Dung-Hai Lee, and Steven Kivelson. *Fermi-surface reconstruction in a smectic phase of a high-temperature superconductor*. Phys. Rev. B **84** (2011), 012507.
- [67] Ivailo Dimov, Pallab Goswami, Xun Jia, and Sudip Chakravarty. *Competing order, Fermi surface reconstruction, and quantum oscillations in underdoped high-temperature superconductors*. Phys. Rev. B **78** (2008), 134529.
- [68] N. Harrison and S. E. Sebastian. *Magnetotransport signatures of a single nodal electron pocket constructed from Fermi arcs*. Phys. Rev. B **92** (2015), 224505.
- [69] G. Blatter, M. V. Feigel'man, V. B. Geshkenbein, A. I. Larkin, and V. M. Vinokur. *Vortices in high-temperature superconductors*. Rev. Mod. Phys. **66** (1994), 1125.
- [70] Yayu Wang, S. Ono, Y. Onose, G. Gu, Yoichi Ando, Y. Tokura, S. Uchida, and N. P. Ong. *Dependence of Upper Critical Field and Pairing Strength on Doping in Cuprates*. Science **299** (2003), 86.
- [71] T. Senthil and Patrick A. Lee. *Synthesis of the phenomenology of the underdoped cuprates*. Phys. Rev. B **79** (2009), 245116.
- [72] B. J. Ramshaw, James Day, Baptiste Vignolle, David LeBoeuf, P. Dosanjh, Cyril Proust, Louis Taillefer, Ruixing Liang, W. N. Hardy, and D. A. Bonn. *Vortex lattice melting and H_{c2} in underdoped $YBa_2Cu_3O_y$* . Phys. Rev. B **86** (2012), 174501.
- [73] M. Tinkham. *Introduction to superconductivity*. Dover publications, Mineola, New York (1996).

- [74] Sumilan Banerjee, Shizhong Zhang, and Mohit Randeria. *Theory of quantum oscillations in the vortex-liquid state of high- T_c superconductors*. Nature Communications **4** (2013), 1700.
- [75] K. v. Klitzing, G. Dorda, and M. Pepper. *New Method for High-Accuracy Determination of the Fine-Structure Constant Based on Quantized Hall Resistance*. Phys. Rev. Lett. **45** (1980), 494.
- [76] Xiao-Gang Wen. *Quantum Field Theory of Many-Body Systems: From the Origin of Sound to an Origin of Light and Electrons*. Higher Education Press, translated in chinese edition (2004).
- [77] M. Z. Hasan and C. L. Kane. *Colloquium : Topological insulators*. Rev. Mod. Phys. **82** (2010), 3045.
- [78] Xiao-Liang Qi and Shou-Cheng Zhang. *Topological insulators and superconductors*. Rev. Mod. Phys. **83** (2011), 1057.
- [79] Richard E. Prange, Steven M. Girvin, K. V. Klitzing, M. E. Cage, A. M. Chang, F. D. M. Haldane, R. B. Laughlin, A. M. M. Pruisken, and D. J. Thouless. *The Quantum Hall Effect*. Springer-Verlag, second edition (1990).
- [80] P. W. Anderson. *Absence of Diffusion in Certain Random Lattices*. Phys. Rev. **109** (1958), 1492.
- [81] J. K. Jain. *Composite-fermion approach for the fractional quantum Hall effect*. Phys. Rev. Lett. **63** (1989), 199.
- [82] Ganpathy Murthy and R. Shankar. *Hamiltonian theories of the fractional quantum Hall effect*. Rev. Mod. Phys. **75** (2003), 1101.
- [83] W. Pan, J. S. Xia, H. L. Stormer, D. C. Tsui, C. Vicente, E. D. Adams, N. S. Sullivan, L. N. Pfeiffer, K. W. Baldwin, and K. W. West. *Experimental studies of the fractional quantum Hall effect in the first excited Landau level*. Phys. Rev. B **77** (2008), 075307.
- [84] J. P. Eisenstein, K. B. Cooper, L. N. Pfeiffer, and K. W. West. *Insulating and Fractional Quantum Hall States in the First Excited Landau Level*. Phys. Rev. Lett. **88** (2002), 076801.
- [85] J. S. Xia, W. Pan, C. L. Vicente, E. D. Adams, N. S. Sullivan, H. L. Stormer, D. C. Tsui, L. N. Pfeiffer, K. W. Baldwin, and K. W. West. *Electron Correlation in the Second Landau Level: A Competition Between Many Nearly Degenerate Quantum Phases*. Phys. Rev. Lett. **93** (2004), 176809.
- [86] J. Shabani, T. Gokmen, Y. T. Chiu, and M. Shayegan. *Evidence for Developing Fractional Quantum Hall States at Even Denominator $1/2$ and $1/4$ Fillings in Asymmetric Wide Quantum Wells*. Phys. Rev. Lett. **103** (2009), 256802.
- [87] Vadim Kalmeyer and Shou-Cheng Zhang. *Metallic phase of the quantum Hall system at even-denominator filling fractions*. Phys. Rev. B **46** (1992), 9889.

- [88] R. L. Willett, R. R. Ruel, K. W. West, and L. N. Pfeiffer. *Experimental demonstration of a Fermi surface at one-half filling of the lowest Landau level*. Phys. Rev. Lett. **71** (1993), 3846.
- [89] R. L. Willett, R. R. Ruel, M. A. Paalanen, K. W. West, and L. N. Pfeiffer. *Enhanced finite-wave-vector conductivity at multiple even-denominator filling factors in two-dimensional electron systems*. Phys. Rev. B **47** (1993), 7344.
- [90] R. R. Du, H. L. Stormer, D. C. Tsui, L. N. Pfeiffer, and K. W. West. *Experimental evidence for new particles in the fractional quantum Hall effect*. Phys. Rev. Lett. **70** (1993), 2944.
- [91] V. J. Goldman, B. Su, and J. K. Jain. *Detection of composite fermions by magnetic focusing*. Phys. Rev. Lett. **72** (1994), 2065.
- [92] W. Kang, H. L. Stormer, L. N. Pfeiffer, K. W. Baldwin, and K. W. West. *How real are composite fermions?* Phys. Rev. Lett. **71** (1993), 3850.
- [93] Robert L. Willett. *Experimental evidence for composite fermions*. Advances in Physics **46** (1997), 447.
- [94] S. A. Kivelson, D-H. Lee, Y. Krotov, and J. Gan. *Composite-fermion Hall conductance at $\nu = 1/2$* . Phys. Rev. B **55** (1997), 15552.
- [95] Dung-Hai Lee. *Neutral Fermions at Filling Factor $\nu = 1/2$* . Phys. Rev. Lett. **80** (1998), 4745.
- [96] F. D. M. Haldane and E. H. Rezayi. *Spin-singlet wave function for the half-integral quantum Hall effect*. Phys. Rev. Lett. **60** (1988), 956.
- [97] J. P. Eisenstein, R. Willett, H. L. Stormer, D. C. Tsui, A. C. Gossard, and J. H. English. *Collapse of the Even-Denominator Fractional Quantum Hall Effect in Tilted Fields*. Phys. Rev. Lett. **61** (1988), 997.
- [98] R. H. Morf. *Transition from Quantum Hall to Compressible States in the Second Landau Level: New Light on the $\nu = 5/2$ Enigma*. Phys. Rev. Lett. **80** (1998), 1505.
- [99] E. H. Rezayi and F. D. M. Haldane. *Incompressible Paired Hall State, Stripe Order, and the Composite Fermion Liquid Phase in Half-Filled Landau Levels*. Phys. Rev. Lett. **84** (2000), 4685.
- [100] Sung-Sik Lee, Shinsei Ryu, Chetan Nayak, and Matthew P. A. Fisher. *Particle-Hole Symmetry and the $\nu = \frac{5}{2}$ Quantum Hall State*. Phys. Rev. Lett. **99** (2007), 236807.
- [101] Michael Levin, Bertrand I. Halperin, and Bernd Rosenow. *Particle-Hole Symmetry and the Pfaffian State*. Phys. Rev. Lett. **99** (2007), 236806.
- [102] X. G. Wen. *Non-Abelian statistics in the fractional quantum Hall states*. Phys. Rev. Lett. **66** (1991), 802.
- [103] B. I. Halperin. *Theory of the quantized Hall conductance*. Helv. Phys. Acta **56** (1983), 75.

- [104] X. G. Wen and A. Zee. *Classification of Abelian quantum Hall states and matrix formulation of topological fluids*. Phys. Rev. B **46** (1992), 2290.
- [105] Parsa Bonderson and J. K. Slingerland. *Fractional quantum Hall hierarchy and the second Landau level*. Phys. Rev. B **78** (2008), 125323.
- [106] B. J. Overbosch and Xiao-Gang Wen. *Phase transition on the edge of the $\nu = 5/2$ Pfaffian and anti-Pfaffian quantum Hall state*. <http://arxiv.org/abs/0804.2087> (2008).
- [107] Guang Yang and D. E. Feldman. *Experimental constraints and a possible quantum Hall state at $\nu = 5/2$* . Phys. Rev. B **90** (2014), 161306.
- [108] J. M. Leinaas and J. Myrheim. *On the theory of identical particles*. Il Nuovo Cimento B (1971-1996) **37** (1977), 1.
- [109] Frank Wilczek. *Quantum Mechanics of Fractional-Spin Particles*. Phys. Rev. Lett. **49** (1982), 957.
- [110] Xi Lin, Ruirui Du, and Xincheng Xie. *Recent experimental progress of fractional quantum Hall effect: $5/2$ filling state and graphene*. National Science Review **1** (2014), 564.
- [111] J. R. Schrieffer. *Theory of Superconductivity*. Perseus Books (1999).
- [112] Chetan Nayak and Frank Wilczek. *Non-Fermi liquid fixed point in $2 + 1$ dimensions*. Nuclear Physics B **417** (1994), 359 .
- [113] Chetan Nayak and Frank Wilczek. *Renormalization group approach to low temperature properties of a non-Fermi liquid metal*. Nuclear Physics B **430** (1994), 534 .
- [114] Max A. Metlitski, David F. Mross, Subir Sachdev, and T. Senthil. *Cooper pairing in non-Fermi liquids*. Phys. Rev. B **91** (2015), 115111.
- [115] David Bohm and David Pines. *A Collective Description of Electron Interactions. I. Magnetic Interactions*. Phys. Rev. **82** (1951), 625.
- [116] David Pines and David Bohm. *A Collective Description of Electron Interactions: II. Collective vs Individual Particle Aspects of the Interactions*. Phys. Rev. **85** (1952), 338.
- [117] David Bohm and David Pines. *A Collective Description of Electron Interactions: III. Coulomb Interactions in a Degenerate Electron Gas*. Phys. Rev. **92** (1953), 609.
- [118] Murray Gell-Mann and Keith A. Brueckner. *Correlation Energy of an Electron Gas at High Density*. Phys. Rev. **106** (1957), 364.
- [119] Gabriele F. Giuliani and Giovanni Vignale. *Quantum Theory of the Electron Liquid*. Cambridge University Press (2005).
- [120] N. E. Bonesteel. *Singular Pair Breaking in the Composite Fermi Liquid Description of the Half-Filled Landau Level*. Phys. Rev. Lett. **82** (1999), 984.

- [121] R. Shankar. *Renormalization-group approach to interacting fermions*. Rev. Mod. Phys. **66** (1994), 129.
- [122] W. Kohn and J. M. Luttinger. *New Mechanism for Superconductivity*. Phys. Rev. Lett. **15** (1965), 524.
- [123] Suk Bum Chung, Ipsita Mandal, Srinivas Raghu, and Sudip Chakravarty. *Higher angular momentum pairing from transverse gauge interactions*. Phys. Rev. B **88** (2013), 045127.
- [124] S. M. Girvin. *Particle-hole symmetry in the anomalous quantum Hall effect*. Phys. Rev. B **29** (1984), 6012.
- [125] Chong Wang and T. Senthil. *Half-filled Landau level, topological insulator surfaces, and three-dimensional quantum spin liquids*. Phys. Rev. B **93** (2016), 085110.
- [126] Scott D. Geraedts, Michael P. Zaletel, Roger S. K. Mong, Max A. Metlitski, Ashvin Vishwanath, and Olexei I. Motrunich. *The half-filled Landau level: The case for Dirac composite fermions*. Science **352** (2016), 197.
- [127] Chong Wang and T. Senthil. *Composite fermi liquids in the lowest Landau level*. <http://arxiv.org/abs/1604.06807v1> (2016).
- [128] Ganpathy Murthy and R. Shankar. $\nu = \frac{1}{2}$ Landau level: Half-empty versus half-full. Phys. Rev. B **93** (2016), 085405.
- [129] Steven Kivelson, Dung-Hai Lee, and Shou-Cheng Zhang. *Global phase diagram in the quantum Hall effect*. Phys. Rev. B **46** (1992), 2223.
- [130] L. W. Wong, H. W. Jiang, and W. J. Schaff. *Universality and phase diagram around half-filled Landau levels*. Phys. Rev. B **54** (1996), R17323.
- [131] D. Shahar, D. C. Tsui, M. Shayegan, R. N. Bhatt, and J. E. Cunningham. *Universal Conductivity at the Quantum Hall Liquid to Insulator Transition*. Phys. Rev. Lett. **74** (1995), 4511.
- [132] D. Shahar, D. C. Tsui, M. Shayegan, E. Shimshoni, and S. L. Sondhi. *Evidence for Charge-Flux Duality near the Quantum Hall Liquid-to-Insulator Transition*. Science **274** (1996), 589.
- [133] D. Kamburov, Yang Liu, M. A. Mueed, M. Shayegan, L. N. Pfeiffer, K. W. West, and K. W. Baldwin. *What Determines the Fermi Wave Vector of Composite Fermions?* Phys. Rev. Lett. **113** (2014), 196801.
- [134] D. Kamburov, M. A. Mueed, I. Jo, Yang Liu, M. Shayegan, L. N. Pfeiffer, K. W. West, K. W. Baldwin, J. J. D. Lee, and R. Winkler. *Determination of Fermi contour and spin polarization of $\nu = \frac{3}{2}$ composite fermions via ballistic commensurability measurements*. Phys. Rev. B **90** (2014), 235108.
- [135] Max A. Metlitski and Ashvin Vishwanath. *Particle-vortex duality of two-dimensional Dirac fermion from electric-magnetic duality of three-dimensional topological insulators*. Phys. Rev. B **93** (2016), 245151.

- [136] Shamit Kachru, Michael Mulligan, Gonzalo Torroba, and Huajia Wang. *Mirror symmetry and the half-filled Landau level*. Phys. Rev. B **92** (2015), 235105.
- [137] Andrew C. Potter, Maksym Serbyn, and Ashvin Vishwanath. *Thermoelectric transport signatures of Dirac composite fermions in the half-filled Landau level*. <http://arxiv.org/abs/1512.06852v1> (2015).
- [138] F. D. M. Haldane. *Berry Curvature on the Fermi Surface: Anomalous Hall Effect as a Topological Fermi-Liquid Property*. Phys. Rev. Lett. **93** (2004), 206602.
- [139] Ajit C. Balram, Csaba Tóke, and J. K. Jain. *Luttinger Theorem for the Strongly Correlated Fermi Liquid of Composite Fermions*. Phys. Rev. Lett. **115** (2015), 186805.
- [140] Maissam Barkeshli, Michael Mulligan, and Matthew P. A. Fisher. *Particle-hole symmetry and the composite Fermi liquid*. Phys. Rev. B **92** (2015), 165125.
- [141] Michael Mulligan, S. Raghu, and Matthew P. A. Fisher. *Emergent particle-hole symmetry in the half-filled Landau level*. Phys. Rev. B **94** (2016), 075101.
- [142] Philip Zucker and Dmitri E. Feldman. *Particle-hole symmetry without particle-hole symmetry in the quantum Hall effect at $\nu = 5/2$* . <http://arxiv.org/abs/1603.03754v1> (2016).
- [143] F. D. M. Haldane. *A model wavefunction for the composite fermi liquid, its geometry and entanglement*. APS March Meeting (2016).
- [144] E. A. Yelland, J. Singleton, C. H. Mielke, N. Harrison, F. F. Balakirev, B. Dabrowski, and J. R. Cooper. *Quantum Oscillations in the Underdoped Cuprate YBa₂Cu₄O₈*. Phys. Rev. Lett. **100** (2008), 047003.
- [145] A. F. Bangura, J. D. Fletcher, A. Carrington, J. Levallois, M. Nardone, B. Vignolle, P. J. Heard, N. Doiron-Leyraud, D. LeBoeuf, L. Taillefer, S. Adachi, C. Proust, and N. E. Hussey. *Small Fermi Surface Pockets in Underdoped High Temperature Superconductors: Observation of Shubnikov-de Haas Oscillations in YBa₂Cu₄O₈*. Phys. Rev. Lett. **100** (2008), 047004.
- [146] Daniel Podolsky and Hae-Young Kee. *Quantum oscillations of ortho-II high-temperature cuprates*. Phys. Rev. B **78** (2008), 224516.
- [147] T. Helm, M. V. Kartsovnik, M. Bartkowiak, N. Bittner, M. Lambacher, A. Erb, J. Wosnitza, and R. Gross. *Evolution of the Fermi Surface of the Electron-Doped High-Temperature Superconductor Nd_{2-x}Ce_xCuO₄ Revealed by Shubnikov-de Haas Oscillations*. Phys. Rev. Lett. **103** (2009), 157002.
- [148] T. Helm, M. V. Kartsovnik, I. Sheikin, M. Bartkowiak, F. Wolff-Fabris, N. Bittner, W. Biberacher, M. Lambacher, A. Erb, J. Wosnitza, and R. Gross. *Magnetic Breakdown in the Electron-Doped Cuprate Superconductor Nd_{2-x}Ce_xCuO₄: The Reconstructed Fermi Surface Survives in the Strongly Overdoped Regime*. Phys. Rev. Lett. **105** (2010), 247002.

- [149] M. V. Kartsovnik, T. Helm, C. Putzke, F. Wolff-Fabris, I. Sheikin, S. Lepault, C. Proust, D. Vignolles, N. Bittner, W. Biberacher, A. Erb, J. Wosnitza, and R. Gross. *Fermi surface of the electron-doped cuprate superconductor $Nd_{2-x}Ce_xCuO_4$ probed by high-field magnetotransport*. New Journal of Physics **13** (2011), 015001.
- [150] Jonghyoun Eun, Xun Jia, and Sudip Chakravarty. *Quantum oscillations in electron-doped high-temperature superconductors*. Phys. Rev. B **82** (2010), 094515.
- [151] Jonghyoun Eun and Sudip Chakravarty. *Magnetic breakdown and quantum oscillations in electron-doped high-temperature superconductor $Nd_{2-x}Ce_xCuO_4$* . Phys. Rev. B **84** (2011), 094506.
- [152] Louis Taillefer. *Fermi surface reconstruction in high- T_c superconductors*. Journal of Physics: Condensed Matter **21** (2009), 164212.
- [153] John Singleton, Clarina de la Cruz, R. D. McDonald, Shiliang Li, Moaz Altarawneh, Paul Goddard, Isabel Franke, Dwight Rickel, C. H. Mielke, Xin Yao, and Pengcheng Dai. *Magnetic Quantum Oscillations in $YBa_2Cu_3O_{6.61}$ and $YBa_2Cu_3O_{6.69}$ in Fields of Up to 85 T: Patching the Hole in the Roof of the Superconducting Dome*. Phys. Rev. Lett. **104** (2010), 086403.
- [154] N. Doiron-Leyraud, S. Badoux, S. Renéde Cotret, S. Lepault, D. LeBoeuf, F. Laliberté, E. Hassinger, B. J. Ramshaw, D. A. Bonn, W. N. Hardy, R. Liang, J. H. . Park, D. Vignolles, B. Vignolle, L. Taillefer, and C. Proust. *Evidence for a small hole pocket in the Fermi surface of underdoped $YBa_2Cu_3O_y$* . Nat. Commun. **6** (2015), 6034.
- [155] B. J. Ramshaw, Baptiste Vignolle, James Day, Ruixing Liang, W. N. Hardy, Cyril Proust, and D. A. Bonn. *Angle dependence of quantum oscillations in $YBa_2Cu_3O_{6.59}$ shows free-spin behaviour of quasiparticles*. Nature Physics **7** (2011), 234.
- [156] S. E. Sebastian, N. Harrison, M. M. Altarawneh, F. F. Balakirev, C. H. Mielke, R. Liang, D. A. Bonn, W. N. Hardy, and G. G. Lonzarich. *Direct observation of multiple spin zeroes in the underdoped high temperature superconductor $YBa_2Cu_3O_6 + x$* . ArXiv e-prints (2011). 1103.4178.
- [157] Samuel Lederer and Steven A. Kivelson. *Observable NMR signal from circulating current order in YBCO*. Phys. Rev. B **85** (2012), 155130.
- [158] M. A. Hossain, J. D. F. Mottershead, D. Fournier, A. Bostwick, J. L. McChesney, E. Rotenberg, R. Liang, W. N. Hardy, G. A. Sawatzky, I. S. Elfimov *et al.* *In situ doping control of the surface of high-temperature superconductors*. Nature Physics **4** (2008), 527.
- [159] Andrea Damascelli, Zahid Hussain, and Zhi-Xun Shen. *Angle-resolved photoemission studies of the cuprate superconductors*. Rev. Mod. Phys. **75** (2003), 473.
- [160] E. Pavarini, I. Dasgupta, T. Saha-Dasgupta, O. Jepsen, and O. K. Andersen. *Band-Structure Trend in Hole-Doped Cuprates and Correlation with T_{cmax}* . Phys. Rev. Lett. **87** (2001), 047003.

- [161] Y. Sassa, M. Radović, M. Månsson, E. Razzoli, X. Y. Cui, S. Pailhès, S. Guerrero, M. Shi, P. R. Willmott, F. Miletto Granozio, J. Mesot, M. R. Norman, and L. Patthey. *Ortho-II band folding in $YBa_2Cu_3O_{7-\delta}$ films revealed by angle-resolved photoemission*. Phys. Rev. B **83** (2011), 140511.
- [162] Xun Jia, Pallab Goswami, and Sudip Chakravarty. *Resolution of two apparent paradoxes concerning quantum oscillations in underdoped high- T_c superconductors*. Phys. Rev. B **80** (2009), 134503.
- [163] JL Pichard and G André. *Many-channel transmission: Large volume limit of the distribution of localization lengths and one-parameter scaling*. EPL (Europhysics Letters) **2** (1986), 477.
- [164] Daniel S. Fisher and Patrick A. Lee. *Relation between conductivity and transmission matrix*. Phys. Rev. B **23** (1981), 6851.
- [165] Scott C. Riggs, O. Vafek, J. B. Kemper, J. B. Betts, A. Migliori, F. F. Balakirev, W. N. Hardy, Ruixing Liang, D. A. Bonn, and G. S. Boebinger. *Heat capacity through the magnetic-field-induced resistive transition in an underdoped high-temperature superconductor*. Nature Physics **7** (2011), 332.
- [166] Sudip Chakravarty, Chetan Nayak, and Sumanta Tewari. *Angle-resolved photoemission spectra in the cuprates from the d -density wave theory*. Phys. Rev. B **68** (2003), 100504.
- [167] N. P. Armitage, P. Fournier, and R. L. Greene. *Progress and perspectives on electron-doped cuprates*. Rev. Mod. Phys. **82** (2010), 2421.
- [168] Guo-qing Zheng, W. G. Clark, Y. Kitaoka, K. Asayama, Y. Kodama, P. Kuhns, and W. G. Moulton. *Responses of the pseudogap and d -wave superconductivity to high magnetic fields in the underdoped high- T_c superconductor $YBa_2Cu_4O_8$: An NMR study*. Phys. Rev. B **60** (1999), R9947.
- [169] Shinji Kawasaki, Chengtian Lin, Philip L. Kuhns, Arneil P. Reyes, and Guo-qing Zheng. *Carrier-Concentration Dependence of the Pseudogap Ground State of Superconducting $Bi_2Sr_{2-x}La_xCuO_{6+\delta}$ Revealed by $^{63,65}Cu$ -Nuclear Magnetic Resonance in Very High Magnetic Fields*. Phys. Rev. Lett. **105** (2010), 137002.
- [170] Hoang K. Nguyen and Sudip Chakravarty. *Effects of magnetic field on the d -density-wave order in the cuprates*. Phys. Rev. B **65** (2002), 180519.
- [171] David Garcia-Aldea and Sudip Chakravarty. *Singlet versus triplet particle-hole condensates in quantum oscillations in cuprates*. Phys. Rev. B **82** (2010), 184526.
- [172] M. R. Norman and Jie Lin. *Spin zeros and the origin of Fermi-surface reconstruction in the cuprates*. Phys. Rev. B **82** (2010), 060509.
- [173] Revaz Ramazashvili. *Quantum Oscillations in Antiferromagnetic Conductors with Small Carrier Pockets*. Phys. Rev. Lett. **105** (2010), 216404.
- [174] H. A. Mook, Pengcheng Dai, S. M. Hayden, A. Hiess, J. W. Lynn, S.-H. Lee, and F. Doğan. *Magnetic order in $YBa_2Cu_3O_{6+x}$ superconductors*. Phys. Rev. B **66** (2002), 144513.

- [175] H. A. Mook, Pengcheng Dai, S. M. Hayden, A. Hiess, S-H Lee, and F. Dogan. *Polarized neutron measurement of magnetic order in $\text{YBa}_2\text{Cu}_3\text{O}_{6.45}$* . Phys. Rev. B **69** (2004), 134509.
- [176] Andrey V. Chubukov and Dirk K. Morr. *Electronic structure of underdoped cuprates*. Physics Reports **288** (1997), 355 .
- [177] B. L. Altshuler, A. V. Chubukov, A. Dashevskii, A. M. Finkel'stein, and D. K. Morr. *Luttinger theorem for a spin-density-wave state*. EPL (Europhysics Letters) **41** (1998), 401.
- [178] Suchitra E. Sebastian, N. Harrison, E. Palm, T. P. Murphy, C. H. Mielke, Ruixing Liang, D. A. Bonn, W. N. Hardy, and G. G. Lonzarich. *A multi-component Fermi surface in the vortex state of an underdoped high- T_c superconductor*. Nature **454** (2008), 200.
- [179] G. E. Volovik. *Superconductivity with lines of gap nodes: density of states in the vortex*. JETP Lett **58** (1993), 469.
- [180] C. Marcenat, A. Demuer, K. Beauvois, B. Michon, A. Grockowiak, R. Liang, W. Hardy, D. A. Bonn, and T. Klein. *Calorimetric determination of the magnetic phase diagram of underdoped ortho II $\text{YBa}_2\text{Cu}_2\text{O}_{6.54}$ single crystals*. Nature communications **6** (2015), 7927.
- [181] Michael J. Stephen. *Superconductors in strong magnetic fields: de Haas-van Alphen effect*. Phys. Rev. B **45** (1992), 5481.
- [182] Kazumi Maki. *Quantum oscillation in vortex states of type-II superconductors*. Phys. Rev. B **44** (1991), 2861.
- [183] Jonghyoun Eun, Zhiqiang Wang, and Sudip Chakravarty. *Quantum oscillations in $\text{YBa}_2\text{Cu}_3\text{O}_{6+\delta}$ from period-8 d-density wave order*. Proceedings of the National Academy of Sciences **109** (2012), 13198.
- [184] R. B. Laughlin. *Hartree-Fock computation of the high- T_c cuprate phase diagram*. Phys. Rev. B **89** (2014), 035134.
- [185] R. B. Laughlin. *Fermi-Liquid Computation of the Phase Diagram of High- T_c Cuprate Superconductors with an Orbital Antiferromagnetic Pseudogap*. Phys. Rev. Lett. **112** (2014), 017004.
- [186] Suchitra E. Sebastian, N. Harrison, F. F. Balakirev, M. M. Altarawneh, P. A. Goddard, Ruixing Liang, D. A. Bonn, W. N. Hardy, and G. G. Lonzarich. *Normal-state nodal electronic structure in underdoped high- T_c copper oxides*. Nature **511** (2014), 61.
- [187] Yi Zhang, Akash V. Maharaj, and Steven Kivelson. *Disruption of quantum oscillations by an incommensurate charge density wave*. Phys. Rev. B **91** (2015), 085105.
- [188] Ashot Melikyan and Zlatko Tešanović. *Mixed state of a lattice d-wave superconductor*. Phys. Rev. B **74** (2006), 144501.

- [189] Oskar Vafek and Ashot Melikyan. *Index Theoretic Characterization of d-Wave Superconductors in the Vortex State*. Phys. Rev. Lett. **96** (2006), 167005.
- [190] Vladimir Cvetkovic and Oskar Vafek. *Berry phases and the intrinsic thermal Hall effect in high-temperature cuprate superconductors*. Nature Communications **6** (2015), 6518.
- [191] Bernhard Kramer and Michael Schreiber. *Computational Physics: selected methods, simple exercises, serious applications*. Springer Verlag Berlin Heidelberg (1996).
- [192] Kathryn A. Moler, David L. Sisson, Jeffrey S. Urbach, Malcolm R. Beasley, Aharon Kapitulnik, David J. Baar, Ruixing Liang, and Walter N. Hardy. *Specific heat of YBa₂Cu₃O_{7- δ}* . Phys. Rev. B **55** (1997), 3954.
- [193] N. E. Bonesteel. *Compressible phase of a double-layer electron system with total Landau-level filling factor 1/2*. Phys. Rev. B **48** (1993), 11484.
- [194] N. E. Bonesteel, I. A. McDonald, and C. Nayak. *Gauge Fields and Pairing in Double-Layer Composite Fermion Metals*. Phys. Rev. Lett. **77** (1996), 3009.
- [195] D. T. Son. *Superconductivity by long-range color magnetic interaction in high-density quark matter*. Phys. Rev. D **59** (1999), 094019.
- [196] K. Park, V. Melik-Alaverdian, N. E. Bonesteel, and J. K. Jain. *Possibility of p-wave pairing of composite fermions at $\nu = \frac{1}{2}$* . Phys. Rev. B **58** (1998), R10167.
- [197] D. R. Luhman, W. Pan, D. C. Tsui, L. N. Pfeiffer, K. W. Baldwin, and K. W. West. *Observation of a Fractional Quantum Hall State at $\nu=1/4$ in a Wide GaAs Quantum Well*. Phys. Rev. Lett. **101** (2008), 266804.
- [198] J. Shabani, T. Gokmen, and M. Shayegan. *Correlated States of Electrons in Wide Quantum Wells at Low Fillings: The Role of Charge Distribution Symmetry*. Phys. Rev. Lett. **103** (2009), 046805.
- [199] Yuan-Ming Lu, Yue Yu, and Ziqiang Wang. *Correlation-Hole Induced Paired Quantum Hall States in the Lowest Landau Level*. Phys. Rev. Lett. **105** (2010), 216801.
- [200] Takao Morinari. *Quantum Hall Effect at Half-Filled Landau Level: Pairing of Composite Fermions*. Phys. Rev. Lett. **81** (1998), 3741.
- [201] Takao Morinari. *Composite fermion pairing theory in single-layer systems*. Phys. Rev. B **62** (2000), 15903.
- [202] Vito W Scarola, Kwon Park, and JK Jain. *Cooper instability of composite fermions*. Nature **406** (2000), 863.
- [203] J. Biddle, Michael R. Peterson, and S. Das Sarma. *Variational Monte Carlo study of spin-polarization stability of fractional quantum Hall states against realistic effects in half-filled Landau levels*. Phys. Rev. B **87** (2013), 235134.
- [204] Jian Zhang, R. R. Du, J. A. Simmons, and J. L. Reno. *Resistance minimum observed at Landau level filling factor $\nu = 1/2$ in ultra high magnetic fields*. Phys. Rev. B **81** (2010), 041308.

- [205] R. Cipri and N. E. Bonesteel. *Gauge fluctuations and interlayer coherence in bilayer composite fermion metals*. Phys. Rev. B **89** (2014), 085109.
- [206] Jason Alicea, Olexei I. Motrunich, G. Refael, and Matthew P. A. Fisher. *Interlayer Coherent Composite Fermi Liquid Phase in Quantum Hall Bilayers*. Phys. Rev. Lett. **103** (2009), 256403.
- [207] Zhiqiang Wang, Ipsita Mandal, Suk Bum Chung, and Sudip Chakravarty. *Pairing in half-filled Landau level*. Annals of Physics **351** (2014), 727 .
- [208] A. Principi, Marco Polini, and G. Vignale. *Linear response of doped graphene sheets to vector potentials*. Phys. Rev. B **80** (2009), 075418.
- [209] V. A. Miransky, G. W. Semenoff, I. A. Shovkovy, and L. C. R. Wijewardhana. *Color superconductivity and nondecoupling phenomena in (2+1)-dimensional QCD*. Phys. Rev. D **64** (2001), 025005.
- [210] X. G. Wen and A. Zee. *Shift and spin vector: New topological quantum numbers for the Hall fluids*. Phys. Rev. Lett. **69** (1992), 953.
- [211] Xiao-Gang Wen. *Topological orders and edge excitations in fractional quantum Hall states*. Advances in Physics **44** (1995), 405.
- [212] Parsa Bonderson, Victor Gurarie, and Chetan Nayak. *Plasma analogy and non-Abelian statistics for Ising-type quantum Hall states*. Phys. Rev. B **83** (2011), 075303.
- [213] Siavash Golkar, Matthew M. Roberts, and Dam T. Son. *The Euler current and relativistic parity odd transport*. Journal of High Energy Physics **04** (2015), 110.
- [214] Siavash Golkar, Matthew M. Roberts, and Dam Thanh Son. *Effective field theory of relativistic quantum hall systems*. Journal of High Energy Physics **12** (2014), 138.
- [215] Sergej Moroz, Carlos Hoyos, and Leo Radzihovsky. *Chiral $p \pm ip$ superfluid on a sphere*. Phys. Rev. B **93** (2016), 024521.